UNIVERSITY OF CALGARY

Effect of Refining on Asphaltene Property Distributions

by

Hassan Sadeghi Yamchi

A THESIS

SUBMITTED TO THE FACULTY OF GRADUATE STUDIES

IN PARTIAL FULFILMENT OF THE REQUIREMENTS FOR THE

DEGREE OF MASTER OF SCIENCE

GRADUATE PROGRAM IN CHEMICAL AND PETROLEUM ENGINEERING

CALGARY, ALBERTA

JULY, 2014

Abstract

Asphaltenes are a solubility class and are defined as the part of a crude oil that is soluble in toluene and insoluble in *n*-heptane. Asphaltene precipitation, and subsequent fouling, is a potential issue in refining when feedstock and/or process streams are blended. While asphaltene precipitation from native crude oils can be predicted from a small set of measurements using regular solution based models, these precipitation models have not been applied to reacted crude oils. This study is part of a larger project to extend a previously developed regular solution based precipitation model to reacted crude oils. The three properties required for this model are density, molecular weight, and solubility parameter. The objectives of the study are: 1) to determine the distributions of these properties for self-associated asphaltene nanoaggregates; 2) model asphaltene precipitation from solutions of *n*-heptane and toluene (heptol) using regular solution theory.

To determine these distributions, *n*-heptane extracted asphaltenes from hydrocracked and thermocracked samples were fractionated into solubility cuts. The asphaltenes were dissolved in toluene and then partially precipitated at specified ratios of heptane-to-toluene to generate sets of light (soluble) and heavy (insoluble) cuts. The molecular weight and density were measured for each cut. The refractive index and elemental analysis were also measured for potential use as correlating parameters. The density distributions were determined directly from the data. The molecular weight data were fitted with a self-association model in order to predict the distributions at any given concentration. Asphaltene solubility parameters were determined by fitting the regular solution model to asphaltene precipitation yield data.

The asphaltenes were found to include both associating and non-associating asphaltenes. The amount of non-associating material and the density of the asphaltenes increased as the extent of reaction increased. Thermal cracking appeared to have little effect on asphaltene average monomer molecular weight or the distribution of nanoaggregate molecular weights. Hydrocracking significantly decreased both the average monomer and nanoaggregate molecular weights. It was found that both hydrocracking and thermal cracking made asphaltenes denser and significantly less soluble. The onset point of precipitation for both cases moved to zero concentration of *n*-heptane in heptol solutions.

A previously developed regular solution model was adapted to calculate solubility parameter distribution reacted asphaltenes. The model was modified as follows: density was correlated to the cumulative mass percent of asphaltenes; 2) the correlation of the asphaltene solubility parameter to molecular weight was retuned. Two methods were used to represent the asphaltene molecular weight distributions: the gamma distribution and the distribution from an association model. Since the solubility model predictions are affected by the shape of the molecular weight distributions, different sets of solubility parameter were calculated for each. In general, the gamma distribution adequately represented the molecular weight distributions for both native and reacted asphaltenes and better fit asphaltene yield data.

Acknowledgements

I would first like to thank my supervisor, Dr. Yarranton, for his support. I am extremely grateful to Dr. Yarranton for the freedom that he extended to me during my thesis work. I am truly indebted to him for his time and mentorship throughout my graduate career. I am thankful to have worked in an environment in which new paths could be explored and new ideas brought to fruition.

A special thanks goes to Elaine who ordered many and many pails of solvents, glass wares and VPO needles in the time of need. She was very kind to me specially those times that I messed up everything in the lab. She could have punished me but she never did. The fact that my thesis is very well written and is very organized is because of her. Thanks to her for editing my thesis and creating such fun atmosphere out of my mistakes. I am also grateful to Diana Powers who took the time, and had the patience, to discuss my many strange questions and to share many ideas with me. She always encouraged me not to lose my hope when I was not very optimistic about outcomes of experiments.

While at U of C I was fortunate to work alongside a group of talented people. I am so thankful to all of them in AER group that provided an exciting and fun atmosphere in which to work. I will miss their comradeship. To all of them I wish the best.

I gratefully acknowledge the financial support of the Shell Global Company in the form of a scholarship during my graduate studies in U of C.

Finally, I would like to thank four very important people to me. I thank my two beautiful sisters and my brother who supported me unconditionally in every steps of my life. Words cannot describe my gratitude to them and hopefully I deserve their love. I also thank my father who has been, and continues to be, hugely inspirational to me. I thank him for his love and guidance.

Dedicated to the memory of my mother.

Table of Contents

List of Tables

List of Figures and Illustrations

List of Symbols, Abbreviations and Nomenclature

Symbol	Definition
A	Coefficient in VPO calibration equation
A	Fitting parameter in molecular weight Dstr. Function
A	Fitting parameter in solubility correlation
a	Slope
a	Fitting parameter in density correlation to molecular weight
B	Fitting parameter in molecular weight Dstr. Function
b	Intercept
C	Concentration
C	Fitting parameter in molecular weight Dstr. Function
c	Fitting parameter in solubility correlation
cumf	Cumulative mass fraction in molecular weight distribution
cumw	Cumulative mass fraction in density distribution
D	Fitting parameter in molecular weight Dstr. Function
D	Interaction parameter
d	Fitting parameter in solubility correlation
E	Voltage
f	fugacity
f	Mass frequency
FRI	Refractive index function
H	Enthalpy
HT##	Heptol ratio with ##% *n*-heptane
K	Equilibrium constant
K	Instrument constant in VPO calibration equation
K	Association constant
K	Equilibrium ratio
l	Interaction coefficient
M	Molecular weight
m	Mass
MW	Molecular weight
n	Mole number
P	Propagator molecule
R	Universal gas constant
RI	Refractive index
T	Absolute temperature
T	Terminator molecule
V	Volume
w	Mass fraction
x	Mole Fraction

Greek Symbols

γ	Activity coefficient
ν	Molar volume
δ	Solubility parameter
ρ	Density
β	Binary interaction coefficient
ϕ	Volume fraction
β	Shape factor in gamma distribution
Γ	Gamma function
Δ	Difference

Subscripts

0	Initial
1,2,3,..., n	1^{st}, 2^{nd}, 3^{rd},…, n^{th}
2	Solute
A	Asphaltene
avg	Average
H	Heavy
HT##H	Heavy fraction precipitated from HT##
HT##L	Light fraction soluble in HT##
i, j, k	i^{th}, j^{th}, k^{th}
insol	Insoluble
L	Light
M	Mixture
m	Mixture
mix	Mixture
mono	Monomer
N	Neutral
P	Propagator
P	Pressure
S	Solvent
sol	Soluble
T	Toluene
T	Terminator
t	Total

Superscripts

0	Standard
L	Light phase

H	Heavy phase
l	Light phase
h	Heavy phase
$\bar{}$	Average

Chapter One: Introduction

Crude oils are a complex mixture of hydrocarbons and heteroatomic species, the heaviest of which are the asphaltenes (Speight, 2007). Asphaltenes are a solubility class and are defined as the part of a crude oil that is soluble in toluene and insoluble in *n*-heptane (Speight, 2007). Asphaltenes can precipitate upon a change in temperature, pressure, or composition and this precipitation can lead to deposition and fouling in reservoirs, wellbores, or surface facilities. Asphaltene precipitation is an issue during depressurization of light crude oils (Leontaritis, 1989; Hammami *et al*., 2000), when diluting heavy oils for recovery processes or transport (Andersen, 1999), and during refining when different streams are blended to obtain desired feed or product properties (Wiehe and Kennedy, 2000). Hence, there is a need to model asphaltene precipitation to design processes or mitigate precipitation related issues in existing facilities.

Asphaltene precipitation from native crude oils and crude oil blends has been modeled with both equation of state and regular solution approaches (Hirschberg *et al*., 1984; Kawanaka *et al*., 1991 Yarranton and Masliyah, 1996; Alboudwarej *et al.*, 2003; Akbarzadeh *et al*., 2005; Ting *et al*., 2003; Wang and Buckley, 2004; Vargas *et al*., 2009; Conzalez *et al*., 2007). These models typically require property distributions for the asphaltenes. For example, the regular solution approach, which is used in this thesis, requires the molecular weight, density, and solubility parameter distributions.

One of the complications in determining asphaltene property distributions is the self-association of asphaltenes. Asphaltenes tend to form aggregates of molecules in solution. The probable

mechanisms involving molecules interactions are aromatic π- π bond interactions, hydrogen bonding, and van der Waals forces (Yen *et al.*, 1961; Speight, 1994; Andersen, 2008; Gray *et al.*, 2011). Associated asphaltenes have been described as colloidal suspensions, reverse micelles, and macromolecules. Each of these concepts leads to different precipitation modeling approaches (Ravey *et al*., 1988, Agrawala *et al*., 2001; Merino-Garcia *et al*., 2004, Merino-Garcia *et al*., 2007; Hammami *et al*., 2007). However, the most successful precipitation models, regular solution theory and equations of state, presume in their application that the associated asphaltenes are macromolecules in solution.

Recent regular solution based precipitation models represent the asphaltene nanoaggregate molecular weight distribution with a Gamma function (Alboudwarej *et al*., 2003; Akbarzadeh *et al*., 2005). In the initial model development, a Gamma distribution function was assumed. Later on, Agrawala and Yarranton (2001) modeled asphaltene association analogously to linear polymerization. They used this "terminator/propagator" model and estimated the molecular weight distribution of asphaltene nano-aggregates. Barrera *at al.* (2012) fitted this association model to molecular weight data for fractionated asphaltenes and demonstrated that the fitted molecular weight distributions could indeed be represented with a Gamma distribution function. Density distributions have also been measured for several asphaltenes from native crude oils and a solubility parameter correlation has been developed (Alboudwarej *et al*., 2003; Akbarzadeh *et al*., 2005). Barrera *et al*. (2012) adapted these correlations to model precipitation of asphaltenes from some native crude oils and mildly reacted streams in solutions of heptane and toluene. However, there are as yet few data for asphaltene properties from refinery streams that have undergone significant cracking or hydrotreatment.

Cracking and hydrotreating are expected to change the properties and solubility of asphaltenes. Asphaltenes are generally considered to be polyaromatic hydrocarbons, consisting of aliphatic branches groups along with a variety of associated functional groups, including acids, thiophenes, pyridines, and porphyrins (Speight, 2007; Strausz *et al.*, 1992). Thermal reactions are known to split off the aliphatic side chains from the asphaltenes. Hence, reacted asphaltenes generally become more aromatic and less soluble in most solvents. They appear as sediments (the onset of the coke formation) during visbreaking and cracking processes. Preheating fuel oil prior to combustion causes the precipitation of reacted asphaltene constituents for a similar reason [Speight, 2004]. Note, after reaction, some components that were originally asphaltenes become insoluble in toluene are, by definition, no longer asphaltenes. Hydrotreating has similar effects on asphaltenes as thermal cracking does. The severity of the reaction controls the degree of changes. The most severe reaction condition, *i.e.*, high temperature and pressure and low space velocity causes hydrocracking and high conversion of asphaltenes. Aromaticity increases because alkyl chains are removed. Aromaticity is followed by a reduction of H/C atomic ratio that results from the removal of aliphatic carbons. Hydrotreating also significantly reduces the heteroelement content of asphaltenes (Speight, 2007; Ancheyta *et al*., 2009). These property changes will almost certainly alter the solubility of the asphaltenes. Hence, in order to model asphaltene precipitation from reacted streams, it is first necessary to determine the effect of the reaction on the asphaltene property distributions.

1.1 Objectives of this Thesis

The goal of this thesis is to determine the density, molecular weight, and solubility parameter distributions of highly reacted asphaltenes. The specific objectives are to:

1. fractionate asphaltenes from thermocracking and hydrocracking processes into solubility cuts by selective precipitation from solutions of toluene and *n*-heptane,
2. measure the molecular weight and density of the solubility cuts obtained in Objective 1,
3. reconstruct molecular weight and density distributions of the whole asphaltenes from the cut data using the Terminator/Propagator self-association model; represent the distributions with a Gamma function if possible,
4. measure the yield of asphaltenes precipitated from solutions of *n*-heptane and toluene,
5. calculate the asphaltene solubility parameter distribution from by modeling the yield data from Objective 4 with a regular solution based approach.

1.2 Thesis Structure

The thesis is organized into six chapters. Chapter 2 presents a background to petroleum chemistry with a focus on heavy oils and bitumen. The structure, composition, and self-association of asphaltenes are discussed. Both self-association and phase behavior modeling approaches are reviewed. Finally, oil refining processes and their effect on asphaltene properties are discussed.

Chapter 3 presents the experimental methods employed in this thesis including asphaltene extraction, determination of solids content, asphaltene fractionation, as well as molecular weight, density, refractive index, and asphaltene solubility measurements.

Chapter 4 describes the models used in this thesis. The self-association model which was developed by Agrawala and Yarranton (2001) is presented. This model is used later to determine the molecular weight distribution of cracked asphaltenes. The regular solution model from Akbarzedeh *et al*. (2005) is also presented including the gamma distribution function used to represent the asphaltene molecular weight distribution as well as molar volume and solubility parameter correlations for asphaltenes. This model is used later on to determine the asphaltene solubility parameter distribution.

Chapter 5 presents the density, molecular weight, and yield data and interpretation for all of the asphaltene samples characterized in this thesis. The methodology used by Barrera *et al.* (2012) to determine the molecular weight and density distributions is illustrated with a case study. The use of the regular solution model to determine solubility parameters is also demonstrated in this case study. Then, the density and molecular weight distributions for the reacted asphaltenes are discussed. Finally, the solubility modeling and solubility parameter distributions for these asphaltenes are presented.

Chapter 6 summarizes the findings of this thesis and provides some recommendations for possible future work.

Chapter Two: Literature Review

This chapter reviews concepts related to heavy crude oils, particularly asphaltenes. Petroleum chemistry is reviewed and the classification of oil based on physical properties is discussed. Asphaltenes are defined and their chemistry is reviewed. Asphaltene self-association behavior and modeling are described with a focus on the propagator/terminator model used in this thesis. Asphaltene phase behavior modeling is reviewed with a focus on the regular solution models used in this thesis. Finally, heavy oil refining and the effects of hydrotreating and thermal cracking on asphaltene properties are reviewed.

2.1 Petroleum Chemistry and Classification

Petroleum is a naturally occurring mixture of hydrocarbons that contains some sulfur, nitrogen, and oxygen-containing species as well as some metals. The exact composition differs according to the source of hydrocarbon (Speight, 2001, 2007), but the proportion of elements varies in a narrow range (Speight, 2007; Hammami and Ratulowski, 2007). Table 2.1 shows the elemental composition range. Petroleum can generally be found in liquid (crude oil) and gas (natural gas) states and, in this thesis, the focus is on crude oils, particularly heavy oils and bitumens.

Classification of crude oil is challenging because oils are ill-defined mixtures of hundreds of thousands of different molecular species. Attempts to classify crude oils based on their elemental analysis were not successful because mobile conventional oils were not distinguishable from heavy viscous petroleum. The usual methods to classify crude oils are divided based on: physical properties (*e.g.*, specific density, viscosity), molecular types (*e.g.*, paraffinic, aromatic,

naphthenic), recovery methods (preliminary, secondary, tertiary), and solubility class (amount of saturates, aromatics, resins, asphaltenes) (Speight, 2001, 2007). The classifications used for heavy oils are typically based on specific gravity or solubility classes.

Table 2.1. Elemental composition ranges of crude oil

Element	Composition, wt%
Carbon	83.0–87.0%
Hydrogen	10.0–14.0%
Oxygen	0.05–1.5%
Nitrogen	0.1–2.0%
Sulfur	0.05–6.0%

2.1.1 Petroleum Classification

Based on physical properties of oil, hydrocarbon resources are divided into three main groups: light oil, heavy oil, and extra heavy oil. Light (conventional) oils are liquid petroleums that flow freely at atmospheric conditions. They have a low viscosity, less than 100 mPa·s. The specific gravity of conventional oils is low because light hydrocarbon components are the dominant fractions, and, consequently, the API gravity is high, in the range of 20 to 35 °API. Light crudes produce more gasoline and diesel fuel than heavy oils during refining and, therefore, have a higher price in the energy market.

Heavy oils are very viscous and usually cannot be recovered from a reservoir under natural flow (Mai *et al*, 2006; Speight, 2001, 2007). Their viscosity is high, in the range of 100 to 10000 mPa.s. Enhanced oil recovery methods, such as preheating the reservoir and steam assisted techniques, are usually required for production from these reservoirs. Heavy oil API gravity ranges from 10 to 15 °API.

Bitumens are extra heavy oils and are defined as naturally occurring hydrocarbons with an API gravity less than 10 °API. The viscosity of bitumen typically ranges from 100,000 mPa.s to 1,000,000 mPa.s. Bitumen deposits are mined if near the surface or, if deeper than approximately 100 meters, require the application of thermal or solvent based enhanced oil recovery methods.

2.1.2 Heavy Oil Characterization

Since the composition of the feedstock plays an important role in refinery behavior, there have been many attempts to find ways to characterize petroleum in terms of compositional fractions. It is necessary that the molecular structure of the petroleum constituents not be altered during the separation process. The most common methods that meet this criterion are gas chromatography, distillation, and solubility based fractionation. It is not possible for one fractionation method to be utilized to fully separate the hydrocarbon components of oil, so several integrated techniques are often employed together.

Gas Chromatography

Gas chromatography is a separation method based on the retention time of petroleum constituents in a column which is packed with a solid of large surface area. Retention time is

used to identify the compounds (or carbon number distribution) in a mixture based on calibrations to standards. This retention times can also be correlated to boiling point to provide similar information as a distillation assay. Although gas chromatography is considered to be very practical in analyzing compounds with low molecular weight and high volatility, its use for characterizing heavy fluids is subjected to many limitations. First, the number of components in specific molecular weight range increases markedly due to the complexity of heavy oil while there are not major differences in physical properties of such complex species to differentiate them. Second, this technique is applied to compounds with boiling point range of -273 to 450 °C and therefore it is not applicable for heavy fractions due to their low volatility (Speight, 2007).

Distillation

Distillation is the most common method for the fractionation of petroleum. It was first used to produce kerosene and gradually became the main component of refineries (Jones and Pujado, 2008). Distillation is also used as a characterization method where the fluid is separated into a series of boiling cuts each representing a specific boiling range. The technique is based on the volatility of the components and therefore each cut does not necessarily correlate exactly to molecular weight or type. Nonetheless, the boiling point generally increases with increasing molecular weight.

Two common distillation methods are atmospheric pressure distillation and reduced pressure distillation. Atmospheric pressure distillation is suitable for fractionation of light oil where most of the lower boiling material can be separated from the petroleum. The method is not suitable for heavy oil or bitumen, which contain a high portion of higher boiling components, because little

of the oil is distilled. Since petroleum components decompose at temperatures above 350°C, increasing the upper temperature limit of the distillation is not an option. Instead, reduced pressure distillation is used to fractionate more of the higher boiling components (Speight, 2001, 2007; Robinson, 2006). For example, at 7 kPa, components with boiling range up to nearly 550°C (atmospheric pressure equivalent) are distilled.

Even with vacuum distillation, approximately 60 wt% of heavy oil cannot be fractionated and reports to the nonvolatile vacuum residue (Speight, 2007). The vacuum residue is concentrated in heteroelement constituents (*i.e.,* nitrogen, oxygen and metals) and hydrocarbons with dense aromatic rings (Reynolds and Speight, 1998; Mitchel *et al*., 1973). To characterize these materials, alternative methods have been developed. The most relevant methods for this thesis are solubility based techniques, in particular, SARA fractionation.

Solubility Based Fractionation

Solubility based methods fractionate heavy oils into different solubility classes based on the affinity of constituents of heavy oil to different solvents and adsorbents. SARA fractionation is the most frequently used technique in this category and divides heavy oils to saturates, aromatics, resins, and asphaltenes following the ASTM D2007M method.

Asphaltenes are a true solubility class and include all the materials that are insoluble in a paraffinic hydrocarbon (*i.e.*, *n*-pentane or *n*-heptane), but soluble in an aromatic hydrocarbon such as toluene or benzene. The remaining SAR (maltenes) fractions are adsorption classes. The saturate fraction corresponds to the non-polar material which is not adsorbed on polar adsorbents

and can be recovered with *n*-pentane as the initial eluent from a silica gel/attapulgus clay adsorption column. Aromatics are adsorbed on column packed with silica gel and are eluted by a mixture of *n*-pentane/toluene. Resins are adsorbed on a column of attapulgus clay and are eluted by a mixture of acetone/toluene. Details of SARA fractionation can be found elsewhere (Agrawala and Yarranton, 2001; Alboudwarej *et al*., 2003). This thesis focuses on asphaltenes extracted by *n*-heptane and the details of the experimental method are provided in Chapter 3.

2.2 Asphaltenes

2.2.1 Composition, Structure and Properties

Asphaltenes are brown to black friable solids that have no definite melting point and usually swell on heating to leave a carbonaceous residue (Speight, 2007). Asphaltenes consist of carbon, hydrogen, sulfur, nitrogen, oxygen and small traces of metals. In general, the hydrogen to carbon ratios of asphaltenes from different crude oils vary within a narrow range but notable variations can occur in heteroelement proportions. For instance, the H/C ratio of *n*-pentane extracted asphaltenes are typically 1.15 ±0.5%, while oxygen contents vary from 0.3% to 4.9%, sulfur contents vary from 0.3% to 10.3%, and nitrogen contents vary from 0.6% to 3.3% (Speight 2007). The elemental analysis of some Alberta bitumen asphaltenes are given in Table 2.2.

Table 2.2. Elemental composition of asphaltenes from Alberta bitumens (Speight, 1994)

Source	Atomic Ratio				Molecular Weight, g/mol
	H/C	N/C	O/C	S/C	
Peace River	1.23	0.011	0.017	0.036	7800
Athabasca	1,25	0.012	0.023	0.036	3850

The yield of asphaltenes depends on the solvent and experimental procedure used to precipitate them from a crude oil (Speight, 2007; Mitchell *et al.*, 1973) and the technique employed can also affect the amount of resins that co-precipitate with the asphaltenes. Hence, the elemental composition of asphaltenes precipitated with different solvents can vary; for example, the atomic ratio of hydrogen to carbon of the *n*-heptane asphaltenes is lower than its ratio in *n*-pentane asphaltene (Speight, 1994). This indicates a higher degree of aromaticity in the *n*-heptane precipitate. Nitrogen to carbon, oxygen to carbon and sulfur to carbon are usually higher using *n*-heptane as precipitant (Speight and Maschopedis, 1981). Therefore, it is necessary to specify the solvent and procedure used to obtain the asphaltenes in order to make meaningful interpretations and comparisons with other asphaltene data.

Most of the information available on the structural parameters and carbon skeleton of petroleum fractions and asphaltenes has been derived from spectroscopic studies of these fraction extracted from various petroleums. The data from these studies support the hypothesis that asphaltenes contain condensed polynuclear aromatic ring systems bearing alkyl side chains (Speight *et al*., 1972; Yen *et al*., 1972; Bandurski, 1982; Speight, 2007; Mullins, 1995). The heteroelements (*e.g.*, nitrogen, oxygen and sulfur) are scattered in various locations both within the ring structures and on the side chains. Mass spectroscopic investigations support the idea of occurrence of nitrogen in carbazole moieties (Clerc and O'Neal, 1961). Other studies of asphaltene structures by X-ray absorption near-edge structure (XANES) spectroscopy suggest that, nitrogen is present likely in pyrrolic forms rather than pyridinic types (Mitra-Kirtley *et al*., 1993). Infrared spectroscopy investigations support the idea of oxygen existence in carboxylic, ketone and phenol function locations (Speight and Maschopedis, 1981). Benzothiophenes and

dibenzothiophenes are the common forms of sulfur occurrence in asphaltene structures (Rose and Francisco, 1988; Keleman *et al*., 1990). Other forms such as alkyl-aryl sulfides rarely exist (Yen 1974). Nickel and vanadium has been suggested to be in porphyrins forms (Baker, 1969; Yen, 1975), but it is not well demonstrated if they can be considered as integral part of asphaltene systems or not. Both aromaticity and heteroelement content increase with increasing molecular weight of asphaltene fractions (Speight, 1994; Yen *et al.*, 1972).

Given the uncertainties in the structure of asphaltene molecules and the location of different functional groups in the ring systems, attributing a well-defined particular molecule structure that can represent all aspects of their physical and chemical properties is not possible. However, recent investigations have inferred two different structures, "continental" and "archipelago" type architectures, Figures 2.1 and 2.2, respectively. The continental architecture assumes asphaltene molecules are a relatively flat disk shape with a dominantly aromatic core (usually consisting of more than seven rings) and a periphery of aliphatic chains (Kuznicki *et al.*, 2008; Sheremata *et al.*, 2004; Mullins *et al*., 2007; Murgich, 2003). HNMR spectroscopy, X-ray diffraction and fluorescence depolarization support this interpretation (Yen *et al*., 1972; Sheremata *et al*., 2004). The archipelago structure represents asphaltene molecules with small aromatic groups (up to four rings) which are connected to each other by aliphatic chains with carbon numbers up to 24 (Zhang *et al*., 2007; Murgich *et al*., 2003). This structure is supported by thermal degradation, oxidation and angle neutron scattering (SANS) data (Strausz *et al*., 2002; Sheremata *et al*., 2004).

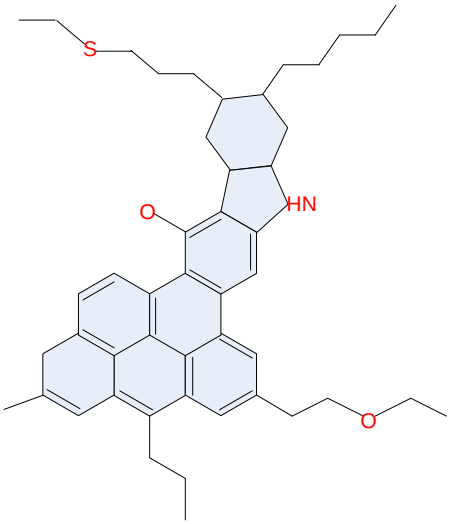

Figure 2.1. Continental model of asphaltene structure (adapted from Kuznicki *et al*., 2008)

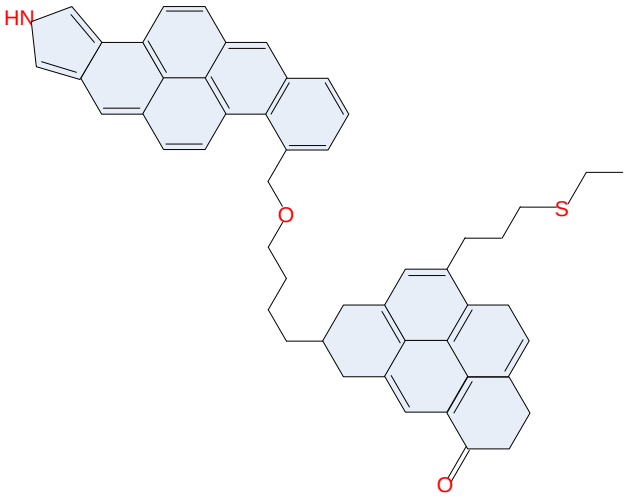

Figure 2.2. Archipelago model of asphaltene structure (adapted from Kuznicki *et al*., 2008)

Recent studies on asphaltene self-association mechanisms and asphaltene property distributions suggest that both structures are likely present. Components of petroleum asphaltene aggregate in petroleum, adhere to wide range of surfaces, occlude components that are porous to solvents and

moreover they are elastic. These properties can be justified only when a range of architectures are suggested that may occur simultaneously (Gray *et al*., 2011). Considering π-π stacking of aromatic rings as dominant force in association of asphaltene (continental structure) could be wrong since the formation of larger aggregates requires other interactions engaged with alkyl-aromatic structures (archipelago structures).

2.2.2 Molecular Weight and Self-Association

The measured molecular weights of asphaltenes range from a few hundred to a few hundred thousand $g \cdot mol^{-1}$, depending on the technique used. Vapor pressure osmometry (VPO) measurements show that the apparent molecular weight increases with increasing asphaltene concentration and decreases with increasing temperature (Moschopedis et al 1976; Yarranton *et al*., 2000; Wiehe, 1992). The changes in molecular weight are attributed to asphaltene self-association where the reported molecular weight corresponds to an average molecular weight of the asphaltene nano-aggregates. Calorimetric titration (Murgich *et al*., 2002; Merino-Garcia and Andersen 2005), small angle neutron scattering (Gawrys and Kilpatrich, 2005; Storm and Sheu, 1995), and interfacial tension measurement (Yarranton *et al*., 2000; Rogel, 2000) confirm self-association in asphaltenes.

Asphaltenes molecular weight measured from different methods and sources provide a consistent average monomer molecular weight of approximately 1000 g/mol (Yarranton *et al*., 2000; Qian *et al*., 2007; Guzman *et al*., 2009; McKenna *et al*., 2010; Mullins *et al*., 2012). For example, molecular weights from VPO suggest monomer molecular weights of 1000 to 2000 g/mol

(Barrera *et al*., 2013; Moschopedis *et al*., 1976). Fluorescence depolarization (FD) gives asphaltene molecular weights between 500 to 1000 $g \cdot mol^{-1}$ (Groenzin and Mullins, 2000). Diffusion measurements such as Taylor dispersion, nuclear magnetic resonance (NMR) and fluorescence correlation spectroscopy are consistent with FD data (Wargadalam *et al*., 2002; Frees *et al*., 2007; Andrews *et al*., 2006; Schneider *et al*., 2007).

VPO measurements indicate average nonaaggregate molecular weights of 5,000 to 10,000 g/mol with a range of molecular weights exceeding 30000 g/mol. The VPO data are in good agreement with those measured by gel permeation chromatography (GPC) and molecular film methods (Peramanu *et al*., 1999; Guzman *et al*., 2009; Strausz *et al*., 2002). GPC has the advantage of not being limited by the low vapor pressure of asphaltenes; however, the results obtained from this method can be affected by asphaltene adsorption which can cause calibration error for higher molecular weights (Speight, 2001). Recent time-of-flight data for nanoaggregate molecular weight are consistent with VPO measurments (McKenna *at al*., 2013). On the other hand observed molecular weight of aggregates from combination of ultracentrifugation and X-ray scattering measurements are an order of magnitude larger than VPO results (Eyssautier *et al*., 2012).

The mechanisms for asphaltene association may include: π-π bond interactions (stacking), formation of charge transfer molecules (Speight *et al*., 1994; Yen, 1974; Gray *et al*, 2011), acid-base interactions, hydrogen bonding between functional groups such as: hydroxyls and carboxylic acids with weak nitrogen bases, Vanadium and nickel contribution through axial

coordination to bases, and association of polar and alkyl groups in hydrophobic pockets driven by Van der Waals forces (Gray *et al*., 2011)

2.2.3 Self-Association Models

Different views of asphaltene structure and self-association mechanisms have led to different self-association concepts including reverse micellization, colloids, and olimerization. Models for each concept are discussed below.

2.2.3.1 Reverse Micellar Self-Association Model

Asphaltenes resemble surfactants in that they consist of a hydrocarbon skeleton with polar functional groups distributed throughout the structure. Like surfactants, they are surface active and are known to stabilize water-in-oil emulsions. Surfactants are known to self-aggregate at sufficient concentration. The aggregates found in the aqueous phase are termed micelles and are structured so that the hydrocarbon parts of the surfactants are concentrated in the center of the aggregate away from the water phase while the polar groups are concentrated at the surface of the micelle. The equivalent aggregates in an organic phase have the reverse structure and are termed reverse micelles. Here, the polar, hydrophobic, groups of the surfactants aggregate together in a core and the nonpolar, hydrophilic, tails are extended away from the center. The concentration at which micelles appear is termed the critical micelle concentration (CMC).

The CMC is determined experimentally as a change in the slope of a plot of surface tension against surfactant concentration (Friberg 2007). At low surfactant concentrations, surfactant exists as monomers in aqueous solution and at the surface. Once an air/water or oil/water

interface is saturated with surfactant, the surface tension decreases linearly with the log of surfactant concentration. However, at the CMC, the excess surfactant now forms micelles and the surfactant monomer concentration changes little. The micelles are not surface active, and therefore, surface tension remains constant above the CMC.

It has been hypothesized that asphaltene aggregates are reverse micelles (Sachanen, 1945). However, it has been shown that the asphaltenes do not exhibit a CMC (Yarranton *et al*., 2000). Both vapour pressure osmometry molecular weight and isothermal titration calorimetry data showed that the aggregation number of asphaltenes (5 to 10 molecules per aggregate) was too small for the segregation of polar and non-polar groups that define a micelle (Yarranton *et al*., 2000; Merino-Garcia, 2007). These data also did not show the abrupt change in aggregate size expected at a CMC, or even a change in slope as might be expected with mixed surfactants, but rather were consistent with stepwise association (Merino-Garcia, 2007). Size exclusion chromatography experiments also showed asphaltene association in concentrations lower than typical CMCs (Andersen, 1994).

2.2.3.2 Colloidal Self-Association Model

The colloidal self-association model assumes that asphaltene molecules are primarily continental structures each consisting of primarily of a condensed aromatic sheet. It is hypothesized that these sheets form colloidal stacks held together by π-π bonds. The stacks are expected to aggregate strongly if exposed but are stabilized as suspended colloids by resins adsorbed on the surface of the colloid (Yen *et al*., 1967; Mullins *et al*., 2007).

The colloidal model arose from x-ray crystallography experiments where π-π bonding was observed between aromatic sheets in dry asphaltenes separated from the source oil. Small-angle x-ray scattering and small-angle neutron scattering support the colloidal model and suggest spherical or disk-shape particles dispersed in crude oils (Ravey *et al*., 1988; Carnahan *et al*., 1993).

A variant of the colloidal model is similar to the reverse micelle model but is not driven by hydrophobic/hydrophilic interactions (Merino-Garcia et al., 2004; Sachanen, 1945). Instead, it is hypothesized that the polynuclear aromatic groups of asphaltenes, which have very strong interactions and low solubility in nonpolar aliphatic compounds, might sequestrate in the core while aliphatic chains surround these stacks. Any forces from outside that disturb these balanced interactions will cause to aggregation of the asphaltene molecule which leads to precipitation (Friberg, 2007).

The colloidal structure is linked with a colloidal model of asphaltene precipitation. Short range intermolecular repulsive forces between resins are believed to prevent flocculation of asphaltene particles (Leontaritis and Mansoori, 1987). Any factor that disturbs the equilibrium of the colloidal system can lead to desorption of resins and consequently can cause asphaltene precipitation. Compositional, pressure, and temperature changes can stimulate precipitation of asphaltene molecules (Leontaritis and Mansoori, 1987; Hammami *et al*., 2007). For example, addition of an *n*-alkane to a crude oil can desorb resins and re-established equilibrium can be achieved by reduction in the free surface energy of asphaltene by flocculation (Hemmami *et al*., 2007).

The colloidal models cannot explain the effect of solvents like toluene on asphaltene association and precipitation. Asphaltenes in toluene self-associate but only to a limited extent. Since resins are completely soluble in toluene, they would be stripped from the asphaltenes leading extensive aggregation and precipitation which is not observed (Agrawala and Yarranton, 2001). The alternative is that toluene stabilizes the aggregates but this effect is not consistent with the concentration dependence of asphaltene association. In addition, the colloidal model predicts that asphaltene precipitation is irreversible while other studies have proven reversibility of asphaltene precipitations (Hammami *et al*., 1999; Hirschberg *et al*., 1984). The most successful models for asphaltene association are thermodynamic models which treat asphaltenes as any other component in a solution. Therefore, the colloidal model is not considered further in this thesis.

2.2.3.3 Supramolecular Self-Association Model

Measured molecular weights of asphaltenes by vapor pressure osmometry in toluene and o-dichlorobenzene showed that increasing the asphaltene concentration in a solvent increased asphaltene self-association until a limiting value was reached (Yarranton *et al*., 2000). This step-wise aggregation resembles polymerization reactions and therefore asphaltene self-association was modeled analogously to linear polymerization (Agrawala and Yarranton 2001; Murgich *et al*., 2002; Merino-Garcia 2004). In this model resins are not considered a peptizing agent adsorbed on the surface of asphaltene, but are assumed to be part of polymer-like aggregates which consist of asphaltene and resin molecules. Aggregates are held together by dispersion forces rather than covalent forces.

This aggregation modeling originated from chemical equilibrium theory (Martin, 1996) that assumes all formed molecular aggregates and monomers are in equilibrium. The equilibrium equation in this process is defined as:

$$P_n + P_1 \leftrightarrow P_{n+1} \quad \Rightarrow \quad [P_{n+1}] = K_{n+1}[P_1][P_n] \tag{2.1}$$

where n is the number of the monomers in aggregate and K_n is the equilibrium constant of n^{th} reaction. The reaction is considered to be first order with respect to both propagating and aggregated molecules.

The simplest step-wise association model is based on dimer (P_2) formation and was employed by Murgich *et al*. (2002) to fit data from calorimetric measurements. They used just one *K* value. The next level of complexity, the "Equal K" approach, allows the formation of components with higher aggregation numbers but assumes that the *K* value is constant for all of the equations (Agrawala and Yarranton, 2001; Merino-Garcia *et al*., 2007). Finally, it can be assumed that the *K* value decrease as aggregates become larger and growth becomes sterically hindered; the "Attenuated K" approach (Martin, 1996; Agrawala and Yarranton, 2001; Merino-Garcia *et al*., 2007).

In all three of the above models, it is assumed that there is just one type of monomer molecule with the capability of forming aggregates. Agrawala and Yarranton (2001) posed two types of monomer, "propagators" and "terminators." Propagators, *P*, have two active sites and can link to other molecules to make larger aggregates, while terminators, *T*, have only one active site and when they link to aggregates the aggregate stops growing. This model has an additional fitting parameter, the initial ratio of terminator to propagator momoners, $(T/P)_0$. The stepwise modeling

approach can fit molecular weight data using less parameters rather than the colloidal models and has the advantage that it can be linked with thermodynamic models to predict the molar mass and solubility parameter distributions (Agrawala and Yarranton, 2001).

2.3 Asphaltene Precipitation

Asphaltenes can precipitate upon changes in temperature, pressure, and composition. At ambient conditions, they precipitate as approximately micron sized particles which tend to flocculate and settle (Hammami *et al*., 2000; Andersen, 1999). At temperatures above 120°C, they appear to separate as a continuous liquid phase (Johnston, 2013). As noted previously, colloidal models attribute precipitation to the disruption of a layer of adsorbed resins. Thermodynamic models are consistent with the oligomer view of asphaltene association and assume that asphaltenes are part of a molecular solution which can undergo a conventional solid-liquid or liquid-liquid phase transition to form an asphaltene-rich phase. Thermodynamic models for asphaltene precipitation are generally based on either regular solution theory (Alboudwarej *et al*., 2003; Akbarzadeh *et al*., 2004; Andersen and Speight, 1999; Wang and Buckley, 2001) or equation of state models (Vargas *et al*., 2009; Gonzalez *et al*., 2007). Regular solution theory was used in this thesis and is discussed below.

Thermodynamic models equate the fugacity of each component in each phase. In regular solution models, fugacity is related to the liquid phase activity coefficient which, in turn, is related to solubility parameters via an enthalpy of mixing derivation (Hildebrand and Scott, 1949). Modified regular solution models include an entropy of mixing term for molecules of different

size (Flory, 1942; Huggins, 1941). The combined expression for the activity coefficient is given by:

$$\ln \gamma_i^L = \ln \frac{v_i^L}{v_m^L} + 1 - \frac{v_i^L}{v_m^L} + \frac{v_i^L}{RT}\left(\delta_i - \delta_m\right)^2 \qquad (2.2)$$

where γ is the activity coefficient, v is the molar volume, δ is the solubility parameter of component i, T is temperature, and R is the universal gas constant.

Regular solution base models were first applied to predict asphaltene precipitation from crude oils by Hirschberg *et al*. (1984). They assumed asphaltene to be a single component with a single molar volume and solubility parameter. A vapor-liquid equilibrium (VLE) using the Soave equation of state was first solved to estimate the composition of the liquid. Then liquid-liquid calculations were performed with this assumption that precipitated asphaltenes have no effect on the previous VLE calculations (Hirschberg *et al*., 1984). This model fitted the onset of asphaltene precipitation but was not very successful in reproducing the amount of precipitated asphaltenes.

Kawanaka *et al*. (1991) treated asphaltenes as polydisperse polymers with a range of molar mass and solubility parameters rather than as a uniform component. They utilized the Scott and Magat heterogeneous polymer solution theory to formulate a continuous-mixture model to predict the onset point of asphaltene precipitation and amount of organic deposition from petroleum crude oil (Scott *et al*., 1945; Kawanaka *et al*., 1991). To predict asphaltene deposition, they assumed solid-liquid equilibrium and proposed a gamma distribution as a representative molar mass distribution of asphaltene molecules.

Yarranton and Masliyah (1996) also represented the self-associated asphaltenes as heterogeneous polydisperse polymers which have a molar mass and density distribution. They divided asphaltenes into different solubility cuts by selective precipitation in different ratios of *n*-hexane and toluene. They confirmed that the less soluble asphaltenes were the more polar and dense components. They then correlated molar volumes and solubility parameters to the apparent molecular weight of the associated asphaltenes. Alboudwarej *et al*. (2003) extended Yarranton and Masliyah's model to asphaltene precipitation from Western Canadian heavy oils at ambient conditions. They performed a liquid-liquid flash calculation based on with mole fractions, molar volumes, and solubility parameters as the input to the model. It was assumed that self-association was not altered when the composition changed, for example, with solvent dilution of a bitumen. Akbarzadeh *et al*. (2005) generalized the model to the samples from around the globe at different temperatures and pressures. More recently, Barrera *et al*. (2013) successfully modeled asphaltene precipitation form mildly reacted bitumen using the same methodology.

2.4 Oil Refining

Oil refining includes all the processes that convert petroleum to valuable products. These marketable products differ in terms of their boiling point ranges. Usually, lower boiling point fractions are considered to be more valuable than the higher boiling fractions (Speight, 2007). Refineries generally have three major products: gas and gasoline, naphtha, and fuel- and gas-oils. Gasoline is derived from the lowest boiling point cuts and is a major fuel source. Naphtha can be produced from both lower and middle boiling point cuts and is used as a precursor in gasoline products. Kerosene, distillate fuel oil, light gas-oil, waxy distillate, and lower boiling lubricant

oils are products from the middle boiling range. The remaining highest boiling cuts include higher boiling lubricant oils and the nonvolatile residuum (Speight, 2007).

Generally, the lower boiling products are readily produced from conventional crude oils by distillation. However, with the increasing production of heavy oil and bitumen, more complex refinery processes are required. The refinery processes used to upgrade and refine bitumen are described below.

2.4.1 Thermal Cracking

Thermal processes include all operations that break, rearrange, and/or combine heavy hydrocarbon molecules by application of heat (Speight, 2007; Parkash, 2003). Thermal cracking is one of the preliminary conversion processes used to decompose high molecular weight species into fractions of various size. Thermal cracking is used to produce gasoline, reduce the crude oil viscosity, and to remove the heaviest oil components as coke (Speight, 2007; Haslego 2010). The typical pressure range used in most thermal cracking processes is between 690 and 6900 kPa and the temperature range varies from 455 °C to 540 °C (Speight, 2007). The feedstock is usually the residuum from atmospheric or vacuum distillation processes (Haslego, 2010; Parkash, 2003).

2.4.2 Vis-Breaking

Vis-breaking was first introduced in the late 1940's as a mild thermal cracking process to reduce the viscosity of residua to achieve desired product specifications (Meyers, 2004, Speight, 2007). The vis-broken residua are blended with lighter product oils to obtain fuel oils that meet target viscosity specifications. The lower the viscosity of the residuum, the less light oil required to

meet the fuel oil specifications. Fuel oil is the main product of vis-broking operations, but some material in the gasoline gas-oil boiling ranges are also produced (Leffler, 2008; Meyers, 2004). Typical operational conditions for vis-breaking processes are temperatures from 470 °C to 495 °C and pressures from 350 kPa to 1380 kPa. Low residence times are imposed to prevent coke formation (Speight, 2007).

2.4.3 Hydrogenation

Hydrogen can be added to thermal processes both to convert higher molecular weight material to liquid fuels and to transform material with less economic value to highly valuable products. There are two main types of hydrogenation processes: hydrocracking (destructive) and hydrotreating (non-destructive), (Speight, 2007). Hydrocracking processes involve both the breaking of carbon-carbon bonds and the addition of hydrogen to saturate ring structures. Hydrocracked products have significantly lower boiling ranges than the feed (Jones and Pujado, 2008). Hydrotreating involves adding hydrogen to remove heteroatoms and saturate hydrocarbons. Hydrotreated products have a similar boiling range to the feed but provide more of the most valuable distillation cuts. Each process is explained in more detail below.

2.4.3.1 Hydrotreating

Hydrotreating is a catalytic process that removes contaminants from liquid petroleum fractions and upgrades the feedstock with hydrogen at temperatures and pressures where thermal cracking is minimized (Speight, 2007; Jones and Pujado, 2008). The reactions that take place in these processes are mainly hydrodesulfurization, hydrodenitrogenation and hydrodemetallation (Speight, 2007). Sulfur, nitrogen, oxygen, and metals are the most troublesome impurities and

can deactivate catalysts, contaminate products, and accelerate corrosion in downstream equipment. Hydrotreating will remove nearly 90% of these impurities (Robinson, 2006). Hydrotreating also saturates most olefins and converts many aromatics to naphthenes (Robinson, 2006; Speight, 2007). Other objectives of hydrotreating processes are: gasoline treatment to meet sulfur specifications, kerosene hydrotreating to produce cleaner-burning jet fuel, and lube hydrotreating to improve color and odor (Meyers, 2004; Robinson, 2006).

Hydrogen partial pressure starts from 1.3 MPa if the feedstock is naphtha or diesel fuel and can go up to nearly 13 MPa for residual oil feedstock (Robinson, 2006). Operational temperature range falls between 340 to 380 °C. The conversion factor for hydrotreating is quite low and falls in the range of 5% to 15%.

2.4.3.2 Hydrocracking

The major difference between hydrocracking and hydrotreating is the greater extent of conversion in hydrocracking. Hydrocracking is a more recently developed process compared to the thermal cracking or vis-breaking and arose in response heavier refinery feedstocks with lower hydrogen to carbon atomic ratios than conventional oils. Typical objectives of hydrocracking are to:

- maximize production of naphtha
- produce of middle distillate fuels with higher hydrogen content
- produce ultra-clean lube base stocks
- produce olefin plant feeds (Robinson, 2006)

Feeds of hydrocracking processes are mostly atmospheric or vacuum gas oils from crude distillation units, heavy or light gas oil from delayed cokers or vis-breakers, and cycle oils (light and heavy) from FCC (Fluid Catalytic Cracking) units. Hydrocracking is more severe than hydrotreating in order to produce lower boiling product not just remove impurities (Speight, 2007). Operating temperatures of hydrocracking are about 370 to 400 °C with hydrogen partial pressures ranging from 13 to 20 MPa depending on the feedstock type (Speight, 2007; Robinson, 2006). These severe conditions lead to higher conversion of feedstock (*i.e.*, 60 to 90%).

2.5 Effect of Processing on Asphaltene Properties

Asphaltenes are the most problematic portion of the heavy oils and can cause many issues in the refining of crude oils including: 1) the reduction of the overall rates of hydrotreating reactions; 2) the deactivation of catalysts by depositing on their surface; 3) increased coke formation (coke precursor). Generally, asphaltene precipitation can limit the ultimate level of conversion (Ancheyta *et al*., 2003; Callejas and Martinez, 2000).

Understanding asphaltene behavior during and after hydrotreating and thermal cracking processes requires their characterization since the process alters asphaltene properties. Observations on asphaltene properties after hydrogenation and thermal processing are summarized below.

Hydrogenation

Seki and Kumata (2000) investigated Kuwait asphaltene and resins properties after hydrotreating and found that their molecular weight decreased gradually through the process. They observed

that asphaltenes became more polydispersed as the temperature of the process increased. They also observed a steep increase in aromaticity of the asphaltenes around 400°C and attributed this change to the shortening of alkyl side chains. They also found that the quality, not quantity, of asphaltene plays the most important role in coke deactivation.

Merdrignac *et al*. (2002) observed that with increasing of the severity of the hydroconversion, a general decrease occurred on the molecular size of asphaltenes. Based on size exclusion chromatography, they also concluded that this shift toward to lower molecular mass was the consequence of dealkylation of side alkyl chains during the hydrogenation process. They concluded that the likelihood of conversion of higher mass molecules was high and that the change in the low/high molecular weight peak proportion indicated that structural changes of asphaltenes occur on conversion. Merdrignac *et al*. (2006) further investigated the evolution of asphaltenes under hydroconversion conditions. They showed that, as the conversion increased, asphaltene unit size decreased and the aromaticity of the asphaltene molecules increased due to dealkylation.

Bartholdy and Andersen (1999) showed that around 380°C, hydrocracking reactions dominated hydrogenation reaction mechanisms. They observed that the H/C ratio of the asphaltene was reduced as the temperature of the hydrogenation reaction increased. Buch *et al*. (2003) analyzed high temperature hydrotreated samples by fluorescence depolarization techniques and showed that the cracking of alkane side chains resulted in a reduction of size of the fused ring systems. Therefore, they observed compacted asphaltene molecules remained after hydrotreatment with significant reduction in their molecular size. A portion of the asphaltenes was converted to the

resin type material soluble in heptane which they assumed to be due to structure changes from the hydrogenation.

Ancheyta *et al*. (2003) characterized Maya crude oil and its hydrocracked products and showed that precipitated asphaltenes exhibited changes in composition during catalytic hydrotreating. The severity of the reaction played a key role on these alterations. Significant changes occurred on the structural properties of asphaltenes at 440°C. Nitrogen and metals content increased whereas sulfur content decreased as the reaction temperature was increased. The H/C atomic ratio of the asphaltenes decreased as the reaction temperature increased, indicating that their aromaticity increased.

Thermocracking

Lababidi *et al*. (2013) studied asphaltene property changes during thermal processes. They did metal and element content analysis and gel permeation chromatography experiments to characterize asphaltene molecules and found that asphaltene molecular size decreased and the H/S ratio decreased as the severity of the reaction increased. However, the aromaticity and metal content increased with the severity of the reaction.

A general observation is that cracking processes tend to decrease the size of the asphaltene molecules. Both hydrogenation and thermocracking processes increase asphaltene aromaticity.

Chapter Three: Experimental Methods

In this chapter, the experimental techniques used in this thesis are presented, including asphaltene extraction, determination of solids content, asphaltene fractionation, as well as molecular weight, density, refractive index, and asphaltene solubility measurements.

3.1 Materials

Seven reacted heavy oil samples and their two feedstocks were characterized in this thesis, Table 3.1. Three samples (X series) came from a thermal-cracking pilot process and their feedstock was a Western Canadian bitumen vacuum bottoms (WCB-VB). One hydrocracked sample (HOS) was also generated from this feedstock in a commercial process. Three samples were obtained from a hydrocracking pilot process (RHC series) and their feedstock was the short residue. All samples were provided by Shell Global Solutions.

Table 3.1. Oil samples used in this thesis.

Sample	Description
WCB-VB	Distillation Tower Vacuum Bottoms
X-1357	Thermal-Cracked
X-1359	Thermal-Cracked
X-1360	Thermal-Cracked
HOS	Hydrocracked
Short Residue	Distillation Tower
RHC-18-37	Hydrocracked
RHC-18-19	Hydrocracked
RHC-19-03	Hydrocracked

n-Heptane and toluene were ACS grade solvent purchased from VWR International LLC and were used in precipitation, solids removal, solubility measurements, and asphaltene fractionations. Asphaltene molecular weight measurements were performed with Omnisolve high purity toluene (99.99%) also obtained from VWR. Sucrose octaacetate (98%), octacosane (99%) and polystyrene standard (99%) were purchased from Sigma-Aldrich Chemical Company.

3.2 Asphaltene Preparation and Fractionation

3.2.1 Bulk Precipitation

To recover asphaltenes from an oil sample. *n*-heptane was added to 40 g of the oil sample at a ratio of 40:1 volume (mL)/weight (g) and sonicated for 60 minutes. After 24 hours of total contact the mixture was filtered through a grade #2 Whatman filter until 350 to 400 ml of solution remained in the beaker. 160 ml (10% of initial solvent volume) of *n*-heptane was added to this mixture and the solution was sonicated for 45 minutes and left to settle for 18 hours. Then the solution was filtered through the same filter. These asphaltenes were designated as C7-Asphaltenes.

The filter cake collected on the filter paper was washed at least 3 times per day for five days with *n*-heptane until the supernatant was colorless. Filter papers were placed in a fume hood for one week to dry until a constant weight was achieved. Recoveries of C7-Asphaltenes+Solids were calculated. The solids included inorganic material such as sand and clay, and also organic material which was insoluble in toluene. Separation of the solids is explained in detail in Section 3.2.2.

The filtrate contained deasphalted oil (maltenes) plus *n*-heptane. A rotary evaporator was used to recover *n*-heptane from the maltenes. The maltenes were collected in a jar and set to dry in a vacuum until a constant weight was achieved. The maltenes were not used in this thesis but were used in a related project.

Note, some of the highly reacted samples were solid or semi-solid at ambient conditions and were preheated in a vacuum oven for at least 24 hours to facilitate sampling and mixing. In the worst case, the temperature required for melting was as high as 120°C. We assumed that the properties of samples did not change because 120°C is well below the cracking temperature.

3.2.2 Solids Removal

The asphaltenes recovered from bulk precipitation contained organic solids such as coke, and inorganic solids such as sand, clay, ash, and small amounts of minerals, all of which are insoluble in toluene (Mitchell *et al*., 1973). These solids precipitate along with the asphaltenes without affecting the onset of the precipitation (Albouldwarej *et al*., 2003).

Solids were removed from the asphaltenes with the following procedure. 200 mL of toluene was added to two grams of asphaltene (with solids) to make a 10 kg/m^3 solution. The mixture was dissolved in an ultrasonic bath for 20 minutes and put aside to settle for 60 minutes. The solution was divided into centrifuge tubes and centrifuged at 4000 RPM for 6 minutes. The supernatant (solids-free asphaltene solution) was decanted into small beakers through a Grade #42 Whatman filter paper and the solids were collected in the bottom of the centrifuge tubes. The beakers and

tubes were placed in a 60°C vacuum oven for at least two days to evaporate the toluene. The dried weights of each were recorded and the solids content was calculated gravimetrically.

3.2.3 Asphaltene Solubility Tests

Solubility curves, or fractional yields of asphaltenes, are plots of the percentage of precipitated asphaltenes versus the mass fraction of *n*-heptane in solutions of *n*-heptane and toluene (heptol). This procedure has been described previously [Alboudwarej *et al*., 2003] and is summarized here. A fixed amount of solids-free C7-Asphaltenes (approximately 0.15 grams) was measured into a 30 ml vial. The desired mass of toluene was added to the asphaltenes. This mixture was placed in ultrasonic bath for 20 minutes to dissolve the asphaltenes. The required amount of *n*-heptane was then added to each vial, to obtain a 10 kg/m^3 solution at the specified heptane:toluene ratio, The mixture was then sonicated for an additional 45 minutes. After 24 hours settling, the solutions were centrifuged at 4000 RPM for 5 minutes to separate precipitated asphaltenes from the mixture. Supernatant was decanted and the solids left in the vial were washed with the same heptol mixture several times until a colorless supernatant was observed. The vials were placed in vacuum oven at 60 °C for two days to dry and then weighed and the precipitate yield determined.

3.2.4 Asphaltene Fractionation

Asphaltene fractionation was performed by dissolving asphaltenes in toluene and then adding heptane at a ratio of *n*-heptane:toluene designed to precipitate only some of the asphaltenes [Barrera *et al*., 2013]. The precipitated (insoluble) asphaltenes are referred to as a Heavy Cut and the soluble asphaltenes at the same ratio are termed the Light Cut. For convenience, the Heavy

Cuts are described as “H##H” where “HXX” specifies the heptane mass fraction in the solution and the final “H” specifies the Heavy Cut. Similarly, the light cut was designated “H##L” where L is the Light Cut.

To start a fractionation, clean vials were weighed and 0.3 grams of solids-free asphaltene was added to each. Toluene was combined with the asphaltenes and the mixture was placed in an ultrasonic bath for 20 minutes until the asphaltenes were dissolved. The corresponding volume of heptane according to the desired heptol ratio was added and then the whole mixture was sonicated for 45 minutes. After 24 hours settling, the vials were centrifuged at 4000 RPM for 5 minutes to separate the precipitate from the solution. The supernatant was decanted to a beaker and set aside. The precipitate (Heavy Cut) was washed with the same heptol ratio until a colorless solution was obtained and then placed in a 60°C vacuum oven for two days to dry. The supernatant plus washings were then placed in a fume hood to evaporate the heptol, The residue is the Light Cut.

3.3 Property Measurements

3.3.1 Molecular Weight Measurements

Molecular weights were determined with vapor pressure osmometry. This technique is based on the difference between vapor pressure of a solute-solvent mixture and the pure solvent. The VPO consists of a cell which is saturated with the solvent vapor and two thermistors placed in this chamber. When droplets of pure solvent are placed on both thermistors there is no temperature change and thus no voltage difference. However, when pure solvent is injected on top of one thermistor and solvent contaminated by a solute is injected onto the second, the vapor pressure

difference generates a temperature change and thus a resistance (or voltage) difference. The molecular weight of a solute (M_2) is related to voltage as follows (Goldfarb and Meeks, 1966*):*

$$\frac{\Delta E}{C_2} = K(\frac{1}{M_2} + A_1 C_2 + A_2 C_2^2) \quad (3.1)$$

where ΔE is the voltage difference the two thermistors, C_2 is the solute concentration (g/l), K is the instrument constant, and A_1 and A_2 are non-ideality constants.

The constant, K, is determined from the calibration of the VPO. A calibration material is chosen which produces nearly ideal solutions with the solvent in low concentrations so that the most of higher order terms in Equation 3.1 become negligible:

$$\frac{\Delta E}{C_2} = K(\frac{1}{M_2} + A_1 C_2) \quad (3.2)$$

K is then determined by extrapolation in a plot of $\Delta E/C_2$ versus C_2 to zero concentration.

Once K is fixed, Equation 3.2 is solved to determine the molecular weight of any unknown substance. For non-ideal mixtures, the molecular weight of the solute is calculated from the intercept of the plot of $\Delta E/C_2$ versus C_2. For ideal solutions, the coefficient A_1 value is zero and the M_2 is calculated as follows:

$$M_2 = \frac{K}{\frac{\Delta E}{C_2}} \quad (3.3)$$

Asphaltene molecules in solution (for example with toluene) self-associate. As the asphaltene concentration in toluene increases, higher apparent molecular weights are observed (Agrawala and Yarranton, 2001). Hence, it is not possible to confirm that asphaltene molecules form ideal

solutions with solvents or non-ideal mixtures. However, Sanchez (2012) examined the non-ideality of solutions made from distillation cuts (*i.e.,* boiling point ranges) and toluene. The lower boiling fractions, which include more aliphatic and paraffinic constituents, formed non-ideal solutions in toluene. The higher boiling fractions, which contain mainly aromatic components, formed nearly ideal solutions. In addition, aromatic and resin solubility fractions also appear to form nearly ideal solutions in toluene (Agrawala *et al*., 2001, Yarranton *et al*., 2007, Okafor 2013). Asphaltenes are the most aromatic portion of the crude oil and therefore, in this thesis, it is assumed that asphaltene forms ideal solution in both toluene and 1,3-dichlorobenzene.

A Jupiter Model 833 Vapor Pressure Osmometer (VPO) was used to measure the molecular weight of asphaltenes. Toluene and 1,3-dichlorobenzene were used as solvents. The operating temperature was 50°C for toluene and 110°C for dichlorobenzene. The VPO has a detection limit of $5x10^{-5}$ mol/L when used with toluene or chloroform [VPO manual]. During the measurements, slight variations in voltage readings were observed due to local temperature and atmospheric pressure changes, thus a minimum five times of readings at each condition were taken to minimize fluctuation errors. Instrument calibration was done using sucrose octaacetate (679 g/mol) and octacosane and polystrene were used as standards to determine the instrument constant, *K*. The measured molecular weight of octacosane was within 5% of the correct value. The repeatability of the molecular weight measurements was approximately 15% for all samples.

3.3.2 Density Measurements

Asphaltenes are solids at ambient conditions and their liquid density cannot be measured directly. Instead, the asphaltene densities were determined indirectly from the densities of a series of solutions of asphaltenes in toluene at different concentrations. If the solutions are regular at low asphaltene concentrations, the density of the solution is related to the density of its constituents as follows:

$$\frac{1}{\rho_M} = \frac{1}{\rho_T} + (\frac{1}{\rho_A} - \frac{1}{\rho_T})w_A \tag{3.4}$$

where ρ_M, ρ_T and ρ_A are the mixture, toluene and asphaltene density (kg/m^3), respectively, and w_A is the asphaltene mass fraction. When the specific volume of the mixture is plotted versus asphaltene mass fraction, the asphaltene density is calculated as follows:

$$\frac{1}{\rho_M} = b + aw_A \tag{3.5}$$

$$b = \frac{1}{\rho_T} \tag{3.6}$$

$$a = (\frac{1}{\rho_A} - \frac{1}{\rho_T}) \tag{3.7}$$

$$\rho_A = \frac{1}{a+b} \tag{3.8}$$

where *a* is the slope and *b* is the intercept of the plot.

Solutions of asphaltene in toluene at concentrations up to an asphaltene mass fraction of 6.5% were prepared, as described previously. The densities of these solutions were measured with an Anton Paar Density meter at 20 °C and atmospheric pressure. The precision of the measurement was 0.0001 g/cm^3. The main source of experimental error is the accuracy of the dilution. Serial

dilutions were repeated at least two times for a number of samples to estimate the error. The repeatability of asphaltene densities was found to be 13.4 kg/m^3.

The validity of the assumption of regular solution behavior to asphaltene-toluene mixtures may be a source of error. The limited solubility of asphaltenes limits the measurements to low concentrations. At these concentrations, the densities of irregular and regular solutions are indistinguishable, but the ultimate value of density calculated by each assumption can be noticeably different, Figure 3.1. The density of an irregular solution can be determined by adding an excess volume of mixing term to the mixing rule as follows:

$$\frac{1}{\rho_M} = \frac{w_T}{\rho_T} + \frac{w_A}{\rho_A} + w_A w_T \left(\frac{1}{\rho_A} - \frac{1}{\rho_T}\right)\beta_{AT} \tag{3.9}$$

where w_T is the mass fraction of toluene, and β_{AT} is the binary interaction coefficient between the asphaltenes and toluene. This last term in Equation 3.9 is the excess volume of mixing. The choice of mixing rule is examined further in Chapter 5.

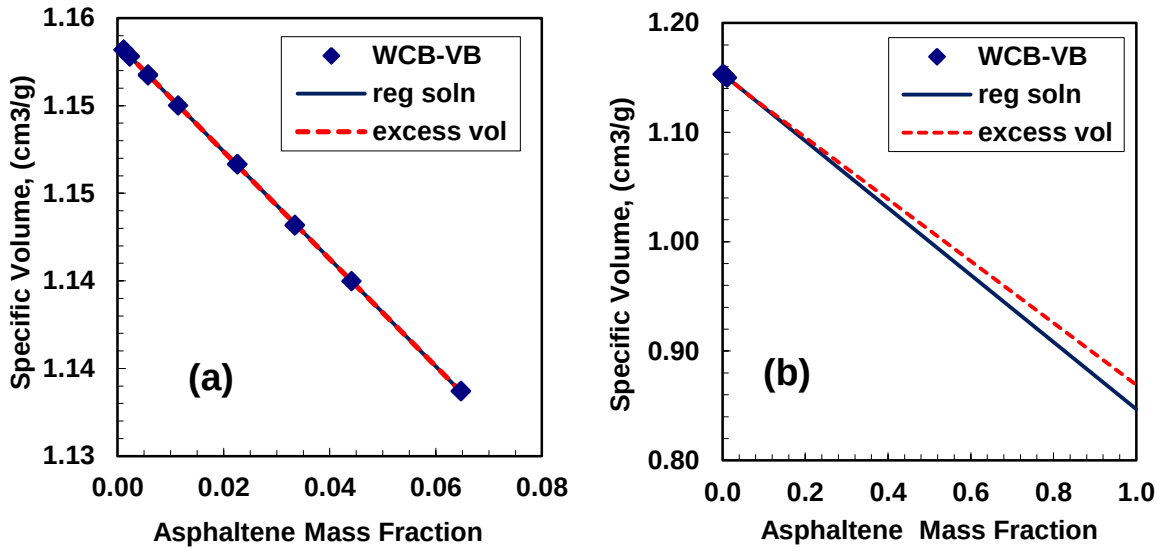

Figure 3.1. Regular and irregular mixing rules fitted to WCB Vacuum Bottom whole asphaltene specific volume data: a) low concentration range; b) full scale.

3.3.3 Refractive Index Measurements

The refractive index (RI) is the ratio of the velocity of light in a vacuum to the velocity of the light in a given substance. The refractive index is related to the hydrocarbon mixture composition (Speight, 2007). Paraffins typically have low values of refractive index and aromatic compounds have higher values of RI. A similar procedure was followed as for the indirect density measurements to measure refractive index at the same concentration ranges. The RI of toluene-asphaltene mixtures were measured on an Anton Paar Abbemat Refractometer at 20°C and atmospheric pressure.

The density and solubility parameter of a component are related to the refractive index function (FRI) given by:

$$FRI = \frac{RI^2-1}{RI^2+2} \tag{3.10}$$

Hence, the RI data are reported and analyzed in terms of FRI. The relationship of FRI to density and solubility parameter is discussed in Chapter 5.

Ideally, the FRI of a solution is related to the volume fraction of its constituents as follows:

$$FRI_{mix} = FRI_A\varphi_A + FRI_T\varphi_T \tag{3.11}$$

where φ is the volume fraction and subscripts *A* and *T* are asphaltenes and toluene, respectively.

The FRI of asphaltenes was determined by fitting low concentration data with the mixing rule (Eq. 3.12), as shown in Figure 3.1a. The precision of the measurement was 0.00001. The main source of experimental error is the accuracy of the dilution. Serial dilutions were repeated at least two times for a number of samples to estimate the error. The repeatability of asphaltene FRI was found to be 0.0065.

As with density, the FRI of asphaltenes in toluene may exhibit excess FRI of mixing, in which case, the FRI of a mixture can be determined as follows:

$$FRI_{mix} = FRI_A\varphi_A + FRI_T\varphi_T - \beta^*_{AT}\varphi_A\varphi_T(FRI_A + FRI_T) \tag{3.12}$$

where β^*_{AT} is the binary FRI interaction parameter for asphaltenes and toluene and the last term in Equation 3.12 is the excess FRI of mixing. Sanchez (2012) and Okafor (2012) found that for distillation fractions, saturates, aromatics and resins, the value of β^*_{iT} increases for the denser fractions such as asphaltenes. Okafor found an average β^*_{iT} of -0.0038 for aromatics and toluene mixtures and predicted a β^*_{AT} of -0.021 for asphaltenes and toluene. The FRI for asphaltenes based on the excess volume mixing rule were consistently about 0.015 less than the FRI

determined from the volumetric mixing rule. Figure 3.2 illustrate the FRI calculation of WCB-VB whole asphaltene using both regular and excess FRI mixing rules.

As will be discussed in Chapter 5, asphaltenes form regular solutions in toluene and o-dichlorobenzene. Since FRI is related to density, it was assumed that the excess FRI of asphaltenes is also negligible and Equation 3.11 was used to determine the asphaltene FRI.

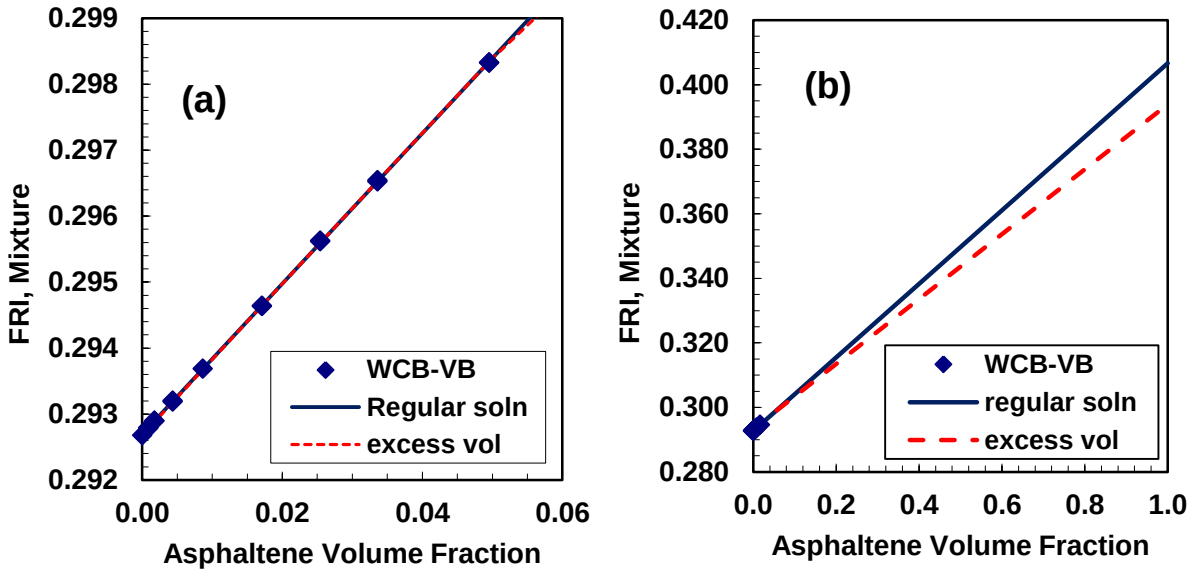

Figure 3.2. Regular solution and excess volume rule fitted to FRI of WCB-VB whole asphaltenes in toluene, a) expanded scale at low asphaltene volume fraction; b) full scale.

Chapter Four: Asphaltene Self-Association and Precipitation Modeling

This chapter describes two models which have been applied in this thesis: 1) a self-association model that will be used to predict asphaltene nano-aggregate molecular weight distributions; 2) a modified regular solution model that will be used to determine asphaltene solubility parameters.

4.1 Self-Association Model

The self-association model used in this thesis was developed by Agrawala and Yarranton (2001) for native asphaltenes and modified by Barrera *et al*. (2013) for both native and mildly reacted asphaltenes. Barrera *et al.* also investigated the effect of including non-associating material, neutrals, on the model performance. The original model and subsequent improvements are presented below.

4.1.1 Original Model

Agrawala and Yarranton (2001) introduced a self-association model with a mechanism analogous to polymerization. They assumed asphaltenes and resins have active sites, such as heteroatoms and aromatic stacks, which were capable of linking to other similar molecules to form larger aggregates. Molecules with multiple active sites could link to form a chain, similar to propagators in polymerization. Molecules with only one site would end a chain, similar to terminators. Molecules with no active sites, neutrals, do not participate in the self-association. Asphaltenes and resins are then considered to be mixtures of propagators and terminators where asphaltenes are predominantly propagators and resins are predominantly terminators. Saturates and aromatics are considered to be neutral. Note that while polymerization reactions apply to

chemical bonds, the reactions in asphaltene self-association represent weaker bonds such as π–π, acid-base, and hydrogen bonding. This simple analogy is almost certainly a gross oversimplification of the real aggregation phenomenon but is sufficient to model the available data.

Propagation

Propagation is the linking of a monomer propagator, P_1, to an aggregate molecule, P_n, where *n* is the number of the monomer molecules in aggregate. Reactions are considered to be first order with respect to both propagator monomer and aggregate molecules. Each reaction is characterized with an association constant, *K*, which is used to determine the aggregate molecule concentrations. For simplification, it is assumed that the constant *K* is equal for all the reactions regardless of aggregate size. Propagation is described in the following reaction equations (Agrawala and Yarranton, 2001):

$$P_1 + P_1 \overset{K}{\leftrightarrow} P_2 \;\longrightarrow\; [P_2] = K[P_1]^2 \tag{4.1}$$

$$P_1 + P_2 \overset{K}{\leftrightarrow} P_3 \;\longrightarrow\; [P_3] = K[P_1][P_2] = K^2[P_1]^3 \tag{4.2}$$

$$P_1 + P_3 \overset{K}{\leftrightarrow} P_4 \;\longrightarrow\; [P_4] = K[P_1][P_3] = K^3[P_1]^4 \tag{4.3}$$

The general equation is given by:

$$P_1 + P_n \overset{K}{\leftrightarrow} P_{n+1} \;\longrightarrow\; [P_{n+1}] = K[P_1][P_n] = K^n[P_1]^{n+1} \tag{4.4}$$

Termination

Termination is a reaction in which in a terminator molecule, *T*, links to a propagator monomer or existing aggregate molecule and terminates further propagation. The reaction is again considered

to be first order with respect to terminator monomers and aggregate molecules. For simplification, the equilibrium constant of termination is assumed to be same for all reactions and is equal to the propagation association constants. This means that the probability of occurrence of monomer-monomer linkage is equal to that of a monomer-aggregate linkage. Another assumption is that it is sufficient for a terminator to stick to just one site of an aggregate to terminate association. It has been found by Yarranton *et al*. (2007) that blocking both propagator sites gave similar results.

The concentration of terminator-aggregates can be expressed as follows:

$$P_1 + T \overset{K}{\leftrightarrow} P_1T \;\longrightarrow\; [P_1T] = KP_1T \tag{4.5}$$

$$P_2 + T \overset{K}{\leftrightarrow} P_2T \;\longrightarrow\; [P_2T] = K[P_2][T] = K^2[P_1]^2[T] \tag{4.6}$$

$$P_3 + T \overset{K}{\leftrightarrow} P_3T \;\longrightarrow\; [P_3T] = K[P_3][T] = K^3[P_1]^3[T] \tag{4.7}$$

The general termination equation is given by:

$$P_n + T \overset{K}{\leftrightarrow} P_nT \;\longrightarrow\; [P_nT] = K[P_n][T] = K^n[P_1]^n[T] \tag{4.8}$$

Mass Balance

In a similar approach to polymerization, the reaction scheme can be solved starting with the mass balance equations for propagators and terminators. If $[P_1]_0$ and $[T]_0$ are the initial concentrations of propagators and terminators, respectively, then the mass balance calculations of propagators is as follows:

$$[P_1]_0 = ([P_1] + 2[P_2] + 3[P_3] + \cdots + n[P_n]) + ([P_1T] + 2[P_2T] + 3[P_3T] + \cdots + n[P_nT]) \tag{4.9}$$

Substitution of aggregate concentrations from Equations 4.1 to 4.8 gives:

$$[P_1]_0 = ([P_1] + 2K[P_1]^2 + 3K^2[P_1]^3 + \cdots + nK^{n-1}[P_1]^n)$$
$$+ (K[P_1][T] + 2K^2[P_1]^2[T] + 3K^3[P_1]^3[T] + \cdots + nK^n[P_1]^n[T])$$
$$= [P_1](1 + K[T])(1 + 2K[P_1] + 3K^2[P_1]^2 + \cdots + nK^n[P_1]^n) \quad (4.10)$$

Equation 4.10 is an infinite series that can be simplified as:

$$[P_1]_0 = [P_1]\frac{(1+K[T])\left(1+K[P_1]+K^2[P_1]^2\right)+\cdots K^n[P_1]^n)}{1-K[P_1]} \quad (4.11)$$

Multiplying the numerator and denominator of right side of Equation by $(1 - K[P_1])$ gives:

$$[P_1]_0 = \frac{[P_1](1+K[T])}{(1-K[P_1])^2} \quad (4.12)$$

Equation 4.12 is a second degree polynomial equation in terms of *[P_1]* and can be expressed as follows:

$$K^2[P_1]_0[P_1]^2 - \left(1 + K(2[P_1]_0[T])\right)[P_1] + [P_1]_0 = 0 \quad (4.13)$$

In a similar way, the mass balance of terminators is given by:

$$[T]_0 = [T] + [P_1T] + [P_2T] + \cdots + [P_nT] \quad (4.14)$$

Equations 4.5 to 4.8 are substituted into Equation 4.14 to obtain:

$$[T]_0 = [T] + K[P_1][T] + K^2[P_1]^2[T] + K^3[P_1]^3[T] + \cdots + K^n[P_1]^n[T] = [T](1 + K[P_1] +$$
$$K^2[P_1]^2 + K^3[P_1]^3 + \cdots + K^n[P_1]^n) \quad (4.15)$$

Multiplying the right side of the above equation by $\frac{1-K[P_1]}{1-K[P_1]}$ gives:

$$[T]_0 = \frac{[T]}{1-K[P_1]} \quad (4.16)$$

Equation 4.16 is rearranged to obtain an expression for [T] as follows:

$$[T] = [T]_0(1 - K[P_1]) \quad (4.17)$$

Substituting Equation 4.17 into Equation 4.13 gives:

$$K^2([P_1]_0 + [T]_0)[P_1]^2 - (1 + K(2[P_1]_0 + [T]_0))[P_1] + [P_1]_0 = 0 \quad (4.18)$$

The equilibrium concentration of propagators, $[P_1]$, is simply the solution of the quadratic Equation 4.17:

$$[P_1] = \frac{1+K(2[P_1]_0+[T]_0)-\sqrt{(1+K(2[P_1]_0+[T]_0))^2-4K^2[P_1]_0([P_1]_0+[T]_0)}}{2K^2([P_1]_0+[T]_0)} \quad (4.19)$$

Once the equilibrium concentration of propagators is known, the equilibrium concentration of terminators can be calculated from Equation 4.17. The concentration of different aggregate sizes in equilibrium condition can be calculated through Equations 4.1 to 4.8. Note that initial concentrations of propagators and terminators ($[P_1]_0$ and $[T]_0$), along with association constant, must be defined to perform all of the above calculations. To ensure that the largest molecules are considered in the system, the maximum number of aggregates, *n*, must be set as high enough to avoid truncation of the upper end of the aggregate distribution.

Implementation of the Model

The inputs to the model are $(\frac{T}{P})_0$ and *K*. The asphaltene mass concentration and the solvent molar volume must also be specified to calculate the molar concentration of the terminators and propagators. The first step is to determine the average molecular weight of the asphaltene monomers before any association. We start with the mole fraction of propagators and terminators molecules in the asphaltenes alone which can be calculated as follows:

$$\frac{x_{T_0}}{x_{P_0}} = \left(\frac{T}{P}\right)_0 \quad (4.20)$$

$$x_{T_0} = \frac{\left(\frac{T}{P}\right)_0}{1+\left(\frac{T}{P}\right)_0} \qquad \text{and} \qquad x_{P_0} = 1 - x_{T_0} \tag{4.21}$$

where x_{To} and x_{Po} are the mole fraction of terminators and propagators in the asphaltenes, respectively, and $(T/P)_0$ is the ratio of terminator to propagator molecules in the whole solution. The average molecular weight of a non-aggregated asphaltene (or monomer molecular weight) is given by:

$$MW_{mono} = x_{T_0} MW_T + (1 - x_{T_0}) MW_P \tag{4.22}$$

where MW_{mono} is the average molecular weight of the asphaltene monomers before any association and MW_T and MW_P are estimated from experimental data. The propagator monomer molecular weight is approximated by extrapolating the molecular weight data of whole asphaltene to zero concentration and the terminator monomer molecular weight is estimated by extrapolating the molecular weight data for the most soluble asphaltene fraction to zero concentration.

The next step is to determine the monomer mole fractions. Assuming the m_A gram of asphaltene is added to V_s liters of solvent of molar volume of υ_s, the total number of moles (n_t) of the system is:

$$n_t = \frac{m_A}{MW_{mono}} + \frac{V_S}{\upsilon_S} \tag{4.23}$$

The initial mole fraction of propagators and terminators is equal to the mole fraction of the asphaltene monomers in the system:

$$[P_1]_0 + [T]_0 = \frac{{}^{m_A}/_{MW_{mono}}}{{}^{m_A}/_{MW_{mono}} + {}^{V_S}/_{\upsilon_S}} \tag{4.24}$$

Recall that asphaltene mass concentration in the system, C_A, is defined as:

$$C_A = \frac{m_A}{V_S} \tag{4.25}$$

and that the initial ratio of terminator to propagator monomers is related to the modeled mole fractions as follows:

$$(\frac{T}{P})_0 = \frac{[T]_0}{[P_1]_0} \tag{4.26}$$

Equations 4.25 and 4.26 are substituted into Equation 4.24 to obtain:

$$[P_1]_0 = \frac{1}{(1+\frac{MW_{mono}}{C_A v_S})(1+(\frac{T}{P})_0)} \tag{4.27}$$

and

$$[T]_0 = [P_1]_0(\frac{T}{P})_0 \tag{4.28}$$

Equations 4.27 and 4.28 are solved with Equation 4.22 and the model inputs. The model output is the average molecular weight of the associated asphaltenes at the input concentration. The average molecular weight of the aggregated system is given by:

$$MW_{avg} = \sum([P_n]MW_{P_n} + [P_nT]MW_{P_nT}) \tag{4.29}$$

The model is run by adjusting fitting parameters, $(\frac{T}{P})_0$ and *K* until the calculated average molecular weight fits the measured experimental molecular weight data. Since the experimental data are scattered and outliers were found to skew regression methods, the model is fitted by manual adjustments (Barrera, 2013). The effect of the fitting parameters has been investigated in previous studies (Agrawala and Yarranton, 2001; Barrera, 2013). The association constant affects the concentration at which limiting value is reached while $(T/P)_0$ affects the limiting value itself.

4.1.2 Conversion of Output to Continuous Molecular Weight Distributions

The output of the model is the mole fraction (or mass fraction) of each aggregate at a specified concentration of asphaltenes in the solvent. Since only average monomer molecular weights are used, the distribution is discrete while the real distribution is almost certainly continuous. Also, as will be discussed in Section 4.2, the output of the model is used as input for regular solution model and a continuous distribution is more convenient (Barrera, 2013).

To determine a continuous cumulative mass frequency distribution of asphaltene aggregates, Barrera (2012) sorted the molecular weight and their corresponding mass fraction in descending order and then used the following form of exponential function to fit to the data using a least squares method:

$$cumf = A_1 + B_1 exp(-exp(\frac{C_1 - MW}{D_1})) \tag{4.30}$$

where *cumf* is the cumulative mass fraction function, *MW* is the molecular weight of the aggregates, and the other terms are fitting parameters. A_1 and B_1 parameters control the upper limit of the distribution while C_1 and D_1 affects the slope and the point in which a maximum value is reached (Barrera, 2013).

Equation 4.30 has the drawback that, after fitting, it calculates some molecular weights less than monomer molecular weights. Therefore, the following alternative fitting equation was developed for this thesis that is constrained to molecular weights at or above the monomer molecular weight.

$$cumf = \left(1 - \exp\left(-A(MW - C)\right)\right) \times B + \tanh(D(MW - C)) \times (1 - B) \tag{4.31}$$

where *C* is the minimum molecular weight and *A*, *B*, and *D* are fitting parameters.

4.1.3 Introducing Neutrals into the Model

Experimental results of this thesis and a previous study (Barrera, 2013) show that a small portion of asphaltene molecules do not self-associate (the neutrals), but must be accounted for in mass balance calculations. In non-aggregated systems with neutrals, the initial mole fraction of terminators and propagators are calculated as follows:

$$x_{T_0} = \frac{(\frac{T}{P})_0}{1+(\frac{T}{P})_0}(1 - x_{N_0}) \quad \text{and} \quad x_P = 1 - x_{T_0} - x_{N_0} \tag{4.32}$$

where $x_{N_0}$is the neutrals mole fraction in asphaltene sample. The molecular weight of the monomer is calculated as:

$$MW_{mono} = x_{T_0} MW_T + \left(1 - x_{T_0} - x_P\right) MW_P + x_{N_0} MW_N \tag{4.33}$$

where MW_N is the neutral monomer molecular weight which is assumed to be equal to the terminator monomer molecular weight.

The initial mole fractions of propagators, terminators, and neutrals in solution are given by:

$$[P_1]_0 = \frac{1}{\left(1+\frac{MW_{mono}}{C_A v_S}\right)\left(1+\left(\frac{T}{P}\right)_0\right)}\left(1 - x_{N_0}\right) \tag{4.34}$$

$$[T]_0 = [P_1]_0 \left(\frac{T}{P}\right)_0 \tag{4.35}$$

$$[N]_0 = \frac{x_{N_0}}{(1+\frac{MW_{mono}}{C_A v_S})} \tag{4.36}$$

In this approach, x_{N_0} is an additional fitting parameter that is added to the model inputs. The initial concentration of propagators, terminators, and neutrals ($[P_1]_0$, $[T]_0$, and $[N]_0$) are calculated and the average molecular weight of the aggregated system is given by the following equation:

$$MW_{avg} = (1 - x_N)\left(\sum_{n=1}^{n}(x_{[P_n]}.MW_{[P_n]} + x_{[P_nT]}.MW_{[P_nT]})\right) + x_N.MW_N \quad (4.37)$$

where x_N is the mole fraction of neutrals in the aggregated system and is different than x_{N_0}. After running the model, the cumulative mass frequency of aggregates is determined from Equation 4.30.

4.2 Modified Regular Solution Model

A regular solution model modified by Albouwarej *et al.* (2003) is used in this thesis. The model applies to asphaltene precipitation and it is assumed that the precipitation is a liquid-liquid equilibrium (or glass-liquid equilibrium) between a heavy asphaltene-rich phase and a light solvent-rich phase. The phase equilibrium is solved with a flash calculation based on the equilibrium ratio of each component. The equilibrium ratio of a component is defined as:

$$K_i^{hl} = \frac{x_i^h}{x_i^l} = \left(\frac{\gamma_i^l}{\gamma_i^h}\right)\left(\frac{f_i^{0l}}{f_i^{0h}}\right)\exp\left[\int_0^P \frac{\Delta v_i dP}{RT}\right] \quad (4.37)$$

where K is the equilibrium ratio, x, γ, and f are the mole fraction, activity coefficient, and fugacity of component i, P is pressure, T is absolute temperature, v is molar volume, R is the universal gas constant, and l, h and o denote the light liquid phase, heavy liquid phase, and standard state, respectively. In a liquid-liquid equilibrium, the term $\left(\frac{f_i^{0l}}{f_i^{0h}}\right)\exp\left[\int_0^P \frac{\Delta v_i dP}{RT}\right]$ is equal to unity and Equation 4.37 reduces to:

$$K_i^{hl} = \frac{x_i^h}{x_i^l} = \left(\frac{\gamma_i^l}{\gamma_i^h}\right) \tag{4.38}$$

Prauznits *et al.* (1999) defined the activity coefficient of a component in an athermal and regular solution as:

$$\ln\gamma_i^L = \ln\frac{v_i^L}{v_m^L} + 1 - \frac{v_i^L}{v_m^L} + \frac{v_i^L}{RT}\sum_j^n\sum_k^n \Phi_j\Phi_k(D_{ij} - 0.5D_{jk}) \tag{4.39}$$

where *m* refers to a mixture and Φ_i is the volume fraction defined as:

$$\Phi_i = \frac{x_i v_i}{\sum x_i v_i} \tag{4.40}$$

and D_{ij} is a interaction parameter which is given by:

$$D_{jk} = (\delta_j - \delta_k)^2 + 2l_{jk}\delta_j\delta_k \tag{4.41}$$

where δ_j is solubility parameter of component j and l_{jk} is the interaction coefficient between components. If the interaction coefficient is equal to zero for all of the components in an equilibrium system, then Equation 4.39 simplifies to:

$$\ln\gamma_i^L = \ln\frac{v_i^L}{v_m^L} + 1 - \frac{v_i^L}{v_m^L} + \frac{v_i^L}{RT}(\delta_i - \delta_m)^2 \tag{4.42}$$

where δ_m is the mixture solubility parameter which can be calculated as:

$$\delta_m = \sum_i^m \Phi_i\delta_i \tag{4.43}$$

Substituting Equation 4.42 into Equation 4.37 gives:

$$K_i^{hl} = \frac{x_i^h}{x_i^l} = \exp[\ln\frac{v_i^l}{v_m^l} - \ln\frac{v_i^h}{v_m^h} + \frac{v_i^h}{v_m^h} - \frac{v_i^l}{v_m^l} + \frac{v_i^l}{RT}\left(\delta_i^l - \delta_m^l\right)^2 - \frac{v_i^h}{RT}\left(\delta_i^h - \delta_i^h\right)^2] \tag{4.44}$$

For easier and more rapid convergence for a solution, it was assumed that the heavy liquid phase only consists of asphaltenes and resins. This assumption is based on experimental observations

that the heavy phase consists mainly of asphaltene and resins (Alboudwarej *et al*., 2003; Akbarzadeh *et al*., 2005). This assumption also leads to better predictions of asphaltene yields at high dilution.

The following flash algorithm is employed to solve the phase equilibrium (Alboudwarej *et al*., 2003):

1. The feed molar composition is given as an input
2. *K* values are initiated using the composition of the feed
3. A standard method (*e.g*. Rachford Rice) is employed to calculate phase amounts
4. The light phase composition is then updated and normalized
5. *K* values are updated and the solution is checked for convergence
6. If error are within tolerance, then the phase amounts and *K* values are reported; otherwise, return to Step 3.

The input properties of the components are their mole fraction, molar volume, and solubility parameter. Temperature and pressure are also input.

4.2.1 Fluid Characterization

In this thesis, asphaltene precipitation from heptane and toluene mixtures is modeled. Each of the solvents is treated as a single component with known properties, but asphaltenes are divided into a series of pseudo-components to represent the molar volume and solubility parameter distributions of the asphaltenes (Yarranton and Masliyah, 1996; Alboudwarej *et al*, 2003). Molar volumes are determined from molecular weight and density data. The molecular weights, molar volumes, and solubility parameters of the relevant components are outlined below.

4.2.1.1 Molecular Weight

The molecular weight of heptane and toluene are well known. The average molecular weight of the asphaltene nano-aggregates is usually measured with VPO in toluene at 50°C. Yarranton and Masliyah (1996) showed that to predict asphaltene precipitation more accurately it is essential for asphaltene to be considered as macromolecular aggregates. Both the Gamma distribution function (Akbarzadeh *et al*., 2002; Alboudwarej *et al*., 2003; Akbarzadeh *et al*., 2005) and the output of the association model discussed in Part 4.1.3 (Barrera, 2012) have been employed to represent the molecular weight of asphaltene aggregates.

The association model approach was described in Section 4.1 but the Gamma distribution is more commonly used. Akbarzadeh *et al*. (2004, 2005) divided asphaltenes into pseudo-components based on the following Gamma distribution function:

$$f(MW) = \frac{1}{\Gamma(\beta)}\left[\frac{\beta}{\bar{M}-MW_{mono}}\right]^{\beta} \times (MW - MW_{mono})^{\beta-1} \times \exp\left[\frac{\beta(MW-MW_{mono})}{\bar{M}-MW_{mono}}\right] \qquad (4.45)$$

where $f(MW)$ is the mass frequency of the given molecular weight, MW_{mono} is the monomer molecular weight, $\bar{M}$ is the average associated molecular weight of asphaltenes, and β is a parameter which determines the shape of the distribution. The distribution can be discretized to different cuts with a constant step size of ΔMW and the mass fraction of each cut can be calculated as:

$$w_i = \frac{\int_{MW_i}^{MW_{i+1}} f(MW)dMW}{\int_{MW_1}^{MW_n} f(MW)dMW} \qquad (4.46)$$

In previous studies, asphaltene were divided into 30 fractions and a maximum value of 30,000 g/mol was recommended for an upper boundary of the molecular weight distribution (Alboudwarej *et al*., 2003; Akbarzadeh *et al.*, 2005; Barrera, 2012). The average molecular weight of the asphaltenes was measured by VPO at a desired concentration and then converted to room temperature equivalent molecular weight with the following correlation:

$$MW_{23} = MW_{50}\exp(0.0073 \times (50 - 23)) \tag{4.47}$$

The asphaltene monomer molar mass was set to a value between 1000 and 1500 g/mol. Values between 2 and 4 were recommended for β.

4.2.1.2 Molar Volumes

Molar volumes of pure solvent can be calculated using the Hankinson-Brobst-Thomson (HBT) technique (Reid *et al*., 1989). To estimate asphaltene molar volume, the density distribution must first be determined, and then molar volumes can be calculated as the ratio of molecular weight to density.

The following correlation was recommended by Adboulwarej *et al*. (2003) to relate asphaltene density to its molecular weight:

$$\rho = 670MW^{0.0639} \tag{4.48}$$

where ρ is the asphaltene density in kg/m^3 and MW is the asphaltene molecular weight in g/mol. Equation 4.48 were based on a limited set of measurements on Athabasca bitumen. More recently, Barrera *et al*. (2012) generalized the density correlation by measuring the properties of asphaltene from different sources. They proposed the following form:

$$\rho = 1100 + 100[1 - \exp\left(-\frac{MW}{3850}\right)] \quad (4.49)$$

where ρ is the density of asphaltene in kg/m^3 and *MW* is asphaltene molecular weight measured by VPO at a concentration of 10 g/L.

4.2.1.3 Solubility Parameter

Solvents:

The solubility parameter, δ, of pure solvents at 25°C is defined as (Barton, 1991):

$$\delta_{25\,℃} = \left(\frac{\Delta H_{25℃}^{\text{vap}^*} - 298.15R}{\upsilon_{25℃}}\right)^{1/2} \quad (4.50)$$

where δ is the solubility parameter in MPa$^{0.5}$, $\Delta H^{\text{vap}*}$ is the molar heat of vaporization in J/mol, *R* is the universal gas constant in J/molK, υ is molar volume in cm^3/mol, and 25°C indicates that the property is determined at 25°C. Barton (1991) reports solubility parameters for a number of pure solvents at 25°C including the value of 18.25 MPa$^{0.5}$ for toluene used in this thesis.

Tharanivasan et al. (2011) determined a correlation for n-alkane solubility parameters. They back calculated $\Delta H_{25℃}^{\text{vap}^*}$ from Equation 4.50 using the known $\delta_{25\,℃}$ values from the literature and then correlated the modified heat of vaporization to molecular weight as follows:

For carbon number ≤ 4:

$$\Delta H_{25℃}^{\text{vap}^*} = 3492.8 + 276.54MW + 0.52400MW^2 \quad (4.51a)$$

For carbon number ≥ 5:

$$\Delta H_{25℃}^{\text{vap}^*} = 103.65 + 367.8MW + 0.0.06030MW^2 \quad (4.51b)$$

They also showed that the calculated $\Delta H_{25℃}^{vap^*}$ fit solubility parameters to within 0.01 $MPa^{0.5}$. Note that the modified heats of vaporization are slightly different than the actual heats of vaporization because they were adjusted to fit the solubility parameter values. The correlations are useful for determining *n*-alkane solubility parameters not available in the literature.

Akbarzadeh *et al*. (2005) developed an expression to take into account temperature effect as:

$$\delta = \delta_{25\,℃}\left(\frac{\upsilon_{25℃}}{\upsilon}\right)^{1/2} - 0.0232(T - 298.15) \tag{4.52}$$

Note that slope of -0.0232 $MPa^{0.5}$/K is consistent with the order of magnitude of the derivation of the solubility parameter ($d\delta/dT$ = -0.03 $MPa^{0.5}$/K) generally found for hydrocarbons (Barton, 1991). Assuming that pressure only affects the molar volume, solubility parameter at any pressure is given by:

$$\delta_{25\,℃,P} = \delta_{25\,℃}\left(\frac{\upsilon_{25℃}}{\upsilon}\right)^{1/2} \tag{4.53}$$

Asphaltenes:

Asphaltene solubility parameters are calculated through empirical correlations. Yarranton and Masliyah (1996) proposed the following equation for asphaltene pseudo components:

$$\delta = (A\rho)^{1/2} \tag{4.54}$$

where δ is the asphaltene solubility parameter ($MPa^{0.5}$) and A is a fitting parameter and approximately equal to the monomer heat of vaporization. Alboudwarej *et al* (2003) estimated that A has a value of 366 J/g by fitting the model to one set of asphaltene-*n*-heptane-toluene precipitation data. Akbarzadeh *et al*. (2005) found that the parameter A depends on temperature

and recommended the following form of the equation by fitting the model to precipitation data for mixtures of asphaltene- *n*-heptane-toluene at 23 and 50 °C:

$$A(T) = -6.667 \times 10^{-4}T + 0.5614 \tag{4.55}$$

Yarranton et al. (2007) later revised the correlation based on more data, as follows:

$$A(T) = -7.5 \times 10^{-4}T + 0.579 \tag{4.56}$$

More recently, Barrera (2012) proposed a new correlation for asphaltene solubility parameters based on experiments on native and mildly reacted bitumen:

$$\delta = (A\rho(cMW)^{d})^{1/2} \tag{4.57}$$

where δ is the solubility parameter of asphaltene pseudo components, ρ is density, MW is molecular weight, *c* and *d* are fitting parameter dependent on the sample, and *A* is a temperature dependent parameter given by:

$$A(T) = -7.5 \times 10^{-4} + 0.579 \tag{4.58}$$

In this these, the values of *c* and *d* are to be determined based on precipitated yield data for a variety of asphaltenes. The following tuning algorithm is used:

1. Enter the operating condition input parameters including: pressure, temperature, solvent composition, and asphaltene concentration.
2. Calculate the molar volume and solubility parameter of the solvents.
3. Enter the parameters associated with the molecular weight distributions.
4. Calculate the density and solubility parameters of asphaltenes fractions.
5. Calculate the mole fraction of each component.
6. Set initial guess for parameters *c*, and *d*.

7. Perform liquid-liquid equilibrium calculations according to the previously introduced flash algorithm. The output is the amount and composition of each phase.
8. Compare the calculated asphaltene yield with experimental results and adjust *c*, and *d* until the error tolerance is acceptable (an average absolute deviation of less than 0.08).

Results of the regular solution modeling and the coefficients for the solubility parameter correlation are discussed in detail in Chapter 5.

Chapter Five: Results and Discussion

In this chapter, asphaltene molecular weight and density distributions are determined for eight crude oils which have been processed under different temperature and pressure conditions. The distributions are reconstructed based on measured properties of asphaltene solubility cuts. Density distributions are calculated directly from the data. Since asphaltenes self-associate, the molecular weight data are modeled with a terminator-propagator model so that the distribution of nano-aggregates can be predicted.

5.1 Samples and Asphaltene Solubility Cuts

Nine crude oil samples were considered for this study and their asphaltene and solids contents are reported in Table 5.1. B3VB is a vacuum distillation tower bottom product and was used as a feed stream for a thermal cracking process. The products of thermal cracking are the X samples (X-1357, X-1359, X-1360). The Short Residue is another unprocessed sample from a distillation tower and was the feedstock for a hydrocracking process. The products of hydrocracking are the RHC samples (19-03, 18-19, 18-37) and HOSB. Table 5.2 summarizes the reaction conditions, where known, and conversion for each sample.

Table 5.1. Asphaltene and solids content of the samples used in this thesis.

Sample	Asphaltene wt%	Solids wt% in Asphaltenes	Solids wt% in Crude Oil
B3VB	43.07	6.57	2.42
X-1357	49.90	10.37	3.25
X-1359	50.00	16.29	8.13
X-1360	50.54	22.80	11.52
Short Residue	16.54	1.32	0.22
RHC-19-03	2.81	33.95	0.95
RHC-18-19	10.49	10.65	1.12
HOSB	12.32	19.67	2.42
RHC-18-37	21.25	19.06	4.05

Table 5.2. Processing conditions for samples from Table 5.1 (NA = not available).

Sample	Temperature (°C)	Pressure (psig)	Extent of Conversion
B3VB	NA	NA	Vacuum Bottoms
X-1357	520+	NA	17.3 wt%
X-1359	520+	NA	31 wt%
X-1360	520+	NA	50.8 wt%
Short Residue	NA	NA	Vacuum Bottoms
RHC-19-03	410	2100	56 vol%
RHC-18-19	432	1960	70 vol%
HOSB	NA	NA	77 vol %
RHC-18-37	440	1960	80 vol %

Figure 5.1 shows the solubility curves of B3VB and Short Residue asphaltenes and Figure 5.2 shows the solubility curves of reacted samples. The yield curves reflect the reaction history of the samples. The B3VB and Short Residue yield curves are similar to each other and to the solubility curves of other native asphaltenes (Barrera, 2012) because these samples were not reacted. On the other hand, the solubility curves of the reacted samples are completely different than those of their feedstocks. The asphaltenes from reacted sources become significantly less soluble and the precipitation onset point moves to zero *n*-heptane concentration as the conversion increases.

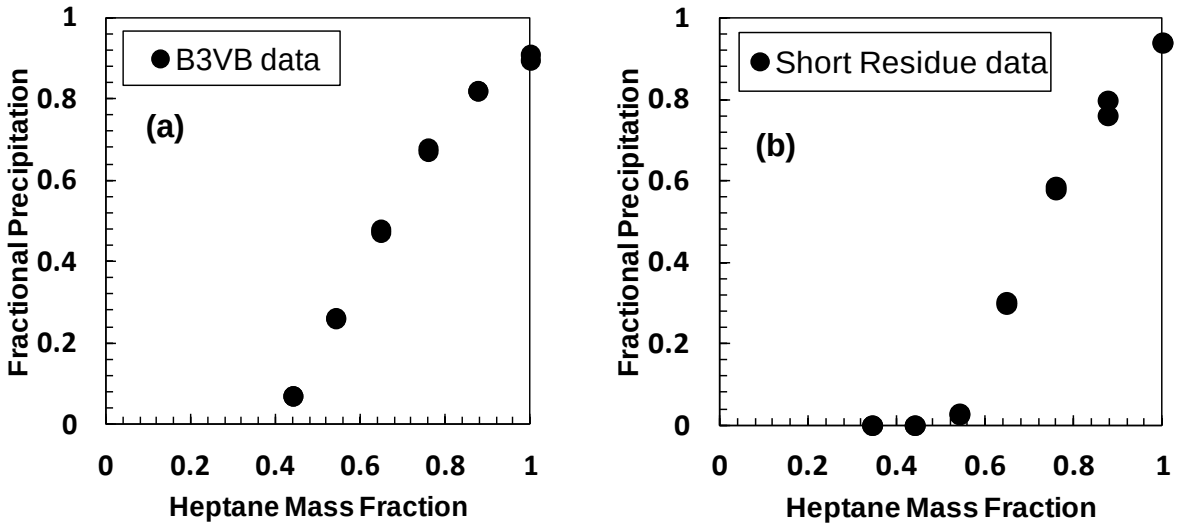

Figure 5.1. Fractional precipitation of asphaltenes from mixtures of heptol: a) B3VB, b) Short Residue.

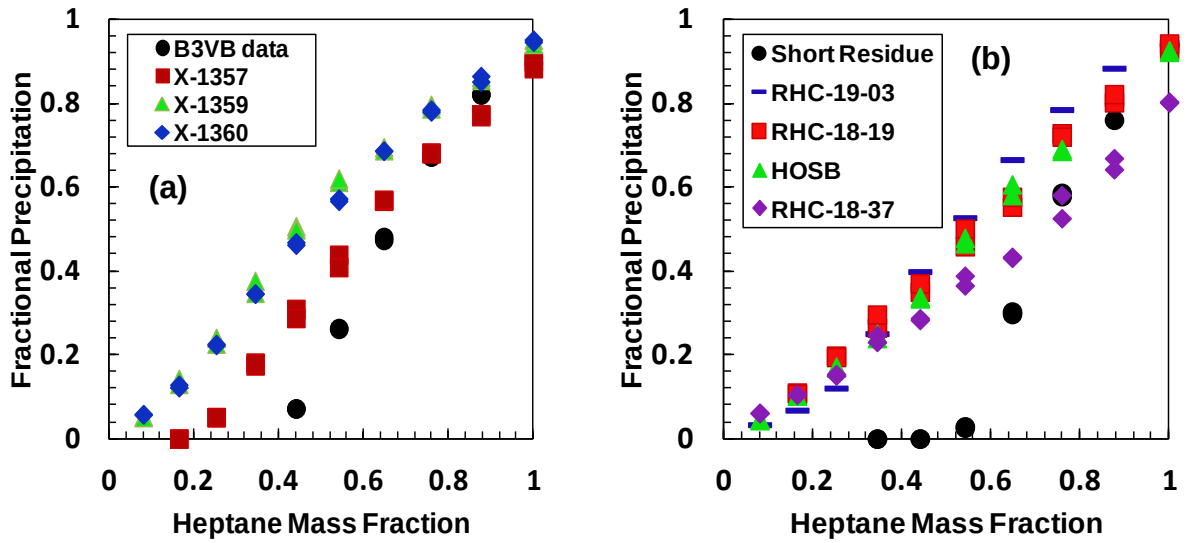

Figure 5.2. Fractional precipitation of asphaltenes from mixtures of heptol: a) Thermocracked, b) Hydrocracked.

The asphaltenes extracted from each oil sample were divided into solubility cuts by selective precipitation from solutions of *n*-heptane and toluene (heptol) as described in Chapter 3. The ratio of n-heptane to toluene was selected to obtain a target yield of asphaltenes based on the solubility curves of whole asphaltene in solutions of *n*-heptane/toluene at 23°C. For all of the samples, two separations were performed: one to obtain the approximately 33% insoluble (heavy) and 67% soluble (light) cuts and one to obtain the approximately 67% insoluble and 33% soluble cuts. For instance, for B3VB, heptol (*n*-heptane + toluene) ratios of HT61 and HT80 were used to obtain the 30% and 70% insoluble cuts, respectively.

After fractionation of the asphaltenes, the molecular weight and density of all cuts along with the whole asphaltenes were measured. In the following sections, the data are presented and the methodology developed by Barrera (2012) is applied to determine the molecular weight and

density distributions of the reacted asphaltenes from the property measurements of the solubility cuts.

Note, all of the measurements in previous work done by Barrera (2012) were prepared in toluene and all of the cuts were completely soluble in toluene. However, in this work it was found that the heaviest cuts of highly reacted asphaltenes were not completely soluble in toluene including X-1359, X-1360, RHC-18-19 and RHC-18-37. Therefore, characterization of these samples was performed using o-dichlorobenzene (DCB) instead of toluene. Asphaltenes self-associate less in DCB than in toluene and a method was developed to convert the DCB based distributions into toluene based distributions as will be described later. It will be also demonstrated that the solvent type had no effect on the measured asphaltene density.

5.2 Molecular Weight Distributions

5.2.1 Molecular Weight Data

Figure 5.3 shows the molecular weight for B3VB and Heavy Oil Stripper Bottoms (HOSB) asphaltenes and a pair of solubility cuts. Note, the molecular weight is the average molecular weight of the asphaltenes including nano-aggregates and therefore is a function of concentration, and temperature. The molecular weight of all cuts increased with increasing asphaltene concentrations, as expected for self-associating materials. The molecular weight of the lightest cut increased only slightly with increasing concentrations, suggesting that it contains little self-associating material. The molecular weight of the asphaltene monomers was estimated from the data for the lightest cut and was in the order of 800 g/mol for these native samples. The molecular weight of the heaviest cut increased significantly with increasing concentration,

indicating it contained a high proportion of self-associating materials. Similar behavior was observed for the reacted samples, as shown in Appendix B.

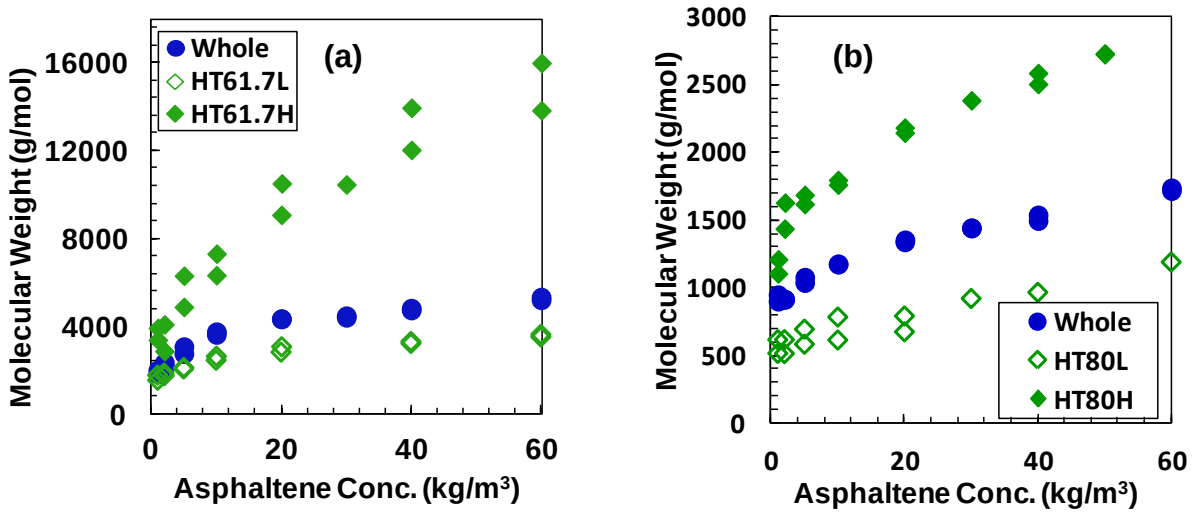

Figure 5.3. Molecular weight in toluene at 50°C for a) B3VB and b) HOSB whole asphaltenes and cuts precipitated using HT61.7 and HT80, respectively.

Figure 5.4 shows both thermal cracking and hydrocracking processes tend to decrease the molecular weight of the asphaltenes; that is, they tend to eliminate self-association. In both cases, the measured molecular weights decreased with an increase in conversion. The decrease in molecular weight was modest for the thermocracked asphaltenes but was significant for the hydrocracked asphaltenes. Thermocracking had no detectable effect on the asphaltene monomer sizes which were in the order of 800 g.mol for the X-series samples. Hydrocracking changed not only the aggregates size, but also dramatically changed the monomer molecular weight to approximately 450 g/mol for the RHC- samples.

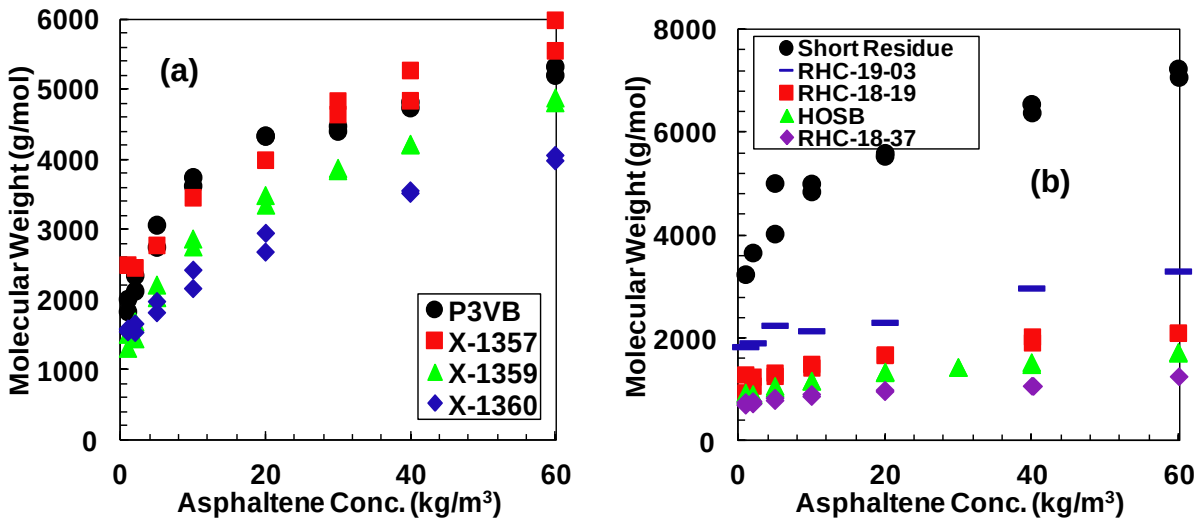

Figure 5.4. Molecular weight of whole asphaltenes: a) Thermocracked, b) Hydrocracked samples.

5.2.2 Modeling Molecular Weight Data

If asphaltenes did not self-associate, their molecular weight would be additive and the molecular weight of the whole asphaltenes could be calculated directly from the molecular weight of the cuts as follows:

$$MW_{whole} = x_{HT\#\#L} MW_{HT\#\#L} + (1 - x_{HT\#\#L}) MW_{HT\#\#H} \quad (5.1)$$

where *MW* is the molecular weight value at specific asphaltene concentration, *HT##L* and *HT##H* are the light and heavy cuts, respectively, with a heptol ratio of *HT##*. Barrera (2012) demonstrated that the molecular weight of whole asphaltene calculated from Equation 5.1 were inconsistent with measured values. Therefore, self-association must be accounted for when interpreting molecular weight data.

When asphaltenes are divided into two solubility cuts, the lower molecular weight aggregates tend to remain soluble and report to light cuts while the high molecular weight aggregates tend to

precipitate and report to the heavy cut. As illustrated in Figure 5.5, each of these cuts will re-associate to a new distribution when they are dissolved in toluene for molecular weight measurements. This new distribution is not necessarily the same as the distribution that the cut had in the original asphaltene mixture in equilibrium with all the other asphaltene aggregates. Therefore, the measured molecular weights are not necessarily additive. To interpret the measured data, the self-association model described in Chapter 4 is used to fit the data to determine the number of the neutral, terminator, and propagator monomers in each cut and the whole asphaltenes, constrained by a material balance. Then, the model can be used to calculate the molecular weight distribution at any given asphaltene concentration.

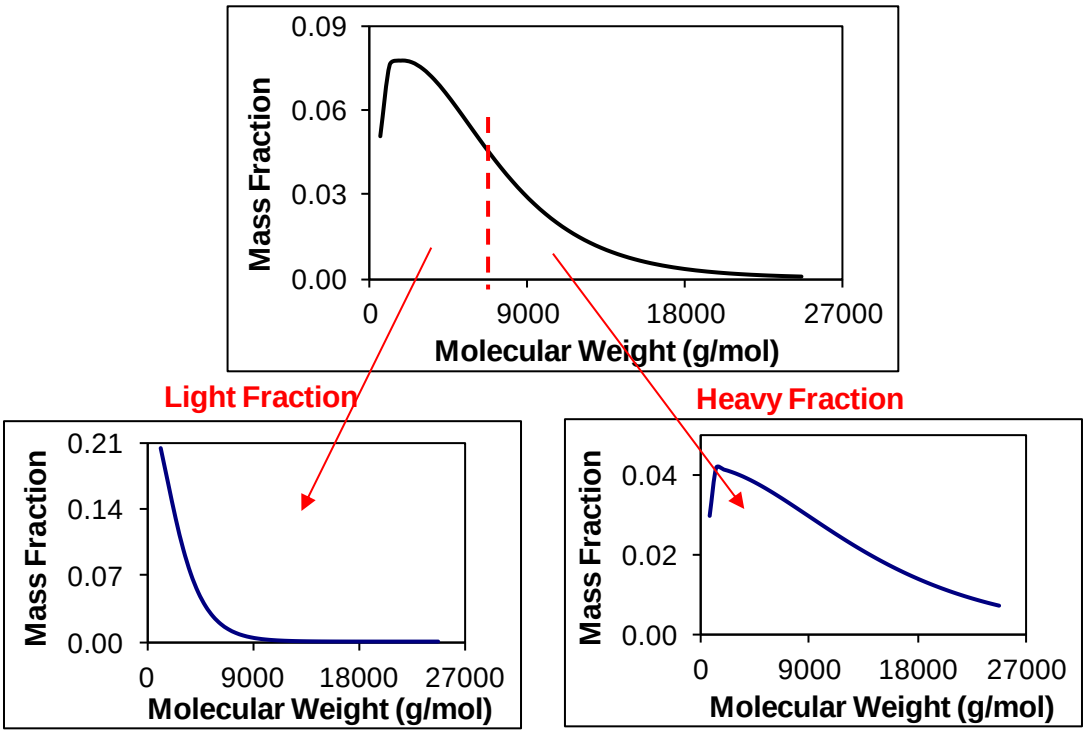

Figure 5.5. Re-association of asphaltenes into new distributions when they are divided into different solubility cuts; adapted from Barrera (2012).

The methodology for the self-association modeling is summarized below. First, initial guesses for the terminator and propagator molecular weights were set based on the molecular weight data at low asphaltene concentrations. An initial guess of the association constant was set based on an initial fit of the whole asphaltene molecular weight data. The initial guesses were adjusted later to optimize the model fit but were not significantly altered.

The main component of the model fitting was a systematic material balance based procedure involving the mole fraction of neutrals and the $(T/P)_0$ ratio. The mole fraction of neutrals was incremented over a range of a values, typically from 0 to 0.25. At each value, the model was fit to the data of the whole asphaltenes and for each of the heavy and light cuts to find the $(T/P)_0$ that best fit the molecular weight data of each cut. Then, the initial number of moles of propagators and terminators were determined for each light and heavy cut based on their molecular weight and $(T/P)_0$. The moles of propagators and terminators in the whole asphaltenes were calculated from each corresponding pair of cuts (*e.g.*, HT80L and HT80H) based on a material balance. The $(T/P)_0$ of the whole asphaltenes from each material balance was compared with the fitted $(T/P)_0$ value. The best fit was taken to be the combination of mole fraction neutrals and $(T/P)_0$ that gave the lowest material balance error.

If the difference between both fitted and calculated values was more than 10%, the monomer molecular weights and the overall *K* value were modified and the procedure was repeated. When the difference was less than 10%, the model was considered to be tuned.

Modeling Molecular Weights Measured in Toluene

Table 5.3 presents the calculated $(T/P)_0$ for all HOS (Heavy Oil Stripper) Bottoms asphaltene cuts, and the fitted value for the whole asphaltenes. The error is less than 7.5% for all of the cuts. The error is reasonable considering the scatter of the molecular weight measurements by VPO (±15%) and the simplifying assumptions used to model asphaltene association. For all other samples, the material balance errors were less than 10%.

Table 5.3. Recalculated $(T/P)_0$ of HOSB asphaltenes

Cut	$(T/P)_0$	Error
Whole	0.170	N/A
HT50	0.181	6.6%
HT80	0.157	7.4%

Figures 5.6 and 5.7 shows the modeled distributions for the HOS Bottoms light cut and heavy cuts, respectively. The model can successfully capture the essential features of asphaltene association including: an increase in molecular weight with increasing concentration, significant association in heavy cuts, and little association in the lightest cut.

Table 5.4 summarizes the input parameters of the terminator-propagator model for the samples that were characterized in toluene. The Short Residue has larger monomer molecular weights, and lower neutral content than the B3VB sample but a similar association constant. A possible reason for these differences is that the Short Residue and B3VB were distilled from bitumen from different source reservoirs. The molecular weight data for the thermocracked sample, X-

1357 (17 wt% thermocracked), were almost identical to its feedstock, B3VB, and consequently the model parameters for these two samples are identical. Hydrocracking appears to increase the number of neutrals and decrease monomer molecular weights with a net effect of reducing self-association.

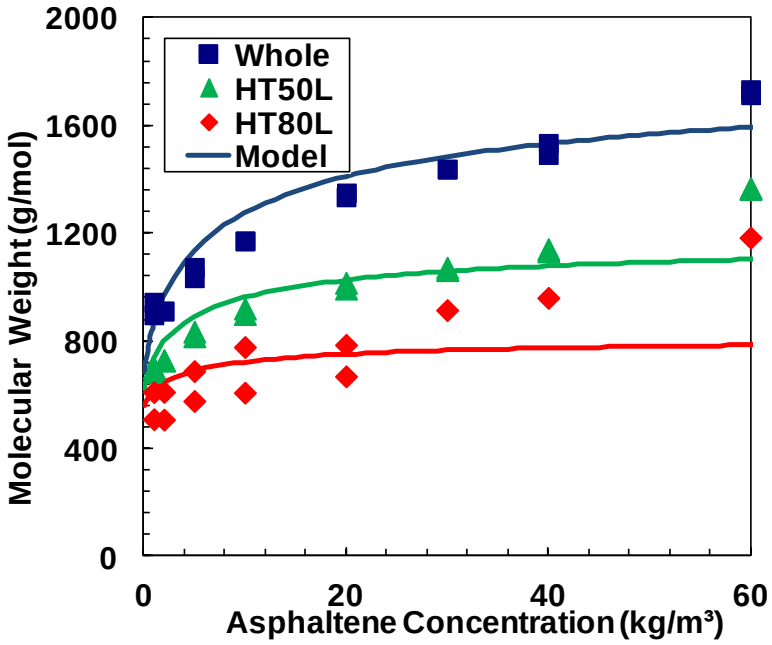

Figure 5.6. Fitting of molecular weight data using the terminator-propagator model for light cuts and whole HOSB asphaltenes.

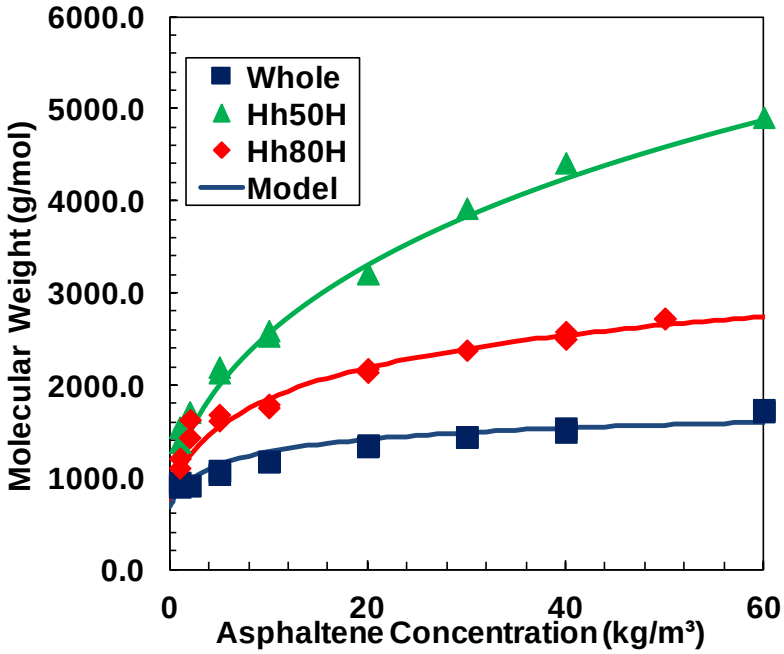

Figure 5.7. Fitting of molecular weight data using the terminator-propagator model for heavy cuts and whole HOSB asphaltenes.

Table 5.4. Input parameters of the terminator-propagator model for samples characterized in toluene

Sample	MW_P (g/mol)	MW_T (g/mol)	MW_N (g/mol)	$(T/P)_0$	K (1/mol)	Mole Frac. N-monomers	Mass Frac. N
B3VB	1200	800	800	0.095	38000	0.125	0.089
X-1357	1200	800	800	0.095	38000	0.125	0.089
Short Residue	2000	1500	1500	0.250	35000	0.072	0.058
HOSB	750	450	450	0.170	7500	0.265	0.187

Modeling Molecular Weights Measured in o-Dichlorobenzene

As mentioned earlier, the heaviest cuts of some samples were not soluble in toluene but were soluble in o-dichlorobenzene (DCB). However, DCB reduces self-association. Figure 5.8 shows

that the molecular weights for whole asphaltenes from B3VB and HOS Bottoms in DCB are substantially less than in toluene (TOL). Therefore, a method is required to convert molecular weights measured in DCB to equivalent molecular weights in toluene.

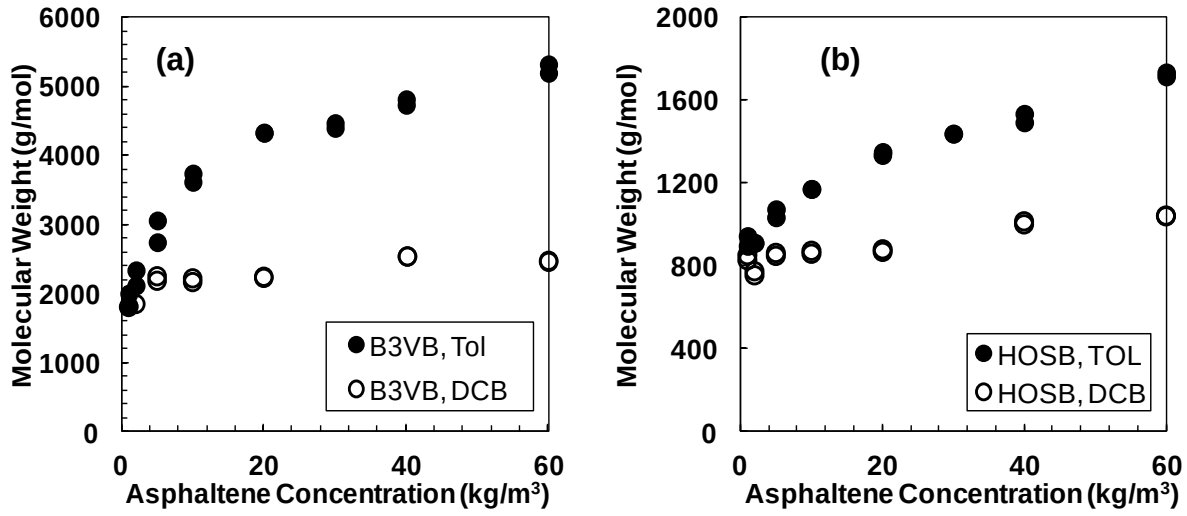

Figure 5.8. Effect of solvent on molecular weight data of whole asphaltenes: a) PRVB, b) HOSB.

First the molecular weight distributions in DCB were constructing following the same methodology for self-association modeling as used for toluene. Table 5.5 presents the input parameters of the terminator-propagator model that best fit the molecular weight data of different samples. Comparing the fit parameters of B3VB and HOSB in toluene with those in DCB, the only differences are between the K and $(T/P)_0$ values. Monomer molecular weights of terminators, propagators, and neutrals as well as the mass fraction of neutrals are the same in both solvents.

Table 5.5. Input parameters of the terminator-propagator model for samples characterized in o-dichlorobenzene

Sample	MW_P (g/mol)	MW_T (g/mol)	MW_N (g/mol)	$(T/P)_0$	K (1/mol)	Mole Frac. N-monomers	Mass Frac. N
B3VB	1200	800	800	0.45	20000	0.117	0.089
X-1359	1000	800	800	0.49	15000	0.120	0.104
X-1360	1000	800	800	0.62	12000	0.157	0.134
HOSB	750	450	450	0.68	5000	0.243	0.187
RHC-18-19	800	700	700	0.62	5000	0.235	0.219
RHC-18-37	650	450	450	0.74	5000	0.240	0.228

Molecular weight data were collected in both solvents for the B3VB and HOSB samples. The ratios of the *K* value in toluene to the *K* value in DCB were determined and were 1.9 and 1.5, respectively. An average ratio of 1.7 was assumed to apply to all other thermocracked samples. For hydrocracked samples, it was observed that all the *K* values in DCB were 5000 (1/mol), Table 5.5. Therefore, the ratio of 1.5 found for the HOSB sample was used for all of the hydrocracked samples. Once the *K* values were determined, the $(T/P)_0$ was found by fitting the molecular weight data of the whole asphaltenes for each sample. Table 5.6 reports the toluene equivalent model parameters calculated from the DCB data.

Table 5.6. Toluene equivalent input parameters of terminator-propagator model

Sample	MW_P (g/mol)	MW_T (g/mol)	MW_N (g/mol)	$(T/P)_0$	K (1/mol)	Mole Frac. N-monomers	Mass Frac. N
X-1359	1000	800	800	0.090	25000	0.125	0.104
X-1360	1000	800	800	0.095	20000	0.165	0.134
RHC-18-19	800	700	700	0.140	7500	0.240	0.219
RHC-18-37	650	450	450	0.400	7500	0.280	0.228

5.2.3 Determining the Continuous Molecular Weight Distribution

Once the parameters of the terminator-propagator model were adjusted and mass balance of all the aggregates was achieved, the molecular weight distributions were determined. However, the output of the model was a discrete distribution of mass fractions for the aggregates that were integer multiples of the monomer molecular weight. A smooth continuous distribution is more realistic given that there is likely a range in monomer molecular weights. Therefore, the discrete distribution was converted into a continuous distribution.

The cumulative mass based molecular weight distribution was fitted with Equation 4.1 using the least squares method. Figure 5.9 shows the fitting to the modeled HOSB whole asphaltenes. Note, the neutrals were assumed to have a uniform molecular weight and cause a step change at the beginning of the distribution. There is a slight deviation in the fitting at lower molecular weights because the step change could not be perfectly matched. Nonetheless, the error of fitting was less than 3% in all cases. The parameters of the fitted Equation 4.1 are presented in Table 5.7.

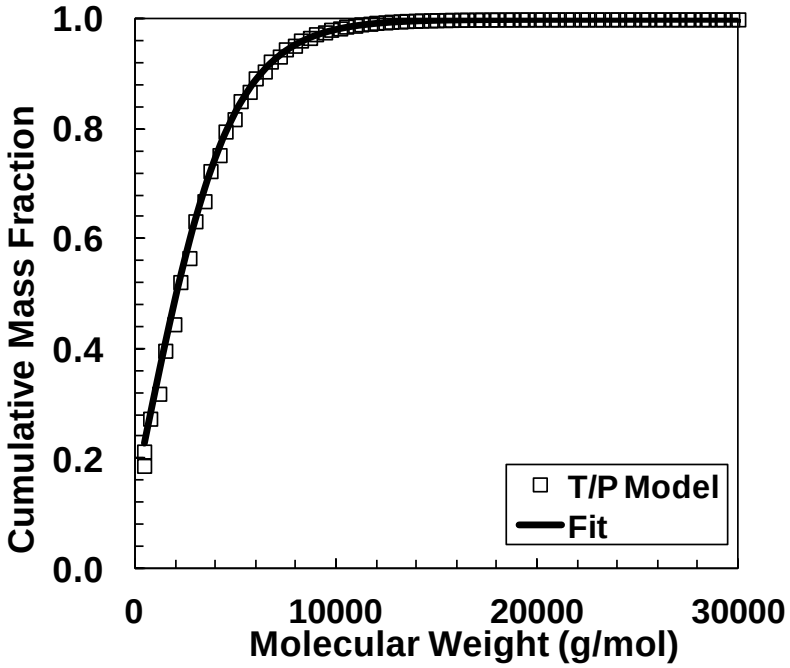

Figure 5.9. Cumulative mass fraction of HOSB asphaltene at 50 °C.

Table 5.7. Fitting parameters of cumulative mass fraction function of samples at 50°C

Sample	A g/mol	B	C	D g/mol	$MW_{av\ @\ 50°C}$ g/mol	$MW_{cumf=0}$ g/mol	MW_{mono} g/mol	MW_{final} g/mol
B3VB	180.4	0.08585	7.528×10^{-5}	799.9	3680	799.9	1078	50000
X-1357	200.2	0.09885	7.528×10^{-5}	799.9	3400	799.9	1078	50000
X-1359	200.2	0.12964	9.998×10^{-5}	799.9	2800	799.9	939	50000
X-1360	120.2	0.18547	1.129×10^{-4}	799.9	2280	799.9	933	45000
Short	32.2	0.09148	7.793×10^{-5}	1499.9	4950	1499.9	1868	60000
RHC-18-19	20.6	0.27107	2.224×10^{-4}	699.9	1460	699.9	760	20000
HOSB	95.3	0.21779	2.316×10^{-4}	449.9	1170	449.9	625	20000
RHC-18-37	23.6	0.35991	3.518×10^{-4}	449.9	890	449.9	564	15000

In order to prepare frequency, as opposed to cumulative, distributions for input into the regular solution model, cumulative distributions were calculated between the average monomer molecular weight, MW_{mono}, using Equation 4.4 and a maximum value, MW_{final}, that accounted for more than 99% of the aggregated molecules, as reported in Table 5.7. Then, the molecular weights between these two values were divided into 40 fractions of constant step size, and the distribution function was determined for each interval. The mass fraction for each interval, w_i, was calculated as:

$$w_i = cumf_i - cumf_{i-1} \tag{5.2}$$

where, *cumf* is the value of distribution function, and i is the number of the component. The average molecular weight of i^{th} interval was calculated as follows:

$$MW_{av,i} = \frac{MW_i + MW_{i-1}}{2} \tag{5.3}$$

For the first interval the average molecular weight was calculated as the average between the molecular weight when the cumulative function is zero ($MW_{cumf=0}$) and the average monomer molecular weight. The average molecular weight of distribution was then determined as:

$$MW_{avg} = \sum_{i=1}^{40} \frac{w_i}{MW_{av,i}} \tag{5.4}$$

The average molecular weight of these distributions are reported in Table 5.7; these values match with the experimentally measured molecular weights at 10 kg/m^3. Figure 5.10 shows the molecular weight distributions for HOSB at 50 °C.

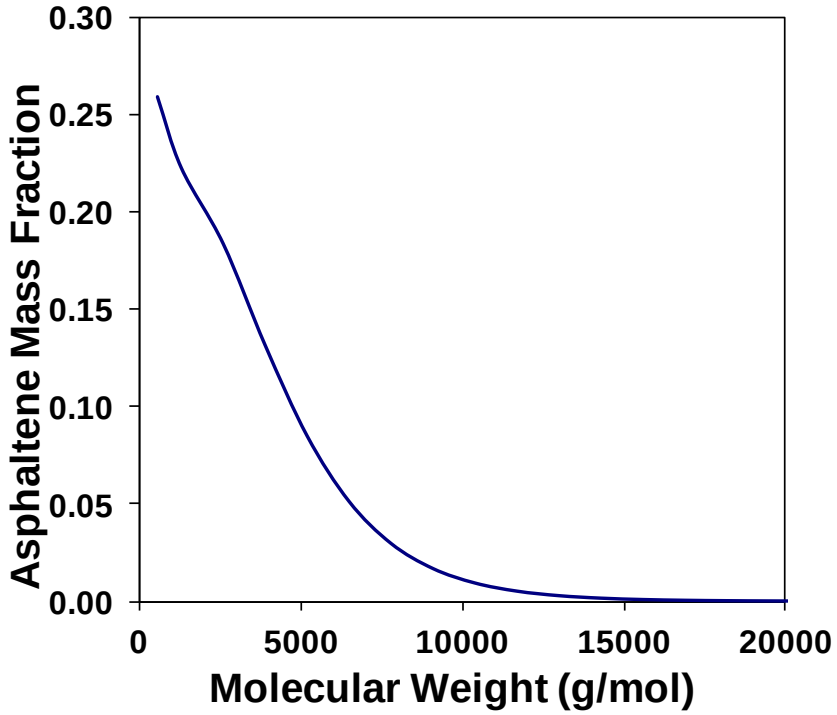

Figure 5.10. Molecular weight distribution of HOSB asphaltenes at 50°C.

Regular solution theory was used to model asphaltene precipitation at room temperature, 23 °C, so it is necessary to correct the molecular weight data to room temperature. In a parallel study, (Ortiz, 2014) found that temperature had no effect on the molecular weight (aggregation) of hydrocracked asphaltenes but it did alter the molecular weight of native and thermocracked asphaltenes. Therefore, the molecular weight distribution of hydrocracked samples at 23°C were assumed to be the same as the distributions measured at 50°C. The molecular weights of native and thermocracked samples were corrected to room temperature as follows (Ortiz, 2014):

$$MW_{23} = MW_{50}\exp(0.0073 \times (50 - 23)) \tag{5.5}$$

The methodology of calculating molecular weight distributions at 23°C is identical to the previous section. After correcting the molecular weight data to account for the temperature effect, $(T/P)_0$ was the only parameter that changed until the average molecular weight of the distribution corresponded to the corrected value at 23°C. Once $(T/P)_0$ was determined and mass fractions of aggregates were calculated, Equation 4.1 was again used to fit the cumulative function. Molecular weight distributions along with average molecular weight at corrected temperature were calculated in a same way as shown previously. Table 5.8 summarizes the fitting parameters to cumulative distribution data, average molecular weight of distributions, and $(T/P)_0$ at 23°C for each sample. Figure 5.11 shows that, as expected, the increase of average molecular weight from 3680 to 4480 g/mol for the B3VB sample gives a broader molecular weight distribution.

Table 5.8. Fitting parameters of cumulative mass fraction function of samples at 23 °C

Sample	A g/mol	B	C	D g/mol	$MW_{av\ @\ 23°C}$ g/mol	$(T/P)_{0\ @\ 23°C}$
B3VB	140.1	0.06468	5.806×10^{-5}	799.9	4480	0.005
X-1357	145.6	0.07380	6.166×10^{-5}	799.9	4200	0.025
X-1359	200.2	0.08853	8.068×10^{-5}	799.9	3420	0.010
X-1360	205.2	0.13389	9.431×10^{-4}	799.9	2780	0.020
Short Residue	140.6	0.05327	6.441×10^{-5}	1499.9	6000	0.150

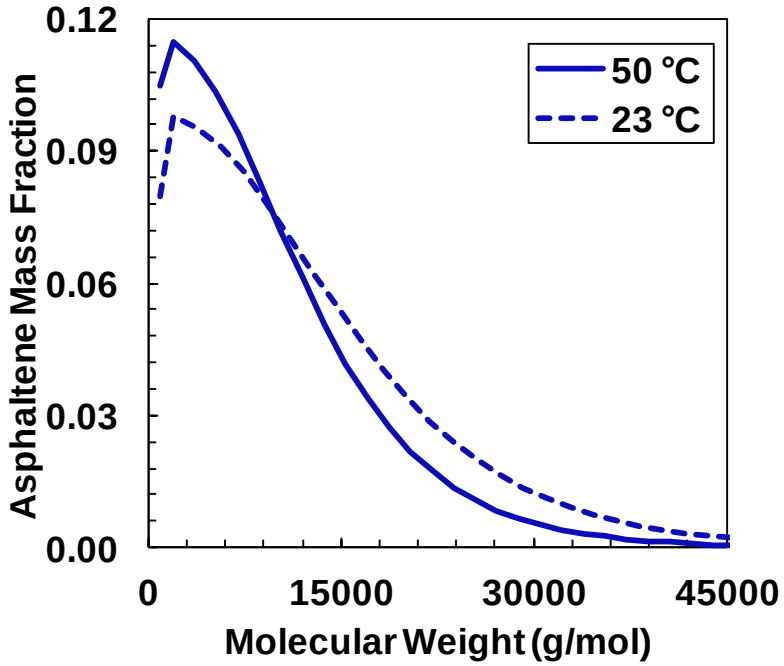

Figure 5.11. Molecular weight distributions of B3VB asphaltenes at 23 and 50 °C.

Figures 5.12 and 5.13 compare molecular weight distributions of reacted samples and their feeds. B3VB and Short Residue are both native samples and have similar molecular weight distributions. Thermocracking had a relative effect on the asphaltene molecular weight distribution, Figure 5.12. The average molecular weight decreased with increasing conversion and the distributions narrowed. Nonetheless, the maximum molecular weights remained at approximately 40,000 g/mol. Most of the difference can be attributed by the increased amount of neutrals at higher conversion. Thermocracking appears to enrich the proportion of neutrals in the asphaltene fraction but does not significantly alter asphaltene self-association. Recall that thermocracking cleaves side chains. This process may create some poorly soluble aromatic cores that do not self-associate (neutrals) but leave many of the asphaltenes still able to associate. Gray *et al.* (2011) noted that there are several possible mechanisms for asphaltene association some of

which involve the side chains or functional groups on the side chains. Hence, removal of side chains may reduce self-association for some asphaltenes. Alternatively, some aromatic cores could aggregate into coke and no longer report to the asphaltenes.

Hydrocracking significantly alters the molecular weight distributions, Figure 5.13. The average molecular weight decreases substantially with increasing conversion, the distributions narrow, and the maximum molecular weight of the distributions shift from 50,000 to approximately 15,000 g/mol. The amount of neutrals also increased significantly. While hydrocracking increases the amount of neutrals, it also appears to significantly reduce asphaltene self-association. Recall that hydrocracking not only cleaves side chains but also removes heteroatoms through hydrogenolosis and hydrodemetallization (Yves Huc, 2011). The strong effect of hydrocracking on association suggests that the heteroatomic groups play a significant role in association.

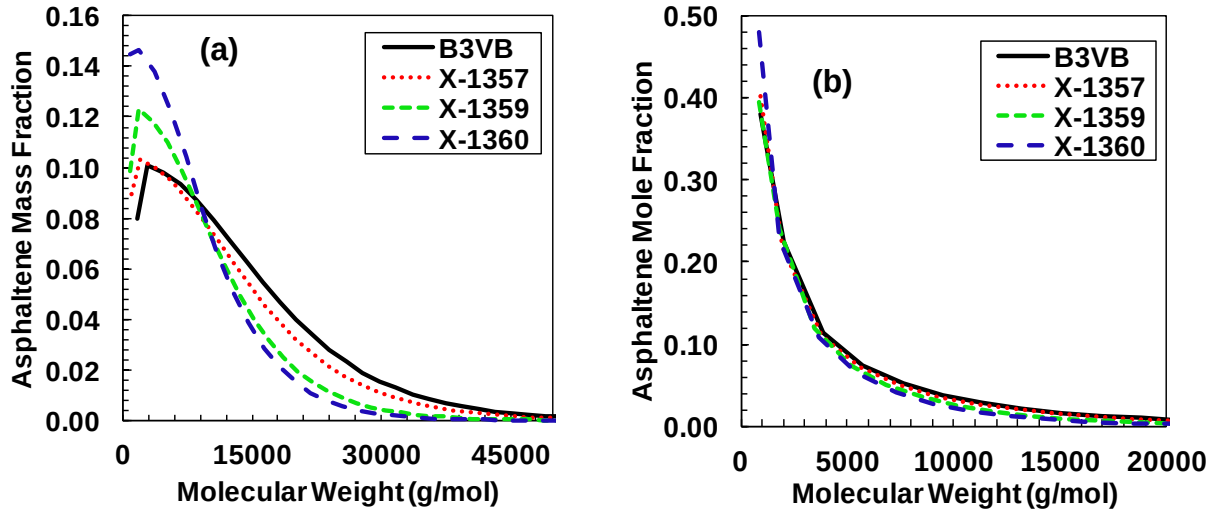

Figure 5.12. Molecular weight distributions of B3VB feed asphaltenes and thermocracked asphaltenes: a) mass basis, b) mole basis.

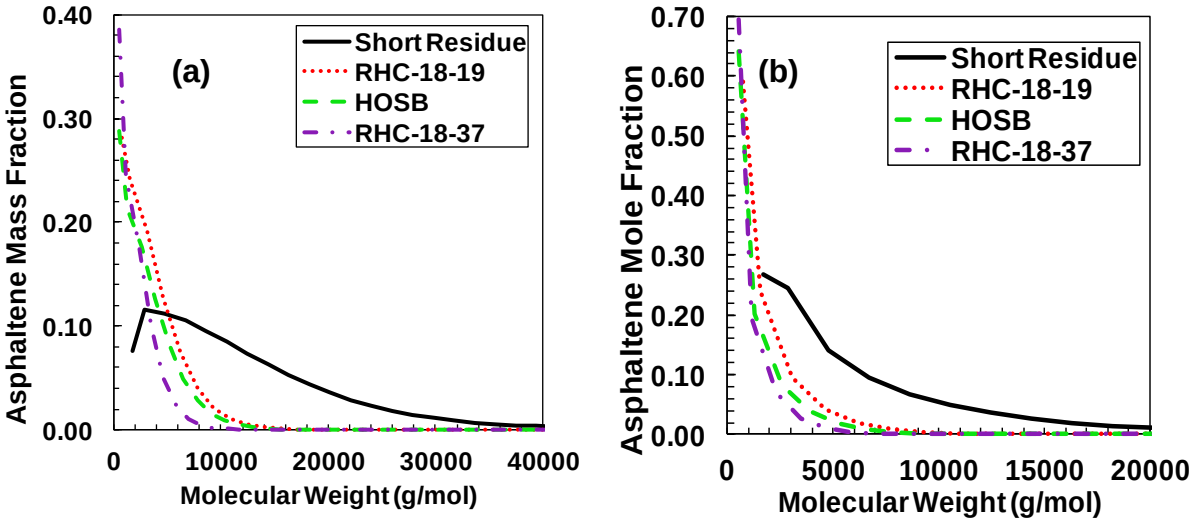

Figure 5.13. Molecular weight distributions of Short Residue feed asphaltenes and hydrocracked asphaltenes: a) mass basis, b) mole basis.

5.2.4 Representing Molecular Weight Distributions with a Gamma Function

While the self-association model is based on all of the available data, it is not practical for most implementations where such data are not available. The Gamma distribution requires less parameters, is easier to implement, and can be tuned to fit typically encountered molecular weight distributions. Therefore, the Gamma distribution was tuned to fit the self-association model distributions.

The parameters required for the Gamma distribution are the average molecular weight, the minimum molecular weight (monomer molecular weight), MW_{final}, and shape factor, β. The average molecular weight in the gamma distribution was the experimentally measured value at asphaltene concentration of 10 kg/m^3 in toluene. The MW_{mono} was taken from Table 5.7. The

MW_{final} and β values were adjusted to match the distributions calculated from the self-association model and are reported in Table 5.9.

Figure 5.14 compares examples of molar frequency distributions for B3VB and HOSB asphaltenes generated by the gamma and terminator-propagator models. The distributions are similar because both have the same average molecular weight. However, the gamma distribution cannot accurately represent the spike corresponding to the large mole fraction of neutrals all at the beginning of the distribution. Therefore, there is a small mismatch between the distributions particularly at lower molecular weights. The same behavior was observed for the rest of samples.

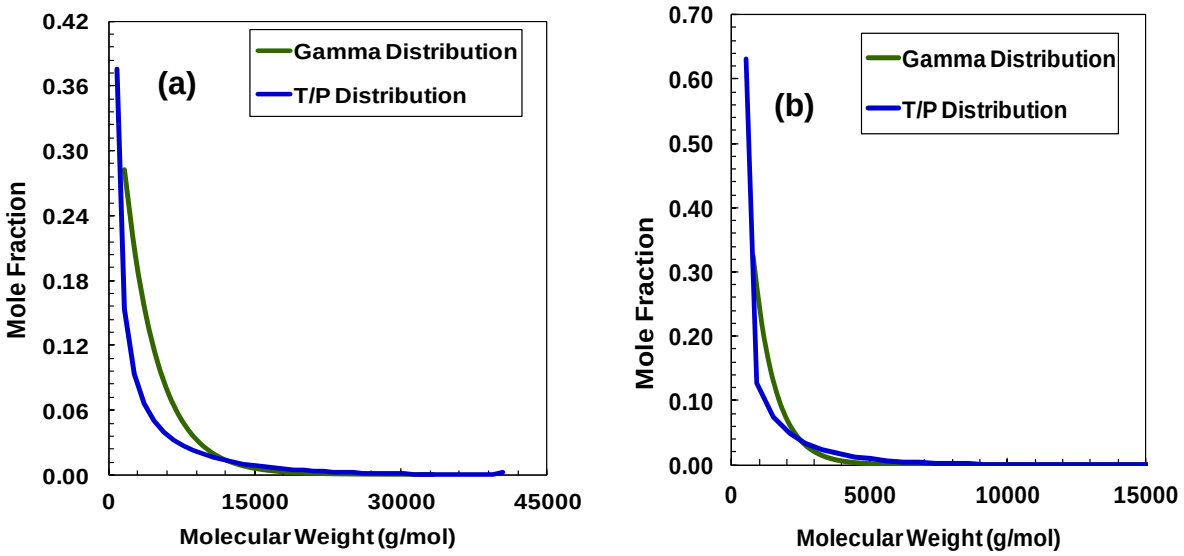

Figure 5.14. Differences between the gamma and terminator and propagator distributions for a) B3VB and b) HOSB asphaltene

Table 5.9. Input parameters of the gamma distributions for different samples

Param.	B3VB	X-1357	X-1359	X-1360	Short Residue	RHC-18-19	HOSB	RHC-18-37
MW_{final}	40000	25000	25000	20000	40000	10000	10000	5000
β	1.0	1.0	1.0	1.0	1.0	1.0	1.0	1.0

5.3 Density Distributions

Figure 5.15 shows the density of whole asphaltenes for thermocracked (left) and hydrocracked (right) samples. For both thermocracking and hydrocracking processes, the asphaltene density increased with increasing conversion. Thermocracking increased the density from 1180.8 kg/m³ for the B3VB feedstock to 1249.0 kg/m³ at 51 wt% conversion. Hydrocracking increased the density from 1121.0 kg/m³ for the Short Residue to 1247.3 kg/m^3 for conversions above 80 vol%.

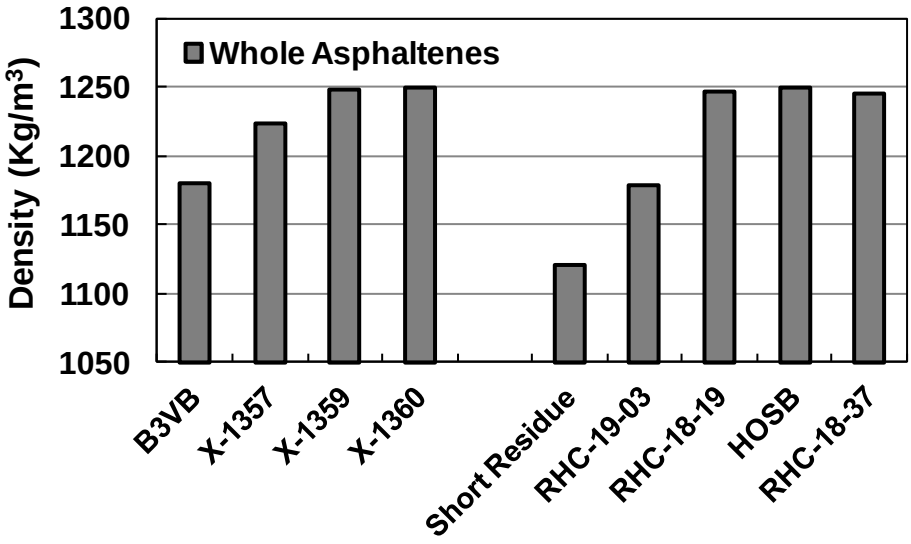

Figure 5.15. Density of whole asphaltenes for the feeds, thermocracked (left) and hydrocracked (right) samples

Density distributions of asphaltenes were determined from the density of the asphaltene solubility cuts. As noted in Chapter 3, a regular solution mixing rule (Equation 3.5) or an excess volume mixing rule must be selected (Equation 3.10). Sanchez (2012) and Okafor (2012) found

that for distillation fractions, saturates, aromatics and resins, an excess volume mixing rule was required (Equation 3.10). They found that the value of the binary interaction parameter of the fraction correlated to the normalized difference in specific volumes of the two components. This correlation suggested that asphaltenes would form irregular solutions in toluene.

However, the density data for asphaltenes in solutions of toluene and of DCB contradict this hypothesis. Densities were calculated from data for each solvent using the regular solution mixing rule. In all cases where densities were measured in both solvents, the asphaltene densities calculated from each solvent dataset were in excellent agreement, Figure 5.16. It is possible that there are excess volumes in both solvents that coincidentally extrapolate to the same end point but it is far more likely that the asphaltene form regular solutions. Note, aromatic solubility fractions also form nearly regular solutions in toluene. It appears that aromatic crude oil components (aromatic, resin, and asphaltene fractions) all form nearly ideal solutions in aromatic solvents. Therefore, all of the density data were fitted with the regular solution mixing rule, Equation 3.5.

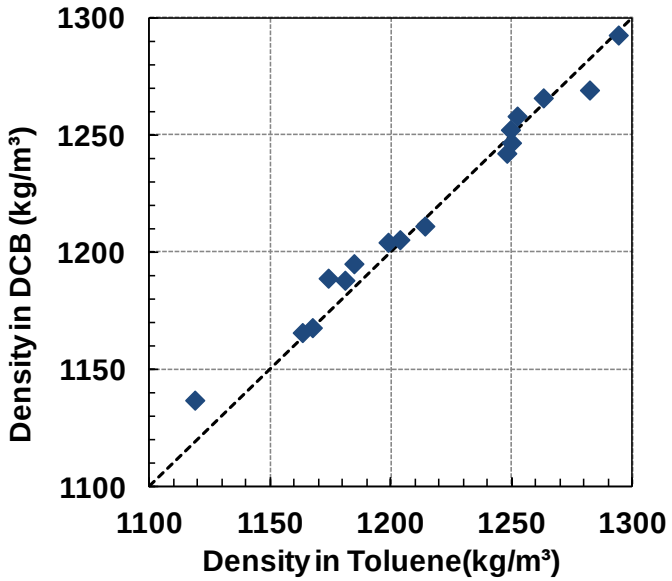

Figure 5.16. Comparison of densities measured in toluene and o-dichlorobenzene (DCB) for B3VB and HOSB whole asphaltenes and their different solubility cuts.

Figure 5.17 shows the density of light and heavy cuts of B3VB and HOSB asphaltenes as a function of mass fraction of the whole asphaltenes. Recall, that the heaviest (with highest molecular weight) asphaltenes precipitate first and the lightest (lowest molecular weight) asphaltenes precipitate last. Hence, the density of a light cut is the average density of asphaltenes from zero to the cumulative mass fraction of the cut. The density of heavy cut is an average density of asphaltene components from the starting cumulative mass fraction of the cut to a mass fraction of one.

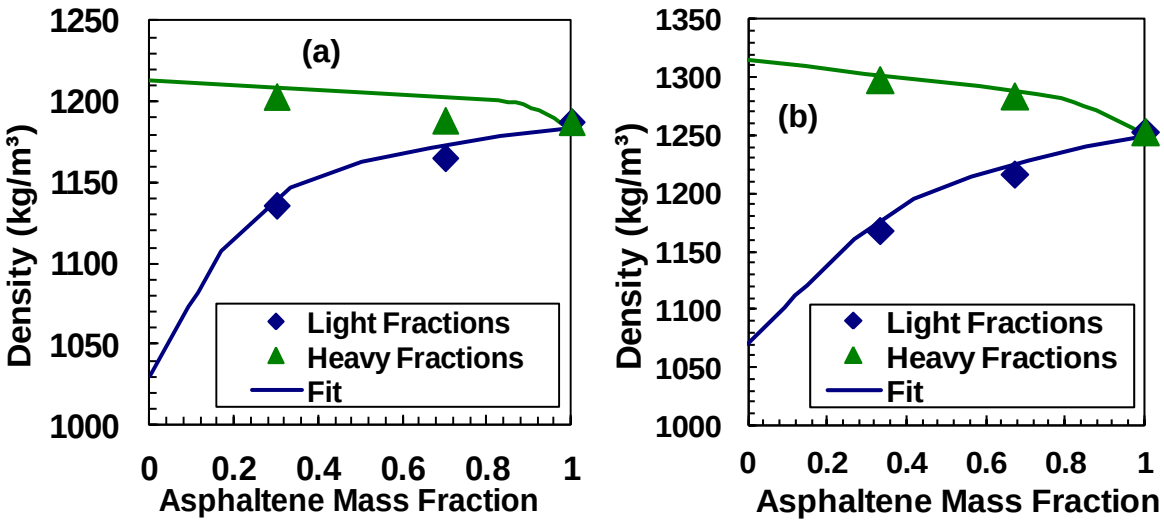

Figure 5.17. Density of light and heavy fractions of: a) B3VB, b) HOSB.

To calculate density distribution in the asphaltene continuum, the first step is determining the incremental density from one cut to the next cut. The increment in mass fraction of the i^{th} light cut, w_i, was calculated as follows:

$$w_i = cumw_i - cumw_{i-1} \tag{5.6}$$

where $cumw_i$ is the experimentally measured cumulative mass fraction of the asphaltenes. For the first cut, $cumw_{i-1}$ is equal to zero. Then, the average mass fraction $\overline{w}_i$ for each increment was calculated as:

$$\overline{w}_i = \frac{w_{i-1}+w_i}{2} \tag{5.7}$$

For the first cut, w_{i-1} is equal to zero. The density of each increment was calculated from the density of each cut from a regular solution mixing rule as follows:

$$\rho_{inc,i} = \frac{\frac{w_i}{w_i+w_{i-1}}}{\frac{1}{\rho_i} - \frac{\frac{w_{i-1}}{w_i+w_{i-1}}}{\rho_{i-1}}} \tag{5.8}$$

For the first cut $\rho_{inc,i} = \rho_i$. A similar procedure was applied for the heavy cuts.

Figure 5.18 shows the increment density calculated from both light and heavy cuts for PRVB and HOSB asphaltenes. Barrera (2012) used two continuous linear density functions to fit increment densities and the densities of light cuts were calculated using the following equations:

$$\bar{\rho}_{sol} = \frac{\int_0^{w_i} dw}{\int_0^{w_i} \frac{1}{\rho(w)} dw} \quad \text{and} \quad \rho(w) = a_L \times w + b_L \tag{5.9}$$

$$\bar{\rho}_{sol} = \frac{a_L w_i}{\ln(\frac{a_L w_i + b_L}{b_L})} \tag{5.10}$$

where a_L, and b_L, are constants for the light cuts. The density of heavy cuts was calculated as follows:

$$\bar{\rho}_{insol} = \frac{\int_{w_i}^{1} dw}{\int_{w_i}^{1} \frac{1}{\rho(w)} dw} \tag{5.11}$$

$$\bar{\rho}_{insol} = \frac{a_H(1-w_i)}{\ln(\frac{a_H + b_H}{a_H w_i + b_H})} \tag{5.12}$$

where a_H, and b_H, are constants for the heavy cuts. The cut densities determined with Equations 5.10 and 5.12 are shown in Figure 5.17.

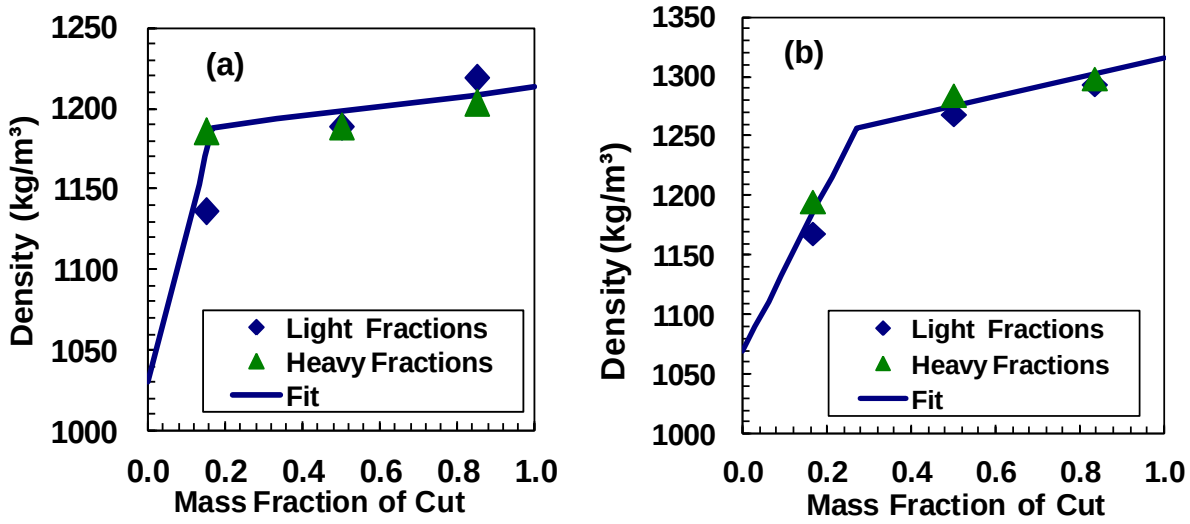

Figure 5.18. Density distribution of a) B3VB and b) HOSB asphaltenes using a linear equation.

In this thesis, an exponential function was used instead of two linear functions to reduce the number of fitting parameters. The following form of density distribution function was assumed:

$$\rho = a + b(1 - \exp(-cw)) \tag{5.13}$$

where *a*, *b*, and *c* are constants. The density of the light and heavy cuts is then calculated as follows:

$$\bar{\rho}_{sol} = \frac{w}{\frac{1}{a'c}\ln\left(\frac{a'e^{cw}-b}{a'-b}\right)} \tag{5.14}$$

$$\bar{\rho}_{insol} = \frac{1-w}{\frac{1}{a'c}\left(\ln\left(\frac{a'e^{c}-b}{a'e^{cw}-b}\right)\right)} \tag{5.15}$$

where, *a'* = *a*+*b*. Figure 5.19 shows the fit of the new correlations for HOSB asphaltene density.

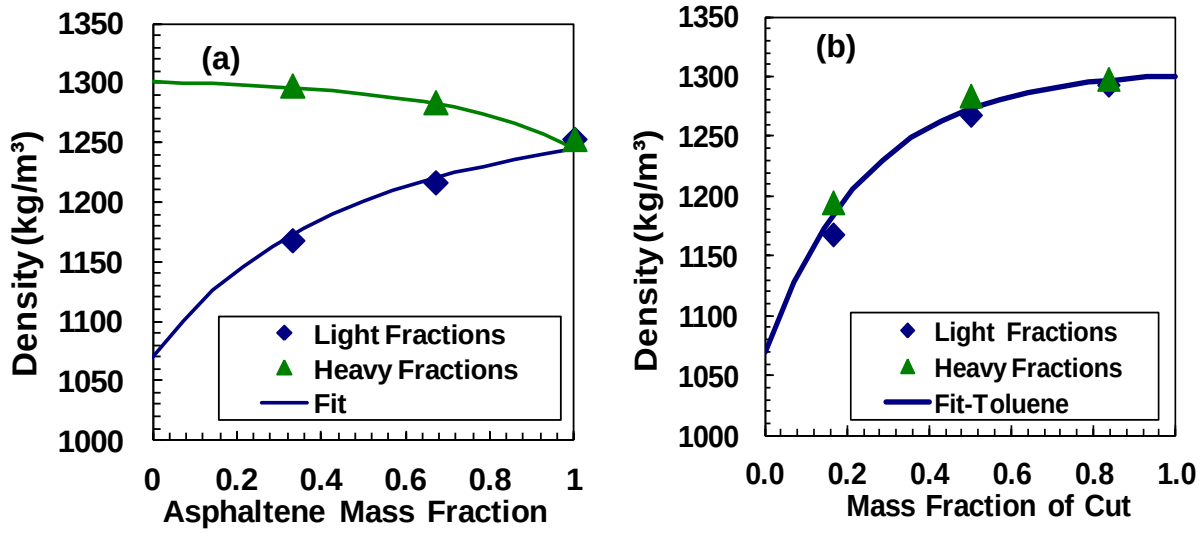

Figure 5.19. HOSB asphaltene densities calculated from Equation 5.13 (a) density of cuts, and (b) density distribution.

Asphaltenes density distributions consist of two distinct parts: a steep rise in the lower mass fractions followed by a plateau section at higher mass fraction. The steep rise corresponds to the lightest and lowest molecular weight cuts where little or no self-association was observed in the molecular weight data. The plateau section corresponds to those cuts which exhibited noticeable self-association. Therefore, it is likely that the asphaltenes which do not self-associate are found in the most soluble and lightest cut of asphaltenes. This non-associating part of asphaltenes are the neutrals and must also be considered in mass balance calculations.

The lower end of density distribution is expected to be close to the density of the resins because asphaltenes are part of a continuum of species from aromatics through the resins to the asphaltenes. The plateau at the upper end of the distribution indicates that self-association produces uniform density aggregates. The density of an aggregate appears to be an average of the

density of the monomers that make up the aggregate. Therefore, aggregates tend to have the same density and the average density of each cut containing predominantly aggregated asphaltenes is the same.

Table 5.10 presents the fitting parameters of density distribution function along with the estimated amount of non-associating materials. Figure 5.20 shows the density distributions of thermocracked and hydrocracked samples, along with their respective feeds. The mass fraction of neutrals are slightly higher than the values determined from the molecular weight data but there is considerable uncertainty with each method. As observed from the molecular weight data, both thermocracking and hydrocracking increase the amount of neutrals.

For both processes, the density of the asphaltenes increases with increasing conversion. However, for the thermocracked samples, the density distributions of X-1359 (30 wt% converted) and X-1360 (50 wt% converted) are similar, suggesting that thermocracking does not change the density beyond approximately 1270 kg/m³. All three hydrocracked asphaltenes (conversions from 50 to 80%) showed similar density distributions also reaching densities of 1270 kg//m³. It appears that 1270 kg/m³ is the upper limit of asphaltene densities in the product of both thermo- and hydrocracking processes.

Table 5.10. Fitting parameters to density distribution data using Equation 5.13 and estimated mass fraction of neutrals.

Sample	a	b	C	Mass Fraction Neutrals (dens)	Mass Fraction Neutrals (MW)
B3VB	1020	180	9.1	0.16	0.09
X-1357	1025	220	9.1	0.17	0.09
X-1359	1085	185	8.0	0.18	0.11
X-1360	1070	205	8.3	0.18	0.14
Short Residue	1045	80	10	0.15	0.06
RHC-18-19	1080	197	5.9	0.22	0.22
HOSB	1070	235	4.0	0.26	0.19
RHC-18-37	1095	194	4.3	0.27	0.23

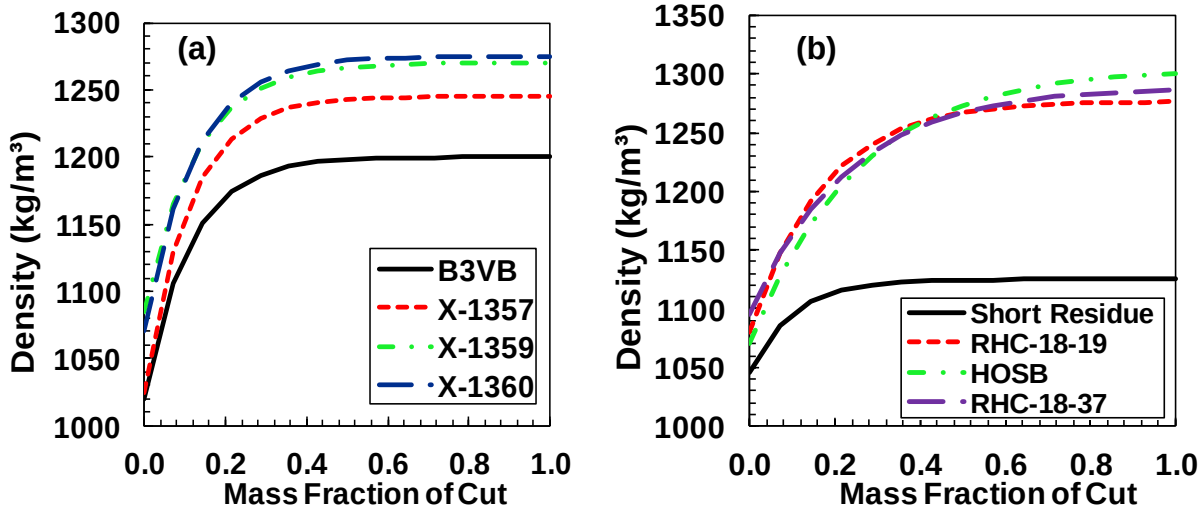

Figure 5.20. Density distributions of feed, thermocracked (a), and hydrocracked (b) asphaltenes.

Note that refractive indices of asphaltene were measured in this thesis for future use as a correlation parameter. Since those results are not employed in final modeling step, all the related data and graphs are provided in the appendices only.

5.4 Correlation of Density to Molecular Weight

Two major inputs to regular solution modeling are molecular weight and molar volume distributions of asphaltenes. Since the definition of molar volume is the ratio of molecular weight over density, it is more convenient to correlate density to molecular weight. Alboudwarej *et al*. (2003) used a power law to relate density to molecular weight as shown in Equation 4.48. Barrera (2012) came up with another expression, Equation (4.49), which was well representative of her own samples. In this thesis, the following equation was employed which is of the same form as Equation 4.49:

$$\rho = \rho_0 + \Delta\rho(1 - \exp(-\frac{MW}{a})) \tag{5.16}$$

where, ρ_0 is the density of lowest for an asphaltene molecule, $\Delta\rho$ is the density difference between lowest and highest molecular weight of asphaltenes, and a is a fitting parameter.

The densities of asphaltene were determined at room temperature and 10 kg/m³ and, therefore, were correlated to the molecular weights corrected to 23°C. Table 5.11 summarizes the fitted parameters of Equation 5.16. However, there is a problem with using this approach. The molecular weight of the asphaltenes depends on concentration and therefore the density distribution at different concentrations and molecular weight distributions will be predicted to change although it is in fact constant. To avoid this issue, the density distribution as a function of

asphaltenes mass fractions (Equation 5.13) was used as an alternative method to input the density distribution into the regular solution model.

Table 5.11. Parameters and fit coefficient for the density correlation in equation 5.16

Sample	P_0	$\Delta\rho$	a
B3VB	1035	170	3000
X-1357	1035	220	2400
Short Residue	1040	85	22400
HOSB	1070	240	1000

5.5 Solubility Parameter Distributions

The regular solution modeling methodology described in Chapter 4 was applied to model the fractional yield of asphaltenes for all the samples considered in this thesis. Note, in previous work (Barrera *et al*, 2013), asphaltene density was correlated to molecular weight but, in this thesis, density is correlated to the mass fraction of asphaltenes. Two types of molecular weight distributions were employed: 1) the Gamma distribution, and 2) the distribution from the terminator-propagator model. Recall that the self-association is based on the most data while the Gamma distribution requires less parameters and is easier to implement. The inputs to the respective distributions were provided in Tables 5.7 and 5.8, and Table 5.9.

Once the densities and molecular weights are set, the only unknown is the solubility parameter of the asphaltenes. The coefficients of the solubility correlation, Equation 4.57, were adjusted to fit the yield data. The equation is reproduced below for convenience.

$$\delta = (A\rho(cMW)^d)^{1/2} \quad (4.57)$$

where *c* and *d* are the fitting parameters.

5.5.1 Results with Density as a Function of Molecular Weight (ρ = f(MW))

Modeling with density as a function of molecular weight was performed only to compare with previous work and only four samples were evaluated for this purpose. Table 5.12 reports the values of parameters *c* and *d* in the solubility correlation when density is considered to be a function of asphaltene molecular weight. Figures 5.21 to 5.24 show the model fits to the yield curves for the samples in Table 5.12. Barrera (2012) found that all native asphaltenes could be modeled with a *d* parameter of 0.0495 and a *c* parameter equal to 0.632 for terminator-propagator distributions and 0.643 for gamma distributions. In this thesis, native asphaltenes (B3VB and Short Residue) also have a *d* of 0.0495 and *c* values which are similar to those from Barrera (2012). However, the more reacted samples (X-1357 and HOSB) have higher *d* values and lower *c* values to match the much broader asphaltene solubility curves.

Both the association model and Gamma distributions fit the precipitation data with little deviation at lower concentrations of *n*-heptane. At higher concentrations (corresponding to the lightest fractions of asphaltenes), the gamma function provided a better fit than the terminator-propagator distribution. This deviation is greatest for the most reacted samples. These samples have more neutrals and it is likely that the solubility parameter distributions of the neutrals would have to be accounted for separately to obtain a better fit. However, there are insufficient data to justify such an approach.

Table 5.12. Fitting parameters used to calculate solubility parameter using Equation 5.16 as density correlation.

Sample	T/P Distribution		Gamma Distribution	
	c	***d***	***c***	***d***
B3VB	0.636	0.0495	0.665	0.0495
X-1357	0.434	0.0900	0.425	0.1000
Short Residue	0.660	0.0495	0.660	0.0495
HOSB	0.547	0.0800	0.465	0.1100

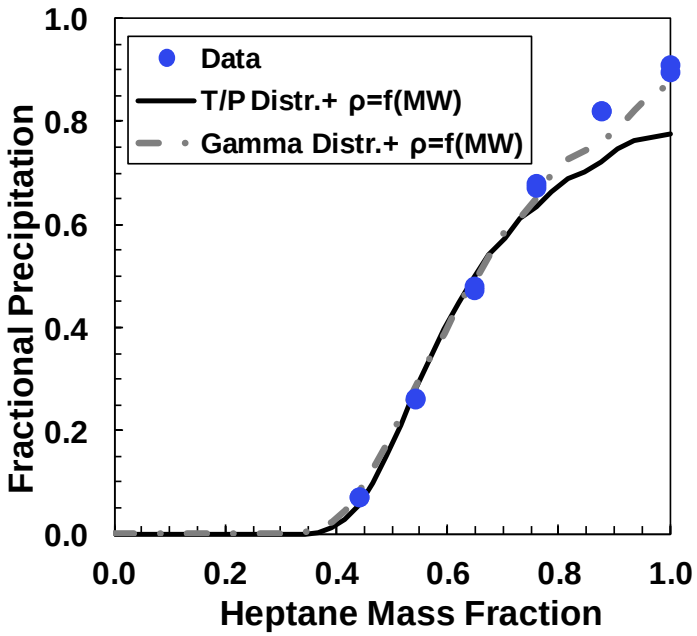

Figure 5.21. Model predictions for fractional yield of B3VB asphaltenes from solutions of *n*-heptane /toluene at 23 °C.

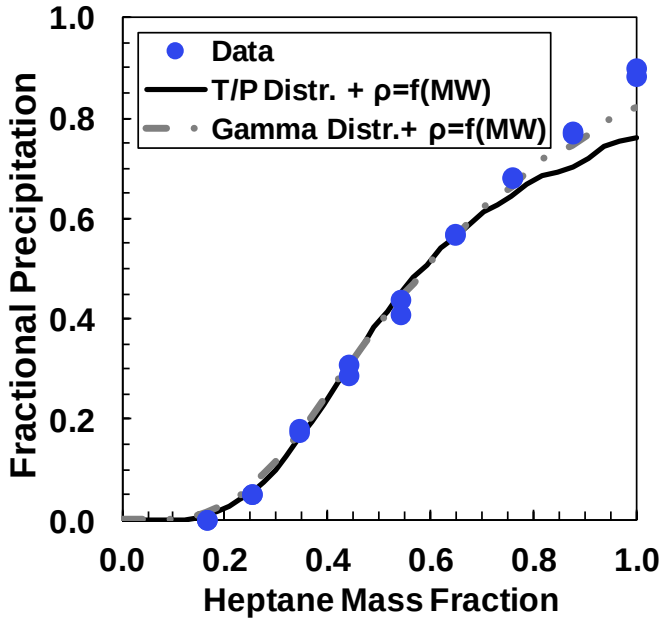

Figure 5.22. Model predictions for fractional yield of X-1357 asphaltenes from solutions of *n*-heptane /toluene at 23 °C.

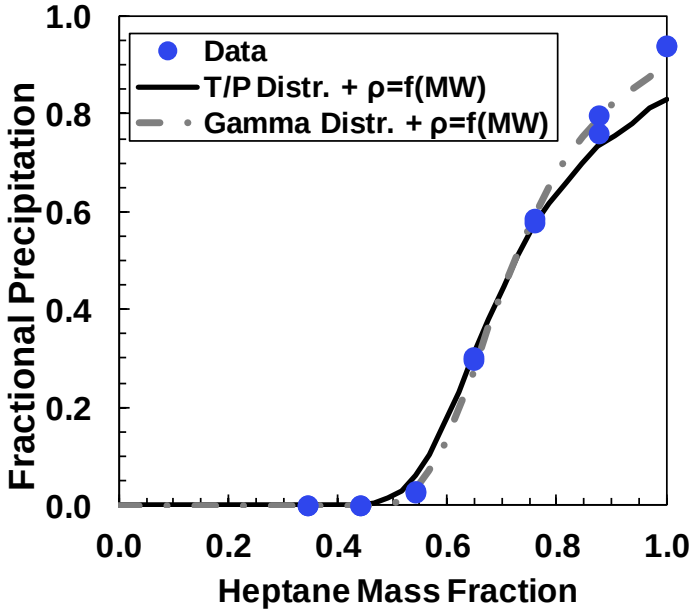

Figure 5.23. Model predictions for fractional yield of Short Residue asphaltenes from solutions of *n*-heptane /toluene at 23 °C.

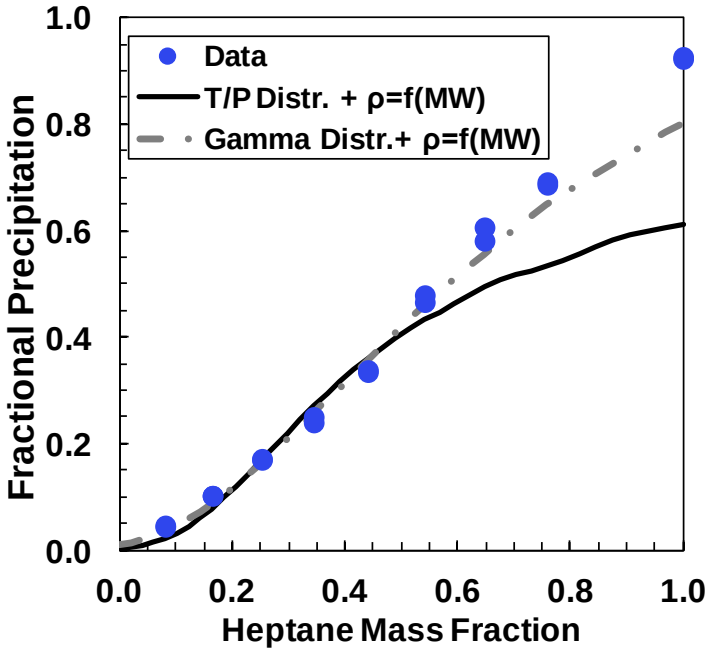

Figure 5.24. Model predictions for fractional yield of HOSB asphaltenes from solutions of *n*-heptane /toluene at 23 C.

5.5.2 Results with Density as a Function of Mass Fraction (ρ = f(w))

Table 5.12 presents fitting parameters for the solubility correlation for all of the samples when the density distribution is input as a function of the asphaltene cumulative mass fraction. Figures 5.25 to 5.28 show the modeling results for thermocracked and hydrocracked samples. The fitted values of *c* and *d* are similar to those from Section 5.5.2 because at 23°C and 10 kg/m³ asphaltene concentration both methods give essentially the same distribution. As before, the reacted samples had lower *c* and higher *d* values than their feedstocks. However, increasing conversion showed an opposite trend with the c value increasing and the d value decreasing with higher conversion. These trends may be an artifact caused by lumping the neutrals with the associated asphaltenes in the characterization.

The Gamma distribution fit the solubility of asphaltene with little deviation both for thermocracked and hydrocracked asphaltenes. However, when using the terminator-propagator distribution, the model under-predicts the precipitation data for reacted samples, particularly the hydrocracked asphaltenes. In general, the gamma distribution adequately represents the molecular weight distributions for both native and reacted asphaltenes and better fits asphaltene yield data.

Table 5.13. Fitting parameters utilized to calculate solubility parameter using Equation 5.13 as density function.

Sample	**T/P Distribution**		**Gamma Distribution**	
	c	***D***	***c***	***D***
B3VB	0.635	0.0495	0.655	0.0495
X-1357	0.395	0.1000	0.384	0.1100
X-1359	0.422	0.1000	0.365	0.1200
X-1360	0.468	0.0900	0.389	0.1200
Short Residue	0.660	0.0495	0.660	0.0495
RHC-18-19	0.555	0.0800	0.355	0.1400
HOSB	0.527	0.0850	0.398	0.1300
RHC-18-37	0.540	0.0900	0.291	0.1800

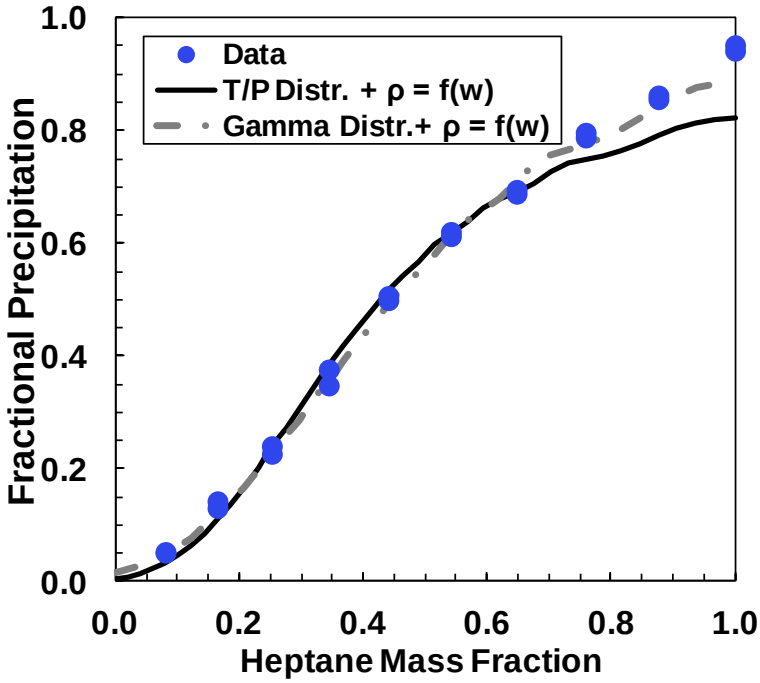

Figure 5.25. Model predictions for fractional yield of X-1359 asphaltenes from solutions of *n*-heptane /toluene at 23 °C.

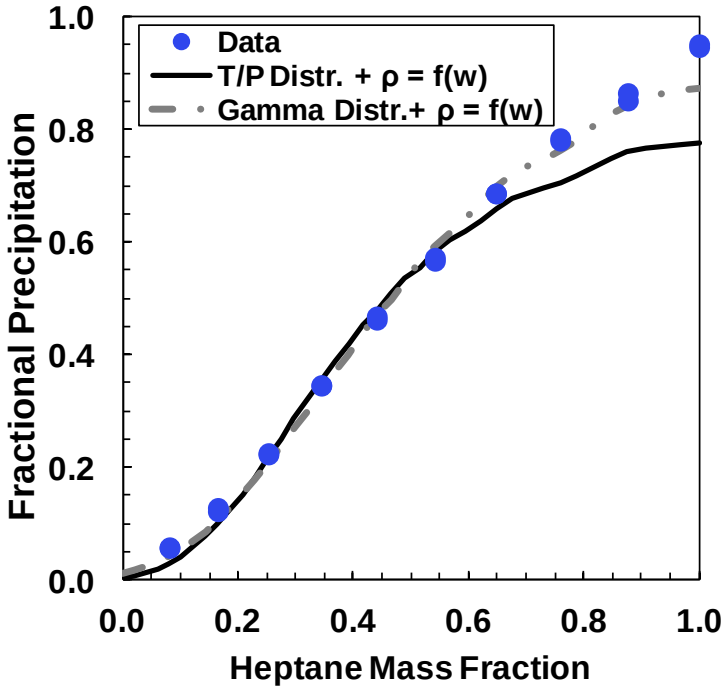

Figure 5.26. Model predictions for fractional yield of X-1360 asphaltenes from solutions of *n*-heptane /toluene at 23 °C.

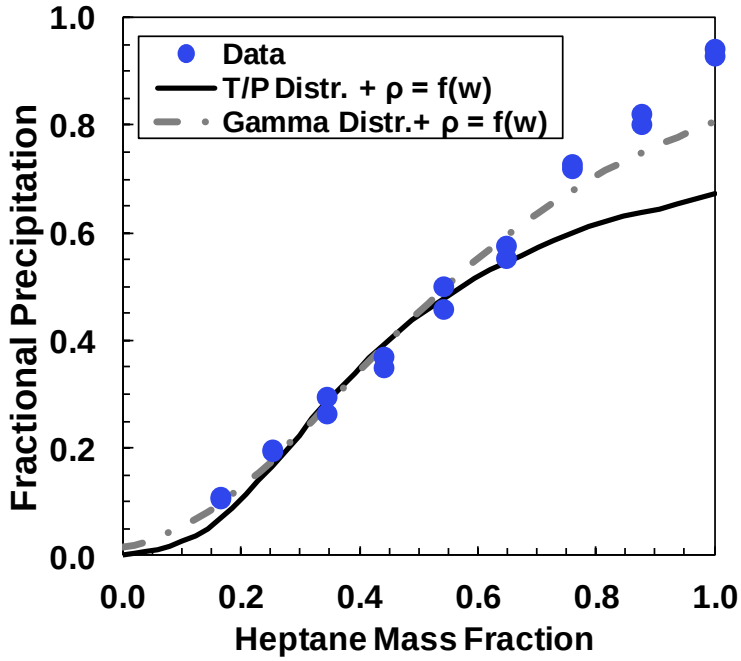

Figure 5.27. Model predictions for fractional yield of RHC-18-39 asphaltenes from solutions of *n*-heptane /toluene at 23 °C.

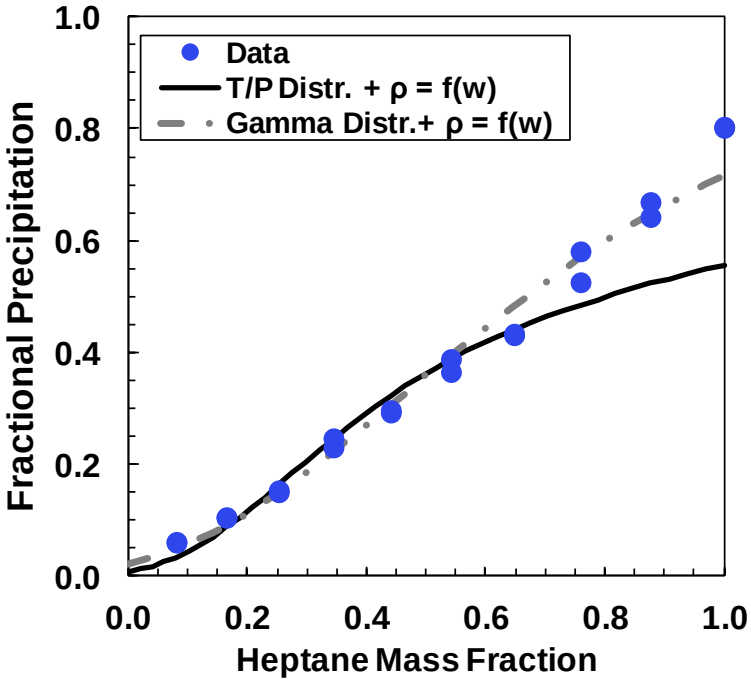

Figure 5.28. Model predictions for fractional yield of RHC-18-37 asphaltenes from solutions of *n*-heptane /toluene at 23 °C.

Chapter Six: Conclusions and Recommendations

The molecular weight and density were measured for solubility cuts of nine asphaltene samples from native, thermocracked, and hydrocracked processes. The property distributions of the whole asphaltenes were reconstructed. Asphaltene yield data were modeled with a regular solution approach to determine the distribution of asphaltene solubility parameters.

6.1 Conclusions

Asphaltene Solubility

The yield curves reflect the reaction history of the samples. Solubility curves of unprocessed samples, B3VB and Short Residue, were similar to each other and to the solubility curves of other native asphaltenes (Barrera, 2012). However, the solubility curves of the reacted samples were completely different than those of their feedstocks. The asphaltenes from reacted sources become significantly less soluble and the precipitation onset point moved to zero concentration of *n*-heptane as the degree of conversion increased.

Asphaltene Molecular Weight Distributions

In every case, the apparent molecular weight increased as asphaltene concentration increased, as was expected for self-associating materials. The molecular weight of the lightest cut increased only slightly with increasing concentrations, suggesting that it contained little self-associating material. The molecular weight of the heaviest cut increased significantly with increasing concentration, indicating it contained a high proportion of self-associating materials. It appeared

that the largest aggregates are the least soluble part of asphaltenes and non-associating material (neutrals) are among the most soluble components of asphaltenes.

The B3VB and Short Residue had similar molecular weight data because both of samples were unprocessed. Thermal cracking and hydrocracking processes were found to decrease the molecular weight of the asphaltenes; that is, they tended to eliminate self-association. In both cases, the measured molecular weights decreased with an increase in conversion extent. The decrease in molecular weight was modest for the thermocracked asphaltenes, but was significant for the hydrocracked asphaltenes. Hydrocracking changed not only the aggregates size, but also dramatically changed the monomer molecular weight from approximately 800 g/mol in the Short Residue feedstock to 450 g/mol for the RHC- samples. The X- series samples all had monomer molecular weights similar to their B3VB feedstock with monomer molecular weights of approximately 800 g/mol.

The terminator-propagator association model successfully fit the molecular weight data for the light and heavy fractions and the whole asphaltenes. This very simple model could capture all of the essential behavior of asphaltenes in solvents. The model was used to predict asphaltene molecular weight distributions at any given asphaltene concentration.

Thermocracking appears to enrich the proportion of neutrals in the asphaltene fraction, but not significantly alter asphaltene self-association. These effects are likely the result of cleaving side chains in asphaltene molecules. This process may create some poorly soluble aromatic cores that do not self-associate (neutrals), but leave many of the asphaltenes still able to associate.

Hydrocracking significantly altered the molecular weight distributions. The average molecular weight decreased substantially with increasing conversion and the distributions narrowed. The amount of neutrals also increased significantly. While hydrocracking increased the amount of neutrals, it also appeared to significantly reduce asphaltene self-association by not only cleaving side chains, but by removing heteroatoms through hydrogenolosis and hydrodemetallization. The strong effect of hydrocracking on association suggests that the heteroatomic groups play a significant role in association.

Density

For both thermocracking and hydrocracking processes, the asphaltene density increased with increased conversion. Thermocracking increased the density from 1181 kg/m³ for the B3VB feedstock to 1249 kg/m³ at 50.8 wt% conversion. Hydrocracking increased the density from 1121 kg/m³ for the Short Residue to 1247 kg/m^3 for conversions above 80 vol%. It is possible that 1250 kg/m³ is a limiting molecular weight of processed asphaltenes.

In all cases, the density increased sharply from the most soluble asphaltenes to the intermediate cuts. However, it changed little from the intermediate to least soluble cuts (the cuts consisting of associated asphaltenes) suggesting that self-association averages the properties of aggregates in terms of density. In other words, the density increases through the neutral components as it does through the aromatic/resin continuum and it becomes almost constant through the aggregated asphaltenes.

Asphaltene Solubility Parameters

A previously developed modified regular solution model was used to fit data on the fractional precipitation of asphaltene from solutions of *n*-heptane and toluene at 23°C. The model was modified as follows: density was correlated to the cumulative mass percent of asphaltenes; 2) the correlation of the asphaltene solubility parameter to molecular weight was retuned.

It was found that the shape of the asphaltene molecular weight distributions can influence predictions of the regular solution model. Therefore, different sets of coefficients were used in solubility parameter correlation when using the gamma or terminator-propagator model. The gamma distribution fit the solubility of asphaltene with little deviation both for thermocracked and hydrocracked asphaltenes. However, when using the terminator-propagator distribution, the model under-predicted the precipitation data for the reacted sample; this issue was significant for hydrocracked asphaltenes. In general, the gamma distribution adequately represented the molecular weight distributions for both native and reacted asphaltenes and better fit asphaltene yield data.

The molecular weight, density, and solubility parameter distributions developed in this thesis can now be used as an input to model asphaltene precipitation from both native and refined crudes. This work is a necessary step to modeling the stability of blends versus precipitation, an important issue for petroleum refiners.

6.2 Recommendations

The next step is to combine the asphaltene property distributions collected in this thesis with the saturate, aromatic, and resin properties determined by Okafor (2014) to model asphaltene precipitation from crude oils and refinery streams. Note, the predictions of asphaltenes fractional yield were lower than experimental data at higher concentrations of *n*-heptane when using the terminator-propagator model for highly reacted samples. A power law between asphaltenes molecular weight and solubility parameter may not be the best correlation and it is recommended to test other forms of functions between these two properties to improve the fit of yield data.

The solubility model still relies on some data fitting. It may be possible to make the model predictive by relating property changes to the reaction history. It is recommended to do more experiments and characterize each sample with reaction indicator such as H/C ratio. It may then be possible to correlate the solubility parameters of asphaltenes to these indicators. Then, the number of measurements required by refiners to characterize stability could be minimized to easily measured properties such as a SARA analysis and an elemental analysis or other indicator properties.

The terminator-propagator model could be improved by introducing a non-uniform association constant. For instance, the asphaltene molecules could be represented as species with two reaction sites. A distribution of reaction constant could be assigned to these sites using a Monte Carlo approach. Species with a low reaction constant would be neutrals and those with a high reaction constant would be propagators. Self-association could be then modeled with a collision simulation applied to a finite number of species.

References

Agrawala, M., & Yarranton, H. (2001). An asphaltene association model analogous to linear polymerization. *Industrial & Engineering Chemistry Research*, *40*(21), 4664--4672.

Agrawala, M. (2001). *Measurement and Modeling of Asphaltene Association* (M.Sc.). University of Calgary.

Akbarzadeh, K., Alboudwarej, H., Svrcek, W., & Yarranton, H. (2005). A generalized regular solution model for asphaltene precipitation from n-alkane diluted heavy oils and bitumens. *Fluid Phase Equilibria*, *232*(1), 159--170.

Akbarzadeh, K., Dhillon, A., Svrcek, W., & Yarranton, H. (2004). Methodology for the characterization and modeling of asphaltene precipitation from heavy oils diluted with n-alkanes. *Energy & Fuels*, *18*(5), 1434--1441.

Alboudwarej, H., Akbarzadeh, K., Beck, J., Svrcek, W., & Yarranton, H. (2003). Regular solution model for asphaltene precipitation from bitumens and solvents. *Aiche Journal*, *49*(11), 2948--2956.

Ancheyta, J., Centeno, G., Trejo, F., & Marroquin, G. (2003). Changes in asphaltene properties during hydrotreating of heavy crudes. *Energy & Fuels*, *17*(5), 1233--1238.

Andersen, S., & Speight, J. (1999). Thermodynamic models for asphaltene solubility and precipitation. *Journal Of Petroleum Science And Engineering*, *22*(1), 53--66.

Andersen, S. (1994). Concentration effects in HPLC-SEC analysis of petroleum asphaltenes. *Journal Of Liquid Chromatography & Related Technologies*, *17*(19), 4065--4079.

Andrews, A., Guerra, R., Mullins, O., & Sen, P. (2006). Diffusivity of asphaltene molecules by fluorescence correlation spectroscopy. *The Journal Of Physical Chemistry A*, *110*(26), 8093--8097.

Bandurski, E. (1982). Structural similarities between oil-generating kerogens and petroleum asphaltenes. *Energy Sources*, *6*(1-2), 47--66.

Barrera, D., Ortiz, D., & Yarranton, H. (2013). Molecular Weight and Density Distributions of Asphaltenes from Crude Oils. *Energy & Fuels*, *27*(5), 2474--2487.

Barrera, D. (2012). *Determination and Application of Asphaltene Property Distributions for Native and Refined Crude Oils* (M.Sc.). University of Calgary.

Bartholdy, J., & Andersen, S. (2000). Changes in asphaltene stability during $_{\text{hydro}}$treating. *Energy & Fuels*, *14*(1), 52--55.

Barton, A. (1991). *Handbook of solubility parameters and other cohesion parameters* (1st ed., pp. 139-215). Boca Raton, Fla.: CRC Press.

Buch, L., Groenzin, H., Buenrostro-Gonzalez, E., Andersen, S., Lira-Galeana, C., & Mullins, O. (2003). Molecular size of asphaltene fractions obtained from residuum hydrotreatment. *Fuel*, *82*(9), 1075--1084.

Bunger, J., & Li, N. (1981). *Chemistry of asphaltenes* (1st ed.). Washington: American Chemical Society.

Calemma, V., Rausa, R., D'Anton, P., & Montanari, L. (1998). Characterization of asphaltenes molecular structure. *Energy & Fuels*, *12*(2), 422--428.

Callejas, M., & Mart'inez, M. (2000). Hydroprocessing of a maya residue. 1. Intrinsic kinetics of asphaltene removal reactions. *Energy & Fuels*, *14*(6), 1304--1308.

Carnahan, N., Quintero, L., Pfund, D., Fulton, J., Smith, R., Capel, M., & Leontaritis, K. (1993). A small angle X-ray scattering study of the effect of pressure on the aggregation of asphaltene fractions in petroleum fluids under near-critical solvent conditions. *Langmuir*, *9*(8), 2035--2044.

Clerc, R., & O'Neal Jr, M. (1961). The mass spectrometric analysis of asphalt. A preliminary investigation. *Analytical Chemistry*, *33*(3), 380--382.

Dickie, J., & Yen, T. (1967). Macrostructures of the asphaltic fractions by various instrumental methods. *Analytical Chemistry*, *39*(14), 1847--1852.

Eyssautier, J., Frot, D., & Barre´, L. (2012). Structure and dynamic properties of colloidal asphaltene aggregates. *Langmuir*, *28*(33), 11997--12004.

Flory, P. (1953). *Principles of polymer chemistry* (1st ed.). Ithaca: Cornell University Press.

Fox, W. (2007). *Effect of Resins on Asphaltene Self-Association and Solubility* (Master of Science). University of Calgary.

Freed, D., Lisitza, N., Sen, P., & Song, Y. (2007). Asphaltene Molecular Composition and Dynamics of Oils from Diffusion Measurements. In O. Mullins, E. Sheu, A. Hammami & A. Marshall, *Asphaltenes, Heavy Oils and Petroleomics* (1st ed., pp. 279-296). New York: Springer.

Friberg, S. (2007). Some emulsion features. *Journal Of Dispersion Science And Technology*, *28*(8), 1299--1308.

Gawrys, K., & Kilpatrick, P. (2005). Asphaltenic aggregates are polydisperse oblate cylinders. *Journal Of Colloid And Interface Science*, *288*(2), 325--334.

Gonzalez, D., Hirasaki, G., Creek, J., & Chapman, W. (2007). Modeling of asphaltene precipitation due to changes in composition using the perturbed chain statistical associating fluid theory equation of state. *Energy & Fuels*, *21*(3), 1231--1242.

Gray, M., Tykwinski, R., Stryker, J., & Tan, X. (2011). Supramolecular assembly model for aggregation of petroleum asphaltenes. *Energy & Fuels*, *25*(7), 3125--3134.

Gray, M., Tykwinski, R., Stryker, J., & Tan, X. (2011). Supramolecular assembly model for

aggregation of petroleum asphaltenes. *Energy & Fuels*, *25*(7), 3125--3134.

Groenzin, H., & Mullins, O. (1999). Asphaltene molecular size and structure. *The Journal Of Physical Chemistry A*, *103*(50), 11237--11245.

Guzman, A., Bueno, A., & Carbognani, L. (2009). Molecular weight determination of asphaltenes from Colombian crudes by size exclusion chromatography (SEC) and vapor pressure osmometry (VPO). *Petroleum Science And Technology*, *27*(8), 801--816.

Guzman, A., Bueno, A., & Carbognani, L. (2009). Molecular weight determination of asphaltenes from Colombian crudes by size exclusion chromatography (SEC) and vapor pressure osmometry (VPO). *Petroleum Science And Technology*, *27*(8), 801--816.

Hammami, A., & Ratulowski, J. (2007). Precipitation and Deposition of Asphaltenes in Production Systems: A Flow Assurance Overview. In O. Mullins, E. Sheu, A. Hammami & A. Marshall, *Asphaltenes, Heavy Oils, and Petroleomics* (1st ed., pp. 617-656). New York: Springer.

Hammami, A., Phelps, C., Monger-McClure, T., & Little, T. (2000). Asphaltene precipitation from live oils: An experimental investigation of onset conditions and reversibility. *Energy & Fuels*, *14*(1), 14--18.

Haslego, C. (2010). Chemical and Process Engineering Resources - Cheresources.com - Index. *Cheresources.com Community*. Retrieved 19 March 2014, from www.CHeresources.com

Hildebrand, J., & Scott, R. (1950). *The solubility of nonelectrolytes* (1st ed.). New York N.Y: Reinhold.

Hirschberg, A., DeJong, L., Schipper, B., Meijer, J., & others,. (1984). Influence of temperature and pressure on asphaltene flocculation. *Society Of Petroleum Engineers Journal*, *24*(03), 283--293.

Hirschberg, A., DeJong, L., Schipper, B., Meijer, J., & others,. (1984). Influence of temperature and pressure on asphaltene flocculation. *Society Of Petroleum Engineers Journal*, *24*(03), 283--293.

Hsu, C., & Robinson, P. (2006). *Practical advances in petroleum processing* (1st ed.). New York: Springer.

Hsu, C., & Robinson, P. (2006). *Practical advances in petroleum processing* (1st ed.). New York: Springer.

Huc, A. (2011). *Heavy crude oils* (1st ed.). Paris: Editions Technip.

Huggins, M. (1941). Solutions of long chain compounds. *Journal Of Chemical Physics*, *9*, 440.

Johnston, K., Satyro, M., Taylor, S., & Yarranton, H. (2014). Modeling Solvent-Bitumen Phase Behavior with a Cubic Equation of State and Asymmetric Mixing Rules. In *63rd Chemical Engineering Conference*.

Jones, D., & Pujado´, P. (2006). *Handbook of petroleum processing* (1st ed.). Dordrecht: Springer.

Kawanaka, S., Park, S., Mansoori, G., & others,. (1991). Organic deposition from reservoir fluids: a thermodynamic predictive technique. *SPE Reservoir Engineering*, *6*(02), 185--192.

Kelemen, S., George, G., & Gorbaty, M. (1990). Direct determination and quantification of sulphur forms in heavy petroleum and coals: 1. The X-ray photoelectron spectroscopy (XPS) approach. *Fuel*, *69*(8), 939--944.

Kuznicki, T., Masliyah, J., & Bhattacharjee, S. (2008). Molecular dynamics study of model molecules resembling asphaltene-like structures in aqueous organic solvent systems. *Energy & Fuels*, *22*(4), 2379--2389.

Lababidi, H., Sabti, H., & AlHumaidan, F. (2014). Changes in asphaltenes during thermal

cracking of residual oils. *Fuel*, *117*, 59--67.

Leffler, W. (2008). *Petroleum refining in nontechnical language* (1st ed.). Tulsa, Okla.: PennWell.

Leontaritis, K., Mansoori, G., & others,. (1987). Asphaltene flocculation during oil production and processing: A thermodynamic colloidal model. *Paper SPE*, *16258*, 4--6.

Mai, A., Bryan, J., Goodarzi, N., & Kantzas, A. (2009). Insights into non-thermal recovery of heavy oil. *Journal Of Canadian Petroleum Technology*, *48*(3), 27--35.

Martin, R. (1996). Comparisons of indefinite self-association models. *Chemical Reviews*, *96*(8), 3043--3064.

McKenna, A., Blakney, G., Xian, F., Glaser, P., Rodgers, R., & Marshall, A. (2010). Heavy petroleum composition. 2. Progression of the Boduszynski model to the limit of distillation by ultrahigh-resolution FT-ICR mass spectrometry. *Energy & Fuels*, *24*(5), 2939--2946.

McKenna, A., Donald, L., Fitzsimmons, J., Juyal, P., Spicer, V., & St, et al. (2013). Heavy petroleum composition. 3. Asphaltene aggregation. *Energy & Fuels*, *27*(3), 1246--1256.

Merdrignac, I., Quoineaud, A., & Gauthier, T. (2006). Evolution of asphaltene structure during hydroconversion conditions. *Energy & Fuels*, *20*(5), 2028--2036.

Merino-Garcia, D., & Andersen, S. (2005). Calorimetric evidence about the application of the concept of cmc to asphaltene self-association. *Journal Of Dispersion Science And Technology*, *26*(2), 217--225.

Merino-Garcia, D., Murgich, J., & Andersen, S. (2004). Asphaltene self-association: Modeling and effect of fractionation with a polar solvent. *Petroleum Science And Technology*, *22*(7-8), 735--758.

Meyers, R. (2004). *Handbook of petroleum refining processes* (1st ed.). New York: McGraw-

Hill.

Mitchell, D., & Speight, J. (1973). The solubility of asphaltenes in hydrocarbon solvents. *Fuel*, *52*(2), 149--152.

Mitra-Kirtley, S., Mullins, O., Van Elp, J., George, S., Chen, J., & Cramer, S. (1993). Determination of the nitrogen chemical structures in petroleum asphaltenes using XANES spectroscopy. *Journal Of The American Chemical Society*, *115*(1), 252--258.

Moschopedis, S., Fryer, J., & Speight, J. (1976). Investigation of asphaltene molecular weights. *Fuel*, *55*(3), 227--232.

Mullins, O., Betancourt, S., Cribbs, M., Dubost, F., Creek, J., Andrews, A., & Venkataramanan, L. (2007). The colloidal structure of crude oil and the structure of oil reservoirs. *Energy & Fuels*, *21*(5), 2785--2794.

Mullins, O., Betancourt, S., Cribbs, M., Dubost, F., Creek, J., Andrews, A., & Venkataramanan, L. (2007). The colloidal structure of crude oil and the structure of oil reservoirs. *Energy & Fuels*, *21*(5), 2785--2794.

Mullins, O., Sabbah, H., Eyssautier, J., Pomerantz, A., Barre´, L., & Andrews, A. et al. (2012). Advances in asphaltene science and the Yen--Mullins model. *Energy & Fuels*, *26*(7), 3986--4003.

Mullins, O. (1995). Chapter 2. In E. Sheu & O. Mullins, *Asphaltene Constituents: Fundamentals and Applications* (1st ed.). New York: Plenum Press.

Murgich, J., & Quimica, C. (2003). Molecular Simulation and the Aggregation of the Heavy Fractions in Crude Oils. *Molecular Simulation*, *29*(6-7), 451-461.

Murgich, J., Merino-Garcia, D., Andersen, S., Manuel del R'io, J., & Galeana, C. (2002). Molecular mechanics and microcalorimetric investigations of the effects of molecular water

on the aggregation of asphaltenes in solutions. *Langmuir*, *18*(23), 9080--9086.

Okafor, J. (2013). *Characterization of Non-Distillable Crude and Refined Oil Fractions for Asphaltene Precipitaion Modeling* (Master of Science). University of Calgary.

Ortiz, D.P. (2014). Personal Communications. University of Calgary.

Parkash, S. (2003). *Refining processes handbook* (1st ed.). Amsterdam: Gulf Professional Pub.

Peramanu, S., Pruden, B., & Rahimi, P. (1999). Molecular weight and specific gravity distributions for Athabasca and Cold Lake bitumens and their saturate, aromatic, resin, and asphaltene fractions. *Industrial & Engineering Chemistry Research*, *38*(8), 3121--3130.

Qian, K., Edwards, K., Siskin, M., Olmstead, W., Mennito, A., Dechert, G., & Hoosain, N. (2007). Desorption and ionization of heavy petroleum molecules and measurement of molecular weight distributions. *Energy & Fuels*, *21*(2), 1042--1047.

Ravey, J., Ducouret, G., & Espinat, D. (1988). Asphaltene macrostructure by small angle neutron scattering. *Fuel*, *67*(11), 1560--1567.

Reid, R., Prausnitz, M., & Poling, B. (1989). *The Properties of Gases & Liquids* (4th ed.). New York: McGraw-Hill.

Rogel, E., Leon, O., Torres, G., & Espidel, J. (2000). Aggregation of asphaltenes in organic solvents using surface tension measurements. *Fuel*, *79*(11), 1389--1394.

Rose, K., & Francisco, M. (1988). A two-step chemistry for highlighting heteroatom species in petroleum materials using carbon-13 NMR spectroscopy. *Journal Of The American Chemical Society*, *110*(2), 637--638.

Sachanen, A. (1945). *The chemical constituents of petroleum* (1st ed.). New York: Reinhold Pub. Corp.

Schneider, M., Andrews, A., Mitra-Kirtley, S., & Mullins, O. (2007). Asphaltene molecular size

by fluorescence correlation spectroscopy. *Energy & Fuels, 21*(5), 2875--2882.

Scott, R. (1945). The Thermodynamics of High-Polymer Solutions: II. The Solubility and Fractionation of a Polymer of Heterogeneous Distribution. *The Journal Of Chemical Physics, 13*(5), 178--187.

Seki, H., & Kumata, F. (2000). Structural change of petroleum asphaltenes and resins by hydrodemetallization. *Energy & Fuels*, *14*(5), 980--985.

Sheremata, J., Gray, M., Dettman, H., & McCaffrey, W. (2004). Quantitative molecular representation and sequential optimization of Athabasca asphaltenes. *Energy & Fuels*, *18*(5), 1377--1384.

Speight, J., & Moschopedis, S. (1981). In N. Li & J. Bunger, *Chemistry of Asphaltenes* (1st ed.). Washington, DC.: American Chemical Society.

Speight, J. (1994). Chemical and Physical Studies of Petroleum Asphaltenes. In T. Yen & G. Chilingar, *Asphaltenes and asphalts* (1st ed., pp. 7-65). Amsterdam: Elsevier Science.

Speight, J. (2001). *Handbook of petroleum analysis* (1st ed.). New York: Wiley-Interscience.

Speight, J. (2004). Petroleum Asphaltenes-Part 1: Asphaltenes, resins and the structure of petroleum. *Oil & Gas Science And Technology*, *59*(5), 467--477.

Speight, J. (2007). *The chemistry and technology of petroleum* (1st ed.). Boca Raton: CRC Press/Taylor & Francis.

Storm, D., & Sheu, E. (1995). Characterization of colloidal asphaltenic particles in heavy oil. *Fuel*, *74*(8), 1140--1145.

Storm, D., & Sheu, E. (1995). Characterization of colloidal asphaltenic particles in heavy oil. *Fuel*, *74*(8), 1140--1145.

Strausz, O., Peng, P., & Murgich, J. (2002). About the colloidal nature of asphaltenes and the

MW of covalent monomeric units. *Energy & Fuels*, *16*(4), 809--822.

Vargas, F., Gonzalez, D., Hirasaki, G., & Chapman, W. (2009). Modeling Asphaltene Phase Behavior in Crude Oil Systems Using the Perturbed Chain Form of the Statistical Associating Fluid Theory (PC-SAFT) Equation of State†. *Energy & Fuels*, *23*(3), 1140--1146.

Wang, J., & Buckley, J. (2001). A two-component solubility model of the onset of asphaltene flocculation in crude oils. *Energy & Fuels*, *15*(5), 1004--1012.

Wargadalam, V., Norinaga, K., & Iino, M. (2002). Size and shape of a coal asphaltene studied by viscosity and diffusion coefficient measurements. *Fuel*, *81*(11), 1403--1407.

Wiehe, I., & Liang, K. (1996). Asphaltenes, resins, and other petroleum macromolecules. *Fluid Phase Equilibria*, *117*(1-2), 201-210.

Yarranton, H., & Masliyah, J. (1996). Molar mass distribution and solubility modeling of asphaltenes. *Aiche Journal*, *42*(12), 3533--3543.

Yarranton, H., Alboudwarej, H., & Jakher, R. (2000). Investigation of asphaltene association with vapor pressure osmometry and interfacial tension measurements. *Industrial & Engineering Chemistry Research*, *39*(8), 2916--2924.

Yen, T. (1972). Present status of the structure of petroleum heavy ends and its significance to various technical applications. *Preprints-American Chemical Society. Division Of Petroleum Chemistry*, *17*(4), F102-F114.

Yen, T. (1974). Structure of petroleum asphaltene and its significance. *Energy Sources, Part Arecovery, Utilization, And Environmental Effects*, *1*(4), 447--463.

Yen, T. (1975). *The Role of trace metals in petroleum* (1st ed.). Ann Arbor - Mich: Ann Arbor Science.

Zhang, L., & Greenfield, M. (2007). Relaxation time, diffusion, and viscosity analysis of model asphalt systems using molecular simulation. *Chemical Physics*, *127*(19), 194502.

APPENDIX A: ERROR ANALYSIS SUMMARY

Tables A.1 to A.24 show the repeatability analysis for density and refractive index measurements. In almost all of the cases the data set are consisted of pairs of measurements. The mean for each pair of measurement is calculated as:

$$\mu = \frac{\sum_{i=1}^{n} y_i}{n} \tag{A.1}$$

where y_i is the experimental measured value and n is the number of repeats. Sample variance, s, could be then determined based on the variances of all data sets and is given by:

$$s = \sqrt{\frac{\sum_{i=1}^{n}(y_i-\mu)^2}{m-1}} \tag{A.2}$$

where m is the number of variances determined for that property measurements. Population variance can be then calculated using Chi-square distribution as follows:

$$\sigma = \sqrt{\frac{\lambda^2 s^2}{(n-1)}} \tag{A.3}$$

Where λ^2 is the chi-square variable (from statistical tables) and σ is the population standard deviation. Eventually, the 95% confidence interval (*CI*) for any single measurement is calculated as 1.645σ and for pair of data as (1.645/ √2)σ. The confidence interval for single measurements is reported in tables.

Absolute deviation (AD) and average absolute deviation (AAD) reported in tables A.25 to A.84 and A103 to A.114

$$\mathrm{AD} = |y_i^* - y_i| \tag{A.4}$$

$$\mathrm{AAD} = \frac{1}{n}\sum_{i=1}^{n}|y_i^* - y_i| \tag{A.5}$$

where y_i^* is the predicted value from the model.

The absolute relative deviation (ARD) reported in tables A.85 to to A.94 is defined as:

$$\text{ARD} = \left|\frac{y_i^* - y_i}{y_i}\right| \tag{A.6}$$

Table A.1. Repeatability of indirect calculation of FRI for B3VB asphaltenes extrapolated from toluene solutions by assuming of regular solution behavior.

Asphaltenes	***n***	***μ*(Expt. FRI)**	s^2
B3VB	2	0.40957	8.17E-09
HT80L	2	0.38186	4.67E-06
HT67.1L	2	0.40060	5.36E-07
HT80H	2	0.41003	1.57E-06
HT67.1H	2	0.42098	2.46E-07
		Average	1.41E-06
		CI	0.0030

Table A.2. Repeatability of indirect calculation of FRI for X-1357 asphaltenes extrapolated from toluene solutions by assuming of regular solution behavior.

Asphaltenes	***n***	***μ*(Expt. FRI)**	s^2
X-1357	2	0.43855	1.02E-08
HT80L	2	0.39062	5.52E-07
HT53L	2	0.42244	1.29E-07
HT53H	2	0.45092	3.46E-07
HT80H	2	0.43976	2.32E-11
		Average	2.08E-07
		CI	0.0012

Table A.3. Repeatability of indirect calculation of FRI for X-1359 asphaltenes extrapolated from toluene solutions by assuming of regular solution behavior.

Asphaltenes	***n***	***μ*(Expt. FRI)**	s^2
X-1359	2	0.45120	3.18E-09
HT68L	2	0.41561	2.65E-07
HT68H	2	0.45456	4.36E-07
		Average	2.35E-07
		CI	0.0014

Table A.4. Repeatability of indirect calculation of FRI for X-1360 asphaltenes extrapolated from toluene solutions by assuming of regular solution behavior.

Asphaltenes	***n***	***μ*(Expt. FRI)**	s^2
X-1360	2.0000	0.45183	2.97E-07
HT67L	2.0000	0.42304	5.01E-06
HT67H	2.0000	0.46078	6.98E-07
		Average	2.00E-06
		CI	0.0040

Table A.5. Repeatability of indirect calculation of FRI for Short Residue asphaltenes extrapolated from toluene solutions by assuming of regular solution behavior.

Asphaltenes	***n***	***μ*(Expt. FRI)**	s^2
Short R.	2	0.38440	5.43E-08
HT71L	2	0.37894	7.03E-07
HT84L	2	0.37230	3.66E-08
HT84H	2	0.38581	2.69E-07
HT71H	2	0.38668	9.62E-10
		Average	2.13E-07
		CI	0.0012

Table A.6. Repeatability of indirect calculation of FRI for HOSB asphaltenes extrapolated from toluene solutions by assuming of regular solution behavior.

Asphaltenes	***n***	***μ*(Expt. FRI)**	s^2
HOSB	2	0.46423	2.04E-07
HT50L	2	0.44707	4.15E-11
HT80L	2	0.42141	3.30E-06
HT80H	2	0.47125	2.83E-06
		Average	1.58E-06
		CI	0.0033

Table A.7. Repeatability of indirect calculation of FRI for B3VB asphaltenes extrapolated from o-dichlorobenzene solutions by assuming of regular solution behavior.

Asphaltenes	***n***	***μ*(Expt. FRI)**	s^2
B3VB	2	0.39765	3.30E-08
HT80L	2	0.37439	3.27E-05
HT67.1L	2	0.39000	1.36E-07
HT80H	2	0.40319	5.12E-08
HT67.1H	2	0.41242	4.63E-07
		Average	6.68E-06
		CI	0.0065

Table A.8. Repeatability of indirect calculation of FRI for X-1359 asphaltenes extrapolated from o-dichlorobenzene solutions by assuming of regular solution behavior.

Asphaltenes	***n***	***μ*(Expt. FRI)**	s^2
X-1359	2	0.43321	5.17E-09
HT35L	2	0.42267	9.72E-09
HT68L	2	0.40163	2.60E-07
HT68H	2	0.44099	4.20E-08
HT35H	2	0.44684	3.40E-10
		Average	6.35E-08
		CI	0.0006

Table A.9. Repeatability of indirect calculation of FRI for X-1360 asphaltenes extrapolated from o-dichlorobenzene solutions by assuming of regular solution behavior.

Asphaltenes	***n***	***μ*(Expt. FRI)**	s^2
X-1360	2	0.43419	3.04E-06
HT38L	2	0.42303	5.95E-09
HT67L	2	0.41080	1.33E-10
HT67H	2	0.44483	1.76E-08
HT38H	2	0.45241	1.86E-07
		Average	6.49E-07
		CI	0.0020

Table A.10. Repeatability of indirect calculation of FRI for HOSB asphaltenes extrapolated from o-dichlorobenzene solutions by assuming of regular solution behavior.

Asphaltenes	***n***	***μ*(Expt. FRI)**	s^2
HOSB	2	0.44669	6.19E-08
HT50L	2	0.43618	1.99E-08
HT80L	2	0.41358	6.50E-07
HT50H	2	0.46788	3.08E-07
HT80H	2	0.46040	6.72E-06
		Average	1.55E-06
		CI	0.0032

Table A.11. Repeatability of indirect calculation of FRI for RHC-18-19 asphaltenes extrapolated from o-dichlorobenzene solutions by assuming of regular solution behavior.

Asphaltenes	***n***	***μ*(Expt. FRI)**	s^2
RHC-18-19	2	0.44387	3.16E-07
HT45L	2	0.42520	1.85E-07
HT76L	2	0.40795	3.30E-07
HT76H	2	0.44645	1.51E-07
HT45H	2	0.45387	1.84E-07
		Average	2.33E-07
		CI	0.0012

Table A.12. Repeatability of indirect calculation of FRI for RHC-18-37 asphaltenes extrapolated from o-dichlorobenzene solutions by assuming of regular solution behavior.

Asphaltenes	***n***	***μ*(Expt. FRI)**	s^2
RHC-18-37	2	0.44113	4.40E-10
HT53L	2	0.42114	2.10E-07
HT91L	2	0.40181	1.69E-08
HT91L	2	0.45376	4.95E-06
HT53H	2	0.46464	1.54E-06
		Average	1.34E-06
		CI	0.0029

Table A.13. Repeatability of indirect calculation of density for B3VB asphaltenes extrapolated from toluene solutions by assuming of regular solution behavior.

Asphaltenes	***n***	***μ*(kg/m^3)**	***s*^{2}**
B3VB	2	1180.9	0.0289
HT80L	2	1118.7	4.3803
HT67.1L	2	1163.2	3.5121
HT80H	2	1173.9	8.8640
HT67.1H	2	1198.7	2.9645
		Average	3.9499
		CI	5.0

Table A.14. Repeatability of indirect calculation of density for X-1357 asphaltenes extrapolated from toluene solutions by assuming of regular solution behavior.

Asphaltenes	***n***	***μ*(kg/m^3)**	***s*^{2}**
X-1357	2	1223.5	0.6404
HT80L	2	1139.8	0.2624
HT53L	2	1195.4	0.7117
HT80H	3	1245.5	1.0495
HT53H	2	1222.2	0.5310
		Average	0.6390
		CI	2.0

Table A.15. Repeatability of indirect calculation of density for X-1359 asphaltenes extrapolated from toluene solutions by assuming of regular solution behavior.

Asphaltenes	***n***	***μ*(kg/m^3)**	***s*^{2}**
X-1359	2	1247.9	1.6379
HT68L	2	1184.6	1.7243
HT68H	2	1252.2	1.4211
		Average	1.5944
		CI	3.6

Table A.16. Repeatability of indirect calculation of density for X-1360 asphaltenes extrapolated from toluene solutions by assuming of regular solution behavior.

Asphaltenes	***n***	***μ*(kg/m^3)**	***s*^{2}**
X-1360	2	1249.9	3.0050
HT67L	2	1203.6	25.2554
HT67H	2	1263.0	3.5812
		Average	10.6138
		CI	9.3

Table A.17. Repeatability of indirect calculation of density for Short Residue asphaltenes extrapolated from toluene solutions by assuming of regular solution behavior.

Asphaltenes	***n***	***μ*(kg/m^3)**	***s*^{2}**
Short R.	2	1121.0	0.0276
HT71L	2	1112.4	3.5694
HT84L	2	1099.8	0.2585
HT84H	2	1124.4	3.4886
HT71L	2	1123.5	0.1961
		Average	1.5080
		CI	3.1

Table A.18. Repeatability of indirect calculation of density for HOSB asphaltenes extrapolated from toluene solutions by assuming of regular solution behavior.

Asphaltenes	***n***	***μ*(kg/m^3)**	***s*^{2}**
HOSB	2	1249.4	42.7909
HT50L	2	1214.0	3.4510
HT80L	2	1167.4	7.2274
HT50H	2	1293.9	25.1010
HT80H	2	1282.2	48.0805
		Average	25.3302
		CI	13.4

Table A.19. Repeatability of indirect calculation of density for B3VB asphaltenes extrapolated from o-dichlorobenzene solutions by assuming of regular solution behavior.

Asphaltenes	***n***	***μ*(kg/m^3)**	***s*^{2}**
B3VB	2	1187.9	0.0001
HT80L	2	1136.7	3.2235
HT67.1L	2	1165.6	0.2197
HT80H	2	1188.8	0.0100
HT67.1H	2	1204.1	4.4980
		Average	1.5902
		CI	3.2

Table A.20. Repeatability of indirect calculation of density for X-1359 asphaltenes extrapolated from o-dichlorobenzene solutions by assuming of regular solution behavior.

Asphaltenes	***n***	***μ*(kg/m^3)**	***s*^{2}**
X-1359	2	1242.2	2.2783
HT35L	2	1228.4	1.2026
HT68L	2	1195.0	0.3817
HT68H	2	1258.0	0.0362
HT35H	2	1272.8	0.4321
		Average	0.8662
		CI	2.4

Table A.21. Repeatability of indirect calculation of density for X-1360 asphaltenes extrapolated from o-dichlorobenzene solutions by assuming of regular solution behavior.

Asphaltenes	***n***	***μ*(kg/m^3)**	***s*^{2}**
X-1360	2	1246.7	0.3680
L1HT38L	2	1232.1	0.0290
HT67L	2	1205.2	0.1511
HT67H	2	1265.8	0.4366
HT38H	2	1285.9	0.0006
		Average	0.1971
		CI	1.6

Table A.22. Repeatability of indirect calculation of density for HOSB asphaltenes extrapolated from o-dichlorobenzene solutions by assuming of regular solution behavior.

Asphaltenes	***n***	***μ*(kg/m^3)**	***s*^{2}**
HOSB	2	1252.2	2.1806
HT50L	2	1211.1	0.0730
HT80L	2	1167.7	77.4055
HT50H	2	1292.6	0.1562
HT80H	2	1269.2	3.6160
		Average	16.6863
		CI	10.4

Table A.23. Repeatability of indirect calculation of density for RHC-18-19 asphaltenes extrapolated from o-dichlorobenzene solutions by assuming of regular solution behavior.

Asphaltenes	***n***	***μ*(kg/m^3)**	***s*^{2}**
RHC-18-19	2	1246.3	0.3156
HT45L	2	1220.9	0.3129
HT76L	2	1191.1	0.0140
HT76H	2	1258.0	0.0410
HT45H	2	1273.5	0.0000
		Average	0.1367
		CI	0.9

Table A.24. Repeatability of indirect calculation of density for RHC-18-37 asphaltenes extrapolated from o-dichlorobenzene solutions by assuming of regular solution behavior.

Asphaltenes	***n***	***μ*(kg/m^3)**	***s*^{2}**
RHC-18-37	2	1246.0	0.7049
HT53L	2	1216.7	0.1541
HT91L	2	1181.5	0.1942
HT91H	2	1269.1	1.2731
HT53H	2	1291.3	11.6307
		Average	2.7914
		CI	4.2

Table A.25. Average absolute deviation for B3VB whole asphaltenes molecular weight data using the terminator-propagator model (toluene measurements).

Asphaltene Concentration (kg/m^3)	Asphaltene Molecular Weight (g/mol)		AD
	Experimental	Calculated	
1	1825	2140	315
2	2117	2544	427
5	2744	3169	425
10	3617	3672	55
20	4331	4159	172
30	4398	4421	23
40	4814	4591	222
60	5318	4806	512
1	2001	2140	139
2	2337	2544	207
5	3059	3169	110
10	3738	3672	66
20	4327	4159	168
30	4468	4421	47
40	4732	4591	141
60	5195	4806	389
		Total AAD	214

Table A.26. Average absolute deviation for B3VB, HT80L fraction molecular weight data using the terminator-propagator model (toluene measurements).

Asphaltene Concentration (kg/m^3)	Asphaltene Molecular Weight (g/mol)		AD
	Experimental	Calculated	
1	984	1410	426
2	1037	1535	498
5	1243	1691	448
10	1407	1790	383
20	1589	1865	276
30	1702	1899	197
40	1735	1918	182
60	1912	1939	27
1	1553	1410	143
2	1278	1535	257
5	1354	1691	337
10	1466	1790	324
20	1590	1865	276
30	1611	1899	288
40	1717	1918	201
60	1842	1939	96
		Total AAD	272

Table A.27. Average absolute deviation for B3VB, HT80H fraction molecular weight data using the terminator-propagator model (toluene measurements).

Asphaltene Concentration (kg/m^3)	Asphaltene Molecular Weight (g/mol)		AD
	Experimental	Calculated	
1	1179	2634	1456
2	1635	3332	1697
5	2265	4598	2333
10	3362	5841	2479
20	5019	7312	2294
30	7332	8254	923
40	8268	8943	675
60	9915	9921	6
1	4068	2634	1434
2	4430	3332	1098
5	4515	4598	83
10	5549	5841	292
20	7136	7312	176
30	8159	8254	95
40	9249	8943	306
60	10709	9921	788
		Total AAD	1008

Table A.28. Average absolute deviation for B3VB, HT61.7L fraction molecular weight data using the terminator-propagator model (toluene measurements).

Asphaltene Concentration (kg/m^3)	Asphaltene Molecular Weight (g/mol)		AD
	Experimental	Calculated	
1	1518	1883	364
2	1723	2169	446
5	2094	2578	484
10	2608	2879	271
20	3043	3145	102
40	3281	3359	77
60	3604	3456	147
1	1750	1883	132
2	1841	2169	328
5	2031	2578	547
10	2429	2879	450
20	2799	3145	346
40	3195	3359	164
60	3492	3456	36
		Total AAD	278

Table A.29. Average absolute deviation for B3VB, HT61.7H fraction molecular weight data using the terminator-propagator model (toluene measurements).

Asphaltene Concentration (kg/m^3)	Asphaltene Molecular Weight (g/mol)		AD
	Experimental	Calculated	
1	3368	2851	517
2	2856	3706	850
5	4870	5387	517
10	6317	7231	915
20	9065	9736	671
30	10453	11574	1122
40	12030	13069	1039
60	13833	15464	1631
1	3910	2851	1059
2	4073	3706	367
5	6291	5387	904
10	7298	7231	67
20	10500	9736	765
40	13949	13069	880
60	15993	15464	529
		Total AAD	789

Table A.30. Summary of average absolute deviation for B3VB asphaltenes molecular weight (toluene measurements).

Fraction	AAD(g/mol)
HT80L	272
HT61L	278
Whole	214
HT80H	1008
HT61H	789
AAD	512

Table A.31. Average absolute deviation for B3VB, whole asphaltenes molecular weight data using the terminator-propagator model (o-dichlorobenzene measurements).

Asphaltene Concentration (kg/m^3)	Asphaltene Molecular Weight (g/mol)		AD
	Experimental	Calculated	
2	2742	1725	1016
5	2183	1998	185
10	2217	2183	34
20	2224	2328	104
40	2533	2427	106
60	2457	2467	10
1	1803	1530	273
2	1846	1725	121
5	2248	1998	250
10	2163	2183	20
20	2240	2328	88
40	2535	2427	107
60	2471	2467	4
		Total AAD	178

Table A.32. Average absolute deviation for B3VB, HT80L fraction molecular weight data using the terminator-propagator model (o-dichlorobenzene measurements).

Asphaltene Concentration (kg/m^3)	Asphaltene Molecular Weight (g/mol)		AD
	Experimental	Calculated	
1	956	1158	203
2	1085	1235	149
5	1281	1331	50
10	1279	1389	110
20	1220	1430	211
40	1277	1457	180
60	1202	1466	264
1	1281	1158	122
2	1415	1235	180
5	1377	1331	46
10	1319	1389	70
20	1227	1430	203
40	1265	1457	192
60	1186	1466	281
		Total AAD	162

Table A.33. Average absolute deviation for B3VB, HT80H fraction molecular weight data using the terminator-propagator model (o-dichlorobenzene measurements).

Asphaltene Concentration (kg/m^3)	Asphaltene Molecular Weight (g/mol)		AD
	Experimental	Calculated	
1	2674	1769	906
2	2878	2070	809
5	2525	2530	5
10	2796	2879	84
20	3045	3181	136
40	3437	3406	30
60	3319	3501	182
1	2314	1769	546
2	2472	2070	403
5	2884	2530	354
10	3228	2879	349
20	3288	3181	107
40	3637	3406	231
60	3407	3501	94
		Total AAD	303

Table A.34. Average absolute deviation for B3VB, HT61.7L fraction molecular weight data using the terminator-propagator model (o-dichlorobenzene measurements).

Asphaltene Concentration (kg/m^3)	Asphaltene Molecular Weight (g/mol)		AD
	Experimental	Calculated	
1	2218	1401	817
2	1750	1549	201
5	1876	1746	129
10	1879	1874	6
20	1728	1969	242
40	1830	2033	203
60	1760	2057	297
1	1964	1401	563
2	1719	1549	170
5	1940	1746	194
10	1958	1874	84
20	1782	1969	187
40	1862	2033	171
60	1754	2057	303
		Total AAD	255

Table A.35. Average absolute deviation for B3VB, HT61.7H fraction molecular weight data using the terminator-propagator model (o-dichlorobenzene measurements).

Asphaltene Concentration (kg/m^3)	Asphaltene Molecular Weight (g/mol)		AD
	Experimental	Calculated	
1	2142	1888	255
2	2716	2252	464
5	3480	2844	636
10	3708	3332	376
20	3815	3791	23
40	4125	4167	42
60	3951	4336	385
1	2115	1888	228
2	3245	2252	993
5	3611	2844	766
10	3697	3332	365
20	3715	3791	76
40	4148	4167	19
60	4010	4336	326
		Total AAD	354

Table A.36. Summary of average absolute deviation for B3VB asphaltenes molecular weight (o-dichlorobenzene measurements).

Fraction	AAD(g/mol)
HT80L	162
HT61L	255
Whole	178
HT80H	303
HT61H	354
AAD	250

Table A.37. Average absolute deviation for X-1357, whole asphaltenes molecular weight data using the terminator-propagator model (toluene measurements).

Asphaltene Concentration (kg/m^3)	Asphaltene Molecular Weight (g/mol)		AD
	Experimental	Calculated	
1	1704	2140	436
2	1863	2544	681
5	2052	3169	1117
10	2280	3672	1391
20	2432	4159	1727
30	4829	4421	408
40	5265	4591	674
60	5981	4806	1174
1	2490	2140	349
2	2449	2544	95
5	2771	3169	398
10	3450	3672	222
20	3986	4159	173
30	4636	4421	216
40	4833	4591	242
60	5545	4806	739
30	4582	4421	161
40	4995	4591	404
60	5674	4806	868
		Total AAD	604

Table A.38. Average absolute deviation for X-1357, HT80L fraction molecular weight data using the terminator-propagator model (toluene measurements).

Asphaltene Concentration (kg/m^3)	Asphaltene Molecular Weight (g/mol)		AD
	Experimental	Calculated	
1	925	1397	472
2	968	1518	549
5	1100	1668	568
10	1216	1762	546
20	1368	1832	464
40	1533	1880	347
60	1673	1899	226
1	832	1397	565
2	912	1518	606
5	1063	1668	605
10	1188	1762	573
20	1363	1832	470
40	1551	1880	329
60	1680	1899	220
		Total AAD	467

Table A.39. Average absolute deviation for X-1357, HT80H fraction molecular weight data using the terminator-propagator model (toluene measurements).

Asphaltene Concentration (kg/m^3)	Asphaltene Molecular Weight (g/mol)		AD
	Experimental	Calculated	
1	2423	2570	147
2	2814	3223	410
5	3799	4384	585
10	4835	5495	660
20	6195	6781	586
40	7882	8174	293
60	9187	9000	187
1	3248	2570	678
2	3996	3223	773
5	3864	4384	520
10	4511	5495	984
20	6200	6781	580
40	7688	8174	487
60	9045	9000	45
		Total AAD	462

Table A.40. Average absolute deviation for X-1357, HT53L fraction molecular weight data using the terminator-propagator model (toluene measurements).

Asphaltene Concentration (kg/m^3)	Asphaltene Molecular Weight (g/mol)		AD
	Experimental	Calculated	
1	1504	1859	356
2	1506	2136	630
5	1866	2527	661
10	2147	2810	663
20	2507	3056	548
40	3004	3248	244
60	3330	3334	4
1	1907	1859	48
2	1534	2136	602
5	2040	2527	487
10	2240	2810	570
20	2625	3056	431
40	3064	3248	184
60	3353	3334	19
		Total AAD	389

Table A.41. Average absolute deviation for X-1357, HT53H fraction molecular weight data using the terminator-propagator model (toluene measurements).

Asphaltene Concentration (kg/m^3)	Asphaltene Molecular Weight (g/mol)		AD
	Experimental	Calculated	
1	2351	2851	500
2	2335	3706	1371
5	4188	5387	1199
10	5861	7231	1370
20	8573	9736	1163
40	13177	13069	108
60	15889	15464	425
1	3721	2851	870
2	5697	3706	1991
5	7670	5387	2283
10	9474	7231	2243
20	11897	9736	2161
40	15640	13069	2571
60	18154	15464	2690
		Total AAD	1496

Table A.42. Summary of average absolute deviation for X-1357 asphaltenes molecular weight (toluene measurements).

Fraction	AAD(g/mol)
HT80L	467
HT53L	389
Whole	604
HT80H	462
HT53H	1496
AAD	684

Table A.43. Average absolute deviation for X-1359, whole asphaltenes molecular weight data using the terminator-propagator model (o-dichlorobenzene measurements).

Asphaltene Concentration (kg/m^3)	Asphaltene Molecular Weight (g/mol)		AD
	Experimental	Calculated	
1	1819	1414	405
2	1871	1572	299
5	1927	1786	141
10	1948	1927	21
20	1878	2034	156
40	2067	2105	38
60	2039	2133	94
1	1857	1414	443
2	1910	1572	339
5	1924	1786	138
10	1921	1927	6
20	1910	2034	124
40	2031	2105	75
60	2035	2133	98
		Total AAD	170

Table A.44. Average absolute deviation for X-1359, HT68L fraction molecular weight data using the terminator-propagator model (o-dichlorobenzene measurements).

Asphaltene Concentration (kg/m^3)	Asphaltene Molecular Weight (g/mol)		AD
	Experimental	Calculated	
1	1456	1074	382
2	1175	1132	43
5	1242	1204	38
10	1123	1248	124
20	1094	1278	184
40	1180	1297	118
60	1234	1305	71
1	1309	1074	234
2	1226	1132	94
5	1244	1204	40
10	1153	1248	94
20	1094	1278	184
40	1183	1297	114
60	1245	1305	60
		Total AAD	127

Table A.45. Average absolute deviation for X-1359, HT68H fraction molecular weight data using the terminator-propagator model (o-dichlorobenzene measurements).

Asphaltene Concentration (kg/m^3)	Asphaltene Molecular Weight (g/mol)		AD
	Experimental	Calculated	
1	2001	1629	372
2	1896	1872	24
5	2240	2229	11
10	2363	2485	122
20	2526	2692	166
40	2843	2838	5
50	2837	2897	60
1	2470	1629	841
2	2012	1872	140
5	2297	2229	68
10	2433	2485	52
20	2504	2692	188
40	2818	2838	20
50	2869	2897	28
		Total AAD	150

Table A.46. Average absolute deviation for X-1359, HT35L fraction molecular weight data using the terminator-propagator model (o-dichlorobenzene measurements).

Asphaltene Concentration (kg/m^3)	Asphaltene Molecular Weight (g/mol)		AD
	Experimental	Calculated	
1	1633	1283	350
2	1544	1397	146
5	1667	1546	122
10	1549	1638	89
20	1541	1706	164
40	1711	1749	38
60	1677	1766	89
1	2755	1283	1471
2	1420	1397	23
5	1619	1546	73
10	1568	1638	70
20	1579	1706	127
40	1730	1749	19
60	1703	1766	63
		Total AAD	203

Table A.47. Average absolute deviation for X-1359, HT35H fraction molecular weight data using the terminator-propagator model (o-dichlorobenzene measurements).

Asphaltene Concentration (kg/m^3)	Asphaltene Molecular Weight (g/mol)		AD
	Experimental	Calculated	
1	3281	1772	1509
2	2600	2087	512
5	2745	2589	155
10	2996	2990	7
20	3287	3354	67
40	3745	3642	103
1	2950	1772	1177
2	2657	2087	570
5	2895	2589	306
10	3066	2990	76
20	3390	3354	36
40	3694	3642	52
		Total AAD	381

Table A.48. Summary of average absolute deviation for X-1359 asphaltenes molecular weight (o-dichlorobenzene measurements).

Fraction	AAD(g/mol)
HT68L	127
HT35L	203
Whole	170
HT68H	150
HT35H	381
AAD	206

Table A.49. Average absolute deviation for X-1360, whole asphaltenes molecular weight data using the terminator-propagator model (o-dichlorobenzene measurements).

Asphaltene Concentration (kg/m^3)	Asphaltene Molecular Weight (g/mol)		AD
	Experimental	Calculated	
1	1234	1264	31
2	1268	1388	121
5	1670	1548	122
10	1602	1645	43
20	1533	1715	182
40	1688	1759	71
60	1671	1776	105
1	1418	1264	154
2	1335	1388	54
5	1672	1548	124
10	1563	1645	82
20	1583	1715	132
40	1688	1759	71
60	1733	1776	43
		Total AAD	95

Table A.50. Average absolute deviation for X-1360, HT67L fraction molecular weight data using the terminator-propagator model (o-dichlorobenzene measurements).

Asphaltene Concentration (kg/m^3)	Asphaltene Molecular Weight (g/mol)		AD
	Experimental	Calculated	
1	984	988	5
2	1027	1033	6
5	1118	1089	30
10	1052	1121	69
20	1043	1144	101
40	1111	1158	47
60	1116	1163	48
1	1002	988	14
2	1030	1033	3
5	1105	1089	16
10	1017	1121	104
20	1009	1144	135
40	1097	1158	61
60	1110	1163	53
		Total AAD	49

Table A.51. Average absolute deviation for X-1360, HT67H fraction molecular weight data using the terminator-propagator model (o-dichlorobenzene measurements).

Asphaltene Concentration (kg/m^3)	Asphaltene Molecular Weight (g/mol)		AD
	Experimental	Calculated	
1	2167	1530	637
2	2222	1761	461
5	2320	2089	231
10	2447	2314	133
20	2421	2488	67
40	2676	2607	70
50	2682	2653	28
1	1904	1530	375
2	2056	1761	295
5	2338	2089	249
10	2394	2314	81
20	2483	2488	6
40	2654	2607	47
50	2706	2653	53
		Total AAD	195

Table A.52. Average absolute deviation for X-1360, HT38L fraction molecular weight data using the terminator-propagator model (o-dichlorobenzene measurements).

Asphaltene Concentration (kg/m^3)	Asphaltene Molecular Weight (g/mol)		AD
	Experimental	Calculated	
1	983	1147	164
2	948	1233	285
5	1271	1338	67
10	1295	1399	105
20	1325	1441	116
40	1480	1467	14
60	1484	1476	8
1	1372	1147	226
2	1238	1233	5
5	1324	1338	14
10	1326	1399	73
20	1315	1441	126
40	1479	1467	12
60	1478	1476	2
		Total AAD	87

Table A.53. Average absolute deviation for X-1360, HT38H fraction molecular weight data using the terminator-propagator model (o-dichlorobenzene measurements).

Asphaltene Concentration (kg/m^3)	Asphaltene Molecular Weight (g/mol)		AD
	Experimental	Calculated	
1	2542	1683	858
2	2369	1999	371
5	3530	2499	1031
10	3165	2896	270
20	3163	3256	93
40	3583	3537	46
1	2354	1683	670
2	2504	1999	505
5	2828	2499	329
10	3119	2896	223
20	3211	3256	45
40	3510	3537	27
		Total AAD	372

Table A.54. Summary of average absolute deviation for X-1360 asphaltenes molecular weight (o-dichlorobenzene measurements).

Fraction	AAD(g/mol)
HT67L	49
HT38L	87
Whole	95
HT67H	195
HT38H	372
AAD	160

Table A.55. Average absolute deviation for Short Residue, whole asphaltenes molecular weight data using the terminator-propagator model (toluene measurements).

Asphaltene Concentration (kg/m^3)	Asphaltene Molecular Weight (g/mol)		AD
	Experimental	Calculated	
2	6096	3611	2485
5	5016	4470	546
10	5007	5164	157
20	5544	5817	273
40	6388	6357	31
60	7078	6605	473
1	3244	3071	173
2	3665	3611	53
5	4033	4470	437
10	4853	5164	311
20	5604	5817	213
40	6556	6357	198
60	7244	6605	639
		Total AAD	461

Table A.56. Average absolute deviation for Short Residue, HT71L fraction molecular weight data using the terminator-propagator model (toluene measurements).

Asphaltene Concentration (kg/m^3)	Asphaltene Molecular Weight (g/mol)		AD
	Experimental	Calculated	
1	1958	2683	724
2	1935	3034	1099
5	3028	3530	502
10	3451	3872	421
20	3798	4143	345
40	4424	4332	92
60	4570	4407	162
1	2432	2683	251
2	2647	3034	388
5	3026	3530	504
10	3476	3872	396
20	3724	4143	419
40	4414	4332	82
60	4633	4407	225
		Total AAD	401

Table A.57. Average absolute deviation for Short Residue, HT71H fraction molecular weight data using the terminator-propagator model (toluene measurements).

Asphaltene Concentration (kg/m^3)	Asphaltene Molecular Weight (g/mol)		AD
	Experimental	Calculated	
1	4578	3763	815
2	5813	4732	1081
5	8248	6606	1642
10	9604	8593	1011
20	10797	11163	366
40	12948	14343	1395
60	14877	16458	1581
1	6773	3763	3010
2	6650	4732	1919
5	8092	6606	1486
10	8965	8593	372
20	10138	11163	1025
40	13180	14343	1162
60	14753	16458	1705
		Total AAD	1327

Table A.58. Average absolute deviation for Short Residue, HT84L fraction molecular weight data using the terminator-propagator model (toluene measurements).

Asphaltene Concentration (kg/m^3)	Asphaltene Molecular Weight (g/mol)		AD
	Experimental	Calculated	
1	1868	2310	442
2	2023	2521	497
5	2639	2791	153
10	2893	2958	65
20	2826	3079	253
40	3144	3155	12
60	3248	3185	64
1	2017	2310	293
2	2230	2521	290
5	2590	2791	201
10	2654	2958	304
20	2709	3079	369
40	3081	3155	74
60	3199	3185	14
		Total AAD	216

Table A.59. Average absolute deviation for Short Residue, HT84H fraction molecular weight data using the terminator-propagator model (toluene measurements).

Asphaltene Concentration (kg/m^3)	Asphaltene Molecular Weight (g/mol)		AD
	Experimental	Calculated	
1	2025	3489	1464
2	3102	4273	1171
5	4929	5672	744
10	6638	6990	352
20	8563	8457	106
40	10752	9935	817
60	11203	10736	467
1	3008	3489	481
2	4584	4273	310
5	6449	5672	777
10	7159	6990	169
20	8205	8457	252
40	10809	9935	873
60	10975	10736	239
		Total AAD	587

Table A.60. Summary of average absolute deviation for Short Residue asphaltenes molecular weight (toluene measurements).

Fraction	AAD(g/mol)
HT84L	216
HT71L	401
Whole	461
HT84H	587
HT71H	1327
AAD	598

Table A.61. Average absolute deviation for RHC-18-19, whole asphaltenes molecular weight data using the terminator-propagator model (o-dichlorobenzene measurements).

Asphaltene Concentration (kg/m^3)	Asphaltene Molecular Weight (g/mol)		AD
	Experimental	Calculated	
1	906	878	29
2	977	950	28
5	993	1066	73
10	1030	1157	127
20	1097	1239	143
40	1260	1303	43
60	1287	1331	44
1	1163	878	285
2	1081	950	131
5	1147	1066	81
10	1146	1157	11
20	1154	1239	85
40	1336	1303	32
60	1336	1331	5
		Total AAD	80

Table A.62. Average absolute deviation for RHC-18-19, HT76L fraction molecular weight data using the terminator-propagator model (o-dichlorobenzene measurements).

Asphaltene Concentration (kg/m^3)	Asphaltene Molecular Weight (g/mol)		AD
	Experimental	Calculated	
1	721	740	19
2	742	755	13
5	801	780	20
10	773	801	28
20	762	820	58
40	861	834	27
60	878	841	37
1	754	740	14
2	746	755	9
5	804	780	24
10	775	801	26
20	758	820	62
40	848	834	14
60	867	841	27
		Total AAD	27

Table A.63. Average absolute deviation for RHC-18-19, HT76H fraction molecular weight data using the terminator-propagator model (o-dichlorobenzene measurements).

Asphaltene Concentration (kg/m^3)	Asphaltene Molecular Weight (g/mol)		AD
	Experimental	Calculated	
1	1844	996	848
2	1392	1127	265
5	1497	1353	144
10	1519	1548	28
20	1581	1736	156
40	1877	1896	19
60	1950	1969	19
1	1606	996	610
2	1618	1127	491
5	1646	1353	292
10	1644	1548	96
20	1643	1736	94
40	1935	1896	39
60	2020	1969	50
		Total AAD	225

Table A.64. Average absolute deviation for RHC-18-19, HT45L fraction molecular weight data using the terminator-propagator model (o-dichlorobenzene measurements).

Asphaltene Concentration (kg/m^3)	Asphaltene Molecular Weight (g/mol)		AD
	Experimental	Calculated	
1	972	805	167
2	978	845	132
5	1003	909	94
10	934	956	22
20	914	995	82
40	1012	1024	11
60	1065	1035	29
1	893	805	88
2	755	845	91
5	902	909	6
10	889	956	66
20	882	995	113
40	1008	1024	15
60	1044	1035	8
		Total AAD	66

Table A.65. Average absolute deviation for RHC-18-19, HT45H fraction molecular weight data using the terminator-propagator model (o-dichlorobenzene measurements).

Asphaltene Concentration (kg/m^3)	Asphaltene Molecular Weight (g/mol)		AD
	Experimental	Calculated	
1	1902	1059	843
2	1790	1226	564
5	2006	1538	468
10	2066	1836	230
20	2122	2167	45
40	2474	2498	24
50	2535	2597	62
1	2152	1059	1093
2	2102	1226	876
5	2082	1538	545
10	2110	1836	274
20	2127	2167	40
40	2459	2498	39
50	2550	2597	47
		Total AAD	368

Table A.66. Summary of average absolute deviation for RHC-18-19 asphaltenes molecular weight (o-dichlorobenzene measurements).

Fraction	AAD(g/mol)
HT76L	27
HT45L	66
Whole	80
HT76H	225
HT45H	368
AAD	153

Table A.67. Average absolute deviation for HOSB, whole asphaltenes molecular weight data using the terminator-propagator model (toluene measurements).

Asphaltene Concentration (kg/m^3)	Asphaltene Molecular Weight (g/mol)		AD
	Experimental	Calculated	
1	897	860	37
2	911	966	55
5	1035	1135	100
10	1171	1274	103
20	1335	1410	75
30	1439	1483	44
40	1493	1531	39
60	1734	1592	141
1	944	860	84
2	912	966	54
5	1074	1135	61
10	1172	1274	102
20	1350	1410	60
30	1438	1483	45
40	1534	1531	3
60	1714	1592	122
		Total AAD	70

Table A.68. Average absolute deviation for HOSB, HT50L fraction molecular weight data using the terminator-propagator model (toluene measurements).

Asphaltene Concentration (kg/m^3)	Asphaltene Molecular Weight (g/mol)		AD
	Experimental	Calculated	
1	701	733	32
2	729	795	66
5	817	890	72
10	900	961	61
20	995	1025	30
30	1072	1057	15
40	1141	1077	64
60	1369	1102	267
1	685	733	48
2	727	795	68
5	835	890	55
10	921	961	40
20	1016	1025	9
30	1063	1057	6
40	1133	1077	55
60	1365	1102	263
		Total AAD	72

Table A.69. Average absolute deviation for HOSB, HT50H fraction molecular weight data using the terminator-propagator model (toluene measurements).

Asphaltene Concentration (kg/m^3)	Asphaltene Molecular Weight (g/mol)		AD
	Experimental	Calculated	
1	1545	1183	361
2	1708	1450	258
5	2197	1978	219
10	2535	2546	11
20	3213	3292	79
30	3922	3818	104
40	4415	4231	184
60	4910	4866	44
1	1382	1183	198
2	1709	1450	259
5	2136	1978	159
10	2593	2546	47
20	3213	3292	79
		Total AAD	154

Table A.70. Average absolute deviation for HOSB, HT80L fraction molecular weight data using the terminator-propagator model (toluene measurements).

Asphaltene Concentration (kg/m^3)	Asphaltene Molecular Weight (g/mol)		AD
	Experimental	Calculated	
1	509	613	103
2	508	643	135
5	577	688	111
10	608	721	113
20	669	750	81
1	610	613	3
2	611	643	33
5	688	688	0
10	778	721	56
20	786	750	36
30	915	764	151
40	960	773	187
60	1184	783	400
		Total AAD	108

Table A.71. Average absolute deviation for HOSB, HT80H fraction molecular weight data using the terminator-propagator model (toluene measurements).

Asphaltene Concentration (kg/m^3)	Asphaltene Molecular Weight (g/mol)		AD
	Experimental	Calculated	
1	1102	1035	67
2	1433	1217	215
5	1615	1542	72
10	1792	1847	55
20	2179	2187	8
40	2501	2539	38
50	2721	2650	71
1	1206	1035	172
2	1625	1217	408
5	1682	1542	140
10	1757	1847	89
20	2142	2187	45
30	2381	2393	12
40	2582	2539	43
50	2728	2650	77
		Total AAD	101

Table A.72. Summary of average absolute deviation for HOSB asphaltenes molecular weight (toluene measurements).

Fraction	AAD(g/mol)
HT80L	108
HT50L	72
Whole	70
HT80H	101
HT50H	154
AAD	101

Table A.73. Average absolute deviation for HOSB, whole asphaltenes molecular weight data using the terminator-propagator model (o-dichlorobenzene measurements).

Asphaltene Concentration (kg/m^3)	Asphaltene Molecular Weight (g/mol)		AD
	Experimental	Calculated	
1	851	691	160
2	754	747	7
5	862	831	30
10	872	894	22
20	879	947	68
40	1014	985	29
60	1039	1002	37
1	827	691	135
2	774	747	27
5	848	831	16
10	858	894	36
20	867	947	80
40	1000	985	14
60	1042	1002	40
		Total AAD	50

Table A.74. Average absolute deviation for HOSB, HT80L fraction molecular weight data using the terminator-propagator model (o-dichlorobenzene measurements).

Asphaltene Concentration (kg/m^3)	Asphaltene Molecular Weight (g/mol)		AD
	Experimental	Calculated	
1	488	539	51
2	567	555	12
5	588	580	9
10	583	597	15
20	574	612	38
1	503	539	36
2	656	555	101
5	616	580	37
10	595	597	2
20	578	612	34
		Total AAD	33

Table A.75. Average absolute deviation for HOSB, HT80H fraction molecular weight data using the terminator-propagator model (o-dichlorobenzene measurements).

Asphaltene Concentration (kg/m^3)	Asphaltene Molecular Weight (g/mol)		AD
	Experimental	Calculated	
1	960	786	174
2	1029	873	156
5	1077	1014	63
10	1059	1124	65
20	1102	1222	120
40	1301	1297	3
60	1292	1330	37
1	915	786	129
2	956	873	82
5	1129	1014	115
10	1112	1124	12
20	1130	1222	92
40	1277	1297	21
60	1336	1330	6
		Total AAD	77

Table A.76. Average absolute deviation for HOSB, HT50L fraction molecular weight data using the terminator-propagator model (o-dichlorobenzene measurements).

Asphaltene Concentration (kg/m^3)	Asphaltene Molecular Weight (g/mol)		AD
	Experimental	Calculated	
1	778	604	174
2	681	636	45
5	720	682	38
10	706	715	8
20	710	741	31
1	792	604	188
2	697	636	61
5	799	682	117
10	732	715	18
20	723	741	17
		Total AAD	70

Table A.77. Average absolute deviation for HOSB, HT50H fraction molecular weight data using the terminator-propagator model (o-dichlorobenzene measurements).

Asphaltene Concentration (kg/m^3)	Asphaltene Molecular Weight (g/mol)		AD
	Experimental	Calculated	
1	1336	866	470
2	1315	985	330
5	1349	1189	160
10	1361	1365	3
20	1416	1538	122
40	1670	1687	17
50	1701	1727	26
1	1348	866	482
2	1199	985	214
5	1405	1189	216
10	1368	1365	3
20	1420	1538	117
40	1691	1687	4
50	1700	1727	27
		Total AAD	157

Table A78. Summary of average absolute deviation for HOSB asphaltenes molecular weight (o-dichlorobenzene measurements).

Fraction	AAD(g/mol)
HT80L	33
HT50L	70
Whole	50
HT80H	77
HT50H	157
AAD	64

Table A.79. Average absolute deviation for RHC-18-37, whole asphaltenes molecular weight data using the terminator-propagator model (o-dichlorobenzene measurements).

Asphaltene Concentration (kg/m^3)	Asphaltene Molecular Weight (g/mol)		AD
	Experimental	Calculated	
1	682	631	51
2	689	679	10
5	743	749	6
10	722	799	77
20	723	840	116
40	827	868	41
60	886	880	5
1	730	631	99
2	710	679	32
5	756	749	7
10	723	799	76
20	739	840	100
40	839	868	29
60	916	880	36
		Total AAD	49

Table A.80. Average absolute deviation for RHC-18-37, HT91L fraction molecular weight data using the terminator-propagator model (o-dichlorobenzene measurements).

Asphaltene Concentration (kg/m^3)	Asphaltene Molecular Weight (g/mol)		AD
	Experimental	Calculated	
1	507	494	13
2	502	503	1
5	515	518	3
10	495	529	33
20	480	538	58
40	535	545	11
60	534	548	14
1	541	494	47
2	516	503	14
5	532	518	14
10	507	529	22
20	490	538	49
40	531	545	14
60	537	548	11
		Total AAD	22

Table A.81. Average absolute deviation for RHC-18-37, HT91H fraction molecular weight data using the terminator-propagator model (o-dichlorobenzene measurements).

Asphaltene Concentration (kg/m^3)	Asphaltene Molecular Weight (g/mol)		AD
	Experimental	Calculated	
1	973	719	254
2	898	799	99
5	928	921	7
10	944	1013	69
20	985	1091	106
40	1115	1147	32
50	1123	1161	38
1	1018	719	298
2	932	799	133
5	1094	921	172
10	996	1013	17
20	1024	1091	67
40	1181	1147	34
50	1189	1161	28
		Total AAD	97

Table A.82. Average absolute deviation for RHC-18-37, HT53L fraction molecular weight data using the terminator-propagator model (o-dichlorobenzene measurements).

Asphaltene Concentration (kg/m^3)	Asphaltene Molecular Weight (g/mol)		AD
	Experimental	Calculated	
1	592	568	24
2	582	597	14
5	615	638	23
10	605	666	60
20	603	688	85
40	674	702	28
60	722	708	14
1	610	568	42
2	599	597	2
5	631	638	7
10	617	666	49
20	607	688	81
40	673	702	30
60	719	708	11
		Total AAD	34

Table A.83. Average absolute deviation for RHC-18-37, HT53H fraction molecular weight data using the terminator-propagator model (o-dichlorobenzene measurements).

Asphaltene Concentration (kg/m^3)	Asphaltene Molecular Weight (g/mol)		AD
	Experimental	Calculated	
1	1198	851	347
2	1254	991	263
5	1487	1237	250
10	1505	1458	47
20	1605	1685	80
40	1919	1891	29
1	1229	851	378
2	1293	991	302
5	1532	1237	295
10	1634	1458	176
20	1684	1685	1
40	1962	1891	71
		Total AAD	187

Table A.84. Summary of average absolute deviation for RHC-18-37 asphaltenes molecular weight (o-dichlorobenzene measurements).

Fraction	AAD(g/mol)
HT91L	22
HT53L	34
Whole	49
HT91H	97
HT53H	187
AAD	65

Table A.85. Recalculation of $(T/P)_0$ for B3VB asphaltene fractions in toluene.

Fraction	$(T/P)_0$	ARD (%)
Whole	0.095	---
HT80	0.104	9.1
HT61.7	0.098	3.2

Table A.86. Recalculation of $(T/P)_0$ for B3VB asphaltene fractions in o-dichlorobenzene.

Fraction	$(T/P)_0$	ARD (%)
Whole	0.480	---
HT80	0.445	7.3
HT61.7	0.459	4.42

Table A.87. Recalculation of $(T/P)_0$ for X-1357 asphaltene fractions in toluene.

Fraction	$(T/P)_0$	ARD (%)
Whole	0.095	---
HT80	0.104	9.9
HT53	0.102	7.5

Table A.88. Recalculation of $(T/P)_0$ for X-1359 asphaltene fractions in o-dichlorobenzene.

Fraction	$(T/P)_0$	ARD (%)
Whole	0.490	---
HT68	0.515	5.0
HT	0.488	0.4

Table A.89. Recalculation of $(T/P)_0$ for X-1360 asphaltene fractions in o-dichlorobenzene.

Fraction	$(T/P)_0$	ARD (%)
Whole	0.620	---
HT67	0.574	7.5
HT38	0.604	2.6

Table A.90. Recalculation of $(T/P)_0$ for Short Residue asphaltene fractions in toluene.

Fraction	$(T/P)_0$	ARD (%)
Whole	0.250	---
HT84	0.245	2.0
HT71	0.273	9.3

Table A.91. Recalculation of $(T/P)_0$ for RHC-18-19 asphaltene fractions in o-dichlorobenzene.

Fraction	$(T/P)_0$	ARD (%)
Whole	0.620	---
HT76	0.563	9.2
HT45	0.555	10.5

Table A.92. Recalculation of $(T/P)_0$ for HOSB asphaltene fractions in toluene.

Fraction	$(T/P)_0$	ARD (%)
Whole	0.170	---
HT80	0.157	7.4
HT50	0.181	6.6

Table A.93. Recalculation of $(T/P)_0$ for HOSB asphaltene fractions in o-dichlorobenzene.

Fraction	$(T/P)_0$	ARD (%)
Whole	0.670	---
HT80	0.668	0.2
HT50	0.743	9.3

Table A.94. Recalculation of $(T/P)_0$ for RHC-18-37 asphaltene fractions in o-dichlorobenzene.

Fraction	$(T/P)_0$	ARD (%)
Whole	0.740	---
HT91	0.690	6.8
HT53	0.670	9.5

Table A.95. Error analysis for B3VB asphaltene solubility measurements in *n*-heptane/toluene mixtures.

Heptol Percentage (v/v)	n	μ(wt/wt)	σ (wt/wt)
50	2	0.0720	0.0000
60	2	0.2629	0.0015
61.7	13	0.3011	0.0071
70	2	0.4777	0.0051
80	16	0.7002	0.0107
90	2	0.8216	0.0006
100	2	0.9041	0.0099

Table A.96. Error analysis for X-1357 asphaltene solubility measurements in *n*-heptane/toluene mixtures

Heptol Percentage (v/v)	n	μ(wt/wt)	σ (wt/wt)
20	2	0.0000	0.0000
30	2	0.0513	0.0001
40	2	0.1781	0.0048
50	2	0.2987	0.0154
53	13	0.3794	0.0166
60	2	0.4241	0.0209
70	2	0.5689	0.0018
80	16	0.6849	0.0080
90	2	0.7717	0.0032
100	2	0.8920	0.0113

Table A.97. Error analysis for X-1359 asphaltene solubility measurements in *n*-heptane/toluene mixtures

Heptol Percentage (v/v)	n	μ(wt/wt)	σ (wt/wt)
10	2	0.0519	0.0010
20	2	0.1366	0.0085
30	2	0.2336	0.0098
35	13	0.3178	0.0189
40	2	0.3623	0.0202
50	2	0.5032	0.0054
60	2	0.6168	0.0055
68	14	0.7054	0.0233
70	2	0.6918	0.0050
80	2	0.7923	0.0061
90	2	0.8594	0.0048
100	2	0.9470	0.0071

Table A.98. Error analysis for X-1360 asphaltene solubility measurements in *n*-heptane/toluene mixtures

Heptol Percentage (v/v)	n	μ(wt/wt)	σ (wt/wt)
10	2	0.0580	0.0009
20	2	0.1255	0.0042
30	2	0.2246	0.0018
38	14	0.3250	0.0157
40	2	0.3461	0.0008
50	2	0.4657	0.0042
60	2	0.5701	0.0040
67	14	0.6514	0.0087
70	2	0.6871	0.0003
80	2	0.7830	0.0032
90	2	0.8587	0.0094
100	2	0.9495	0.0035

Table A.99. Error analysis for Short Residue asphaltene solubility measurements in *n*-heptane/toluene mixtures

Heptol Percentage (v/v)	n	μ(wt/wt)	σ (wt/wt)
50	2	0.0000	0.0000
60	2	0.0277	0.0024
70	2	0.3003	0.0042
71	12	0.3677	0.0110
80	2	0.5826	0.0056
84	14	0.7192	0.0111
90	2	0.7794	0.0263
100	2	0.9400	0.0014

Table A.100. Error analysis for RHC-18-19 asphaltene solubility measurements in *n*-heptane/toluene mixtures

Heptol Percentage (v/v)	n	μ(wt/wt)	σ (wt/wt)
20	2	0.1083	0.0024
30	2	0.1963	0.0024
40	2	0.2803	0.0222
45	14	0.4170	0.0240
50	2	0.3605	0.0143
60	2	0.4802	0.0299
70	2	0.5653	0.0165
76	14	0.6903	0.0205
80	2	0.7247	0.0057
90	2	0.8124	0.0138
100	2	0.9365	0.0092

Table A.101. Error analysis for RHC-18-37 asphaltene solubility measurements in *n*-heptane/toluene mixtures

Heptol Percentage (v/v)	n	μ(wt/wt)	σ (wt/wt)
10	2	0.0613	0.0007
20	2	0.1055	0.0007
30	2	0.1523	0.0024
40	2	0.2388	0.0116
50	2	0.2852	0.0030
53	14	0.3300	0.0230
60	2	0.3771	0.0164
70	2	0.4327	0.0019
80	2	0.5536	0.0390
90	2	0.6560	0.0189
91	14	0.7088	0.0301
100	2	0.8030	0.0014

Table A.102. Error analysis for HOSB asphaltene solubility measurements in *n*-heptane/toluene mixtures

Heptol Percentage (v/v)	n	μ(wt/wt)	σ (wt/wt)
10	2	0.0453	0.0019
20	2	0.1025	0.0001
30	2	0.1708	0.0015
40	2	0.2452	0.0074
50	14	0.3283	0.0264
60	2	0.4727	0.0093
70	2	0.5941	0.0180
80	14	0.6653	0.0184
100	2	0.9250	0.0028

Table A.103. AAD for predictions of B3VB asphaltenes solubility in *n*-heptane/toluene mixtures at 23°C using regular solution approach when density is correlated to molecular weight.

Heptol % (v/v)	Asphaltene Fractional precipitation (wt/wt)				
	Experimental	Gamma Distribution	AAD	T/P Distribution	AAD
50	0.0720	0.0789	0.0069	0.0561	0.0159
60	0.2618	0.2827	0.0209	0.2736	0.0118
70	0.4813	0.4871	0.0057	0.4966	0.0152
80	0.6729	0.6505	0.0224	0.6334	0.0394
90	0.8211	0.7584	0.0628	0.7226	0.0985
100	0.8971	0.8699	0.0272	0.7760	0.1211
50	0.0720	0.0789	0.0069	0.0561	0.0159
60	0.2640	0.2827	0.0187	0.2736	0.0096
70	0.4741	0.4871	0.0130	0.4966	0.0225
80	0.6807	0.6505	0.0302	0.6334	0.0472
90	0.8220	0.7584	0.0636	0.7226	0.0994
100	0.9111	0.8699	0.0412	0.7760	0.1351
		Average	0.0266	**Average**	0.0527

Table A.104. AAD for predictions of B3VB asphaltenes solubility in *n*-heptane/toluene mixtures at 23°C using regular solution approach when density is a function of accumulative mass fraction of asphaltenes.

Heptol % (v/v)	Asphaltene Fractional precipitation (wt/wt)				
	Experimental	Gamma Distribution	AAD	T/P Distribution	AAD
50	0.0720	0.0134	0.0586	0.0392	0.0328
60	0.2618	0.2060	0.0558	0.2373	0.0245
70	0.4813	0.5107	0.0293	0.4954	0.0141
80	0.6729	0.7118	0.0390	0.6612	0.0116
90	0.8211	0.8168	0.0043	0.7518	0.0693
100	0.8971	0.8753	0.0218	0.8247	0.0724
50	0.0720	0.0134	0.0586	0.0392	0.0328
60	0.2640	0.2060	0.0580	0.2373	0.0267
70	0.4741	0.5107	0.0366	0.4954	0.0214
80	0.6807	0.7118	0.0312	0.6612	0.0194
90	0.8220	0.8168	0.0052	0.7518	0.0702
100	0.9111	0.8753	0.0358	0.8247	0.0864
		Average	0.0362	**Average**	0.0401

Table A.105. AAD for predictions of X-1357 asphaltenes solubility in *n*-heptane/toluene mixtures at 23°C using regular solution approach when density is correlated to molecular weight.

Heptol % (v/v)	Asphaltene Fractional precipitation (wt/wt)				
	Experimental	Gamma Distribution	AAD	T/P Distribution	AAD
20	0.0000	0.0144	0.0144	0.0085	0.0085
30	0.0512	0.0677	0.0165	0.0550	0.0038
40	0.1747	0.1716	0.0030	0.1586	0.0160
50	0.3096	0.3067	0.0029	0.3043	0.0052
60	0.4388	0.4447	0.0059	0.4475	0.0086
70	0.5676	0.5609	0.0068	0.5619	0.0057
80	0.6829	0.6631	0.0198	0.6425	0.0404
90	0.7740	0.7445	0.0295	0.7019	0.0721
100	0.9000	0.8218	0.0782	0.7600	0.1400
20	0.0000	0.0144	0.0144	0.0085	0.0085
30	0.0513	0.0677	0.0163	0.0550	0.0037
40	0.1815	0.1716	0.0099	0.1586	0.0229
50	0.2878	0.3067	0.0189	0.3043	0.0165
60	0.4093	0.4447	0.0354	0.4475	0.0381
70	0.5701	0.5609	0.0092	0.5619	0.0082
80	0.6809	0.6631	0.0178	0.6425	0.0384
90	0.7695	0.7445	0.0250	0.7019	0.0676
100	0.8840	0.8218	0.0622	0.7600	0.1240
		Average	0.0214	**Average**	0.0349

Table A.106. AAD for predictions of X-1357 asphaltenes solubility in *n*-heptane/toluene mixtures at 23°C using regular solution approach when density is a function of accumulative mass fraction of asphaltenes.

Heptol % (v/v)	Asphaltene Fractional precipitation (wt/wt)				
	Experimental	Gamma Distribution	AAD	T/P Distribution	AAD
20	0.0000	0.0091	0.0091	0.0142	0.0142
30	0.0512	0.0489	0.0023	0.0639	0.0127
40	0.1747	0.1350	0.0396	0.1617	0.0129
50	0.3096	0.2676	0.0420	0.2964	0.0131
60	0.4388	0.4205	0.0184	0.4360	0.0029
70	0.5676	0.5629	0.0048	0.5552	0.0124
80	0.6829	0.6805	0.0024	0.6404	0.0425
90	0.7740	0.7610	0.0130	0.7073	0.0667
100	0.9000	0.8269	0.0731	0.7626	0.1374
20	0.0000	0.0091	0.0091	0.0142	0.0142
30	0.0513	0.0489	0.0024	0.0639	0.0126
40	0.1815	0.1350	0.0465	0.1617	0.0198
50	0.2878	0.2676	0.0202	0.2964	0.0086
60	0.4093	0.4205	0.0111	0.4360	0.0266
70	0.5701	0.5629	0.0072	0.5552	0.0149
80	0.6809	0.6805	0.0004	0.6404	0.0405
90	0.7695	0.7610	0.0085	0.7073	0.0622
100	0.8840	0.8269	0.0571	0.7626	0.1214
		Average	0.0204	**Average**	0.0353

Table A.107. AAD for predictions of X-1359 asphaltenes solubility in *n*-heptane/toluene mixtures at 23°C using regular solution approach when density is a function of accumulative mass fraction of asphaltenes.

Heptol % (v/v)	Asphaltene Fractional precipitation (wt/wt)				
	Experimental	Gamma Distribution	AAD	T/P Distribution	AAD
10	0.0526	0.0475	0.0051	0.0321	0.0205
20	0.1306	0.1179	0.0127	0.1094	0.0212
30	0.2405	0.2234	0.0171	0.2368	0.0037
40	0.3766	0.3544	0.0222	0.3816	0.0050
50	0.5070	0.4932	0.0138	0.5144	0.0074
60	0.6129	0.6162	0.0033	0.6156	0.0026
70	0.6953	0.7086	0.0133	0.6895	0.0058
80	0.7967	0.7759	0.0208	0.7493	0.0473
90	0.8560	0.8432	0.0128	0.7915	0.0645
100	0.9420	0.8887	0.0533	0.8228	0.1192
10	0.0512	0.0475	0.0037	0.0321	0.0191
20	0.1427	0.1179	0.0248	0.1094	0.0332
30	0.2267	0.2234	0.0033	0.2368	0.0102
40	0.3480	0.3544	0.0064	0.3816	0.0336
50	0.4993	0.4932	0.0061	0.5144	0.0151
60	0.6207	0.6162	0.0045	0.6156	0.0051
70	0.6882	0.7086	0.0204	0.6895	0.0013
80	0.7880	0.7759	0.0121	0.7493	0.0387
90	0.8628	0.8432	0.0196	0.7915	0.0713
100	0.9520	0.8887	0.0633	0.8228	0.1292
		Average	0.0169	**Average**	0.0327

Table A.108. AAD for predictions of X-1360 asphaltenes solubility in *n*-heptane/toluene mixtures at 23°C using regular solution approach when density is a function of accumulative mass fraction of asphaltenes.

Heptol % (v/v)	Asphaltene Fractional precipitation (wt/wt)				
	Experimental	Gamma Distribution	AAD	T/P Distribution	AAD
10	0.0573	0.0420	0.0154	0.0295	0.0279
20	0.1225	0.1057	0.0168	0.0991	0.0234
30	0.2258	0.2070	0.0189	0.2160	0.0099
40	0.3455	0.3337	0.0118	0.3536	0.0081
50	0.4687	0.4703	0.0016	0.4791	0.0104
60	0.5673	0.5928	0.0254	0.5830	0.0157
70	0.6873	0.6971	0.0099	0.6581	0.0292
80	0.7852	0.7628	0.0225	0.7051	0.0802
90	0.8520	0.8428	0.0092	0.7602	0.0918
100	0.9470	0.8737	0.0733	0.7767	0.1703
10	0.0586	0.0420	0.0166	0.0295	0.0291
20	0.1285	0.1057	0.0228	0.0991	0.0294
30	0.2233	0.2070	0.0164	0.2160	0.0073
40	0.3467	0.3337	0.0129	0.3536	0.0069
50	0.4627	0.4703	0.0076	0.4791	0.0164
60	0.5730	0.5928	0.0198	0.5830	0.0101
70	0.6869	0.6971	0.0103	0.6581	0.0288
80	0.7807	0.7628	0.0179	0.7051	0.0756
90	0.8653	0.8428	0.0225	0.7602	0.1052
100	0.9520	0.8737	0.0783	0.7767	0.1753
		Average	0.0215	**Average**	0.0475

Table A.109. AAD for predictions of Short Residue asphaltenes solubility in *n*-heptane/toluene mixtures at 23°C using regular solution approach when density is correlated to molecular weight.

Heptol % (v/v)	Asphaltene Fractional precipitation (wt/wt)				
	Experimental	Gamma Distribution	AAD	T/P Distribution	AAD
40	0.0000	0.0000	0.0000	0.0000	0.0000
50	0.0000	0.0000	0.0000	0.0007	0.0007
60	0.0293	0.0316	0.0022	0.0599	0.0306
70	0.3033	0.2727	0.0306	0.3048	0.0015
80	0.5866	0.5905	0.0039	0.5697	0.0169
90	0.7608	0.7896	0.0288	0.7348	0.0261
100	0.9410	0.9018	0.0392	0.8313	0.1097
40	0.0000	0.0000	0.0000	0.0000	0.0000
50	0.0000	0.0000	0.0000	0.0007	0.0007
60	0.0260	0.0316	0.0056	0.0599	0.0339
70	0.2973	0.2727	0.0246	0.3048	0.0075
80	0.5786	0.5905	0.0119	0.5697	0.0089
90	0.7980	0.7896	0.0084	0.7348	0.0632
100	0.9390	0.9018	0.0372	0.8313	0.1077
		Average	0.0137	**Average**	0.0291

Table A.110. AAD for predictions of Short Residue asphaltenes solubility in *n*-heptane/toluene mixtures at 23°C using regular solution approach when density is a function of accumulative mass fraction of asphaltenes.

Heptol % (v/v)	Asphaltene Fractional precipitation (wt/wt)				
	Experimental	Gamma Distribution	AAD	T/P Distribution	AAD
40	0.0000	0.0000	0.0000	0.0000	0.0000
50	0.0000	0.0000	0.0000	0.0014	0.0014
60	0.0293	0.0316	0.0022	0.0607	0.0314
70	0.3033	0.2743	0.0290	0.3058	0.0024
80	0.5866	0.6041	0.0175	0.5846	0.0019
90	0.7608	0.8027	0.0419	0.7436	0.0172
100	0.9410	0.9031	0.0379	0.8325	0.1085
40	0.0000	0.0000	0.0000	0.0000	0.0000
50	0.0000	0.0000	0.0000	0.0014	0.0014
60	0.0260	0.0316	0.0056	0.0607	0.0347
70	0.2973	0.2743	0.0230	0.3058	0.0084
80	0.5786	0.6041	0.0255	0.5846	0.0061
90	0.7980	0.8027	0.0047	0.7436	0.0544
100	0.9390	0.9031	0.0359	0.8325	0.1065
		Average	0.0159	**Average**	0.0269

Table A.111. AAD for predictions of HOSB asphaltenes solubility in *n*-heptane/toluene mixtures at 23°C using regular solution approach when density is correlated to molecular weight.

Heptol % (v/v)	Asphaltene Fractional precipitation (wt/wt)				
	Experimental	Gamma Distribution	AAD	T/P Distribution	AAD
10	0.0467	0.0355	0.0112	0.0216	0.0250
20	0.1024	0.0867	0.0156	0.0771	0.0253
30	0.1698	0.1630	0.0068	0.1692	0.0006
40	0.2400	0.2562	0.0162	0.2706	0.0306
50	0.3387	0.3581	0.0194	0.3590	0.0203
60	0.4661	0.4600	0.0061	0.4321	0.0340
70	0.6068	0.5562	0.0506	0.4942	0.1126
80	0.6917	0.6489	0.0428	0.5331	0.1585
100	0.9230	0.8021	0.1209	0.6101	0.3129
10	0.0439	0.0355	0.0085	0.0216	0.0223
20	0.1025	0.0867	0.0158	0.0771	0.0255
30	0.1719	0.1630	0.0089	0.1692	0.0027
40	0.2505	0.2562	0.0057	0.2706	0.0201
50	0.3347	0.3581	0.0234	0.3590	0.0243
60	0.4793	0.4600	0.0193	0.4321	0.0472
70	0.5814	0.5562	0.0252	0.4942	0.0872
80	0.6866	0.6489	0.0377	0.5331	0.1534
100	0.9270	0.8021	0.1249	0.6101	0.3169
		Average	0.0311	**Average**	0.0789

Table A.112. AAD for predictions of HOSB asphaltenes solubility in *n*-heptane/toluene mixtures at 23°C using regular solution approach when density is a function of accumulative mass fraction of asphaltenes.

Heptol % (v/v)	Asphaltene Fractional precipitation (wt/wt)				
	Experimental	Gamma Distribution	AAD	T/P Distribution	AAD
10	0.0467	0.0436	0.0030	0.0228	0.0238
20	0.1024	0.0969	0.0055	0.0748	0.0276
30	0.1698	0.1755	0.0058	0.1604	0.0094
40	0.2400	0.2721	0.0321	0.2597	0.0197
50	0.3387	0.3754	0.0367	0.3529	0.0142
60	0.4661	0.4758	0.0097	0.4319	0.0342
70	0.6068	0.5655	0.0413	0.4985	0.1083
80	0.6917	0.6497	0.0420	0.5439	0.1478
100	0.9230	0.7863	0.1367	0.6189	0.3041
10	0.0439	0.0436	0.0003	0.0228	0.0211
20	0.1025	0.0969	0.0056	0.0748	0.0277
30	0.1719	0.1755	0.0036	0.1604	0.0115
40	0.2505	0.2721	0.0216	0.2597	0.0092
50	0.3347	0.3754	0.0407	0.3529	0.0182
60	0.4793	0.4758	0.0035	0.4319	0.0474
70	0.5814	0.5655	0.0159	0.4985	0.0829
80	0.6866	0.6497	0.0369	0.5439	0.1426
100	0.9270	0.7863	0.1407	0.6189	0.3081
		Average	0.0323	**Average**	0.0754

Table A.113. AAD for predictions of RHC-18-19 asphaltenes solubility in *n*-heptane/toluene mixtures at 23°C using regular solution approach when density is a function of accumulative mass fraction of asphaltenes.

Heptol % (v/v)	Asphaltene Fractional precipitation (wt/wt)				
	Experimental	Gamma Distribution	AAD	T/P Distribution	AAD
20	0.1100	0.0969	0.0131	0.0684	0.0416
30	0.1980	0.1769	0.0211	0.1656	0.0324
40	0.2647	0.2777	0.0131	0.2829	0.0183
50	0.3504	0.3878	0.0373	0.3904	0.0400
60	0.5013	0.4960	0.0053	0.4771	0.0242
70	0.5536	0.5939	0.0403	0.5447	0.0089
80	0.7287	0.6771	0.0515	0.6003	0.1284
90	0.8027	0.7493	0.0533	0.6372	0.1655
100	0.9300	0.8074	0.1226	0.6743	0.2557
20	0.1067	0.0969	0.0097	0.0684	0.0383
30	0.1947	0.1769	0.0177	0.1656	0.0291
40	0.2960	0.2777	0.0183	0.2829	0.0131
50	0.3707	0.3878	0.0171	0.3904	0.0197
60	0.4591	0.4960	0.0369	0.4771	0.0181
70	0.5769	0.5939	0.0170	0.5447	0.0322
80	0.7207	0.6771	0.0435	0.6003	0.1204
90	0.8221	0.7493	0.0728	0.6372	0.1849
100	0.9430	0.8074	0.1356	0.6743	0.2687
		Average	0.0403	**Average**	0.0800

Table A.114. AAD for predictions of RHC-18-37 asphaltenes solubility in *n*-heptane/toluene mixtures at 23°C using regular solution approach when density is a function of accumulative mass fraction of asphaltenes.

Heptol % (v/v)	Asphaltene Fractional precipitation (wt/wt)				
	Experimental	Gamma Distribution	AAD	T/P Distribution	AAD
10	0.0618	0.0490	0.0128	0.0337	0.0281
20	0.1050	0.0907	0.0143	0.0870	0.0180
30	0.1540	0.1490	0.0050	0.1628	0.0088
40	0.2470	0.2222	0.0248	0.2453	0.0017
50	0.2973	0.3060	0.0086	0.3218	0.0245
60	0.3655	0.3949	0.0294	0.3873	0.0218
70	0.4340	0.4837	0.0497	0.4411	0.0071
80	0.5812	0.5684	0.0129	0.4850	0.0962
90	0.6693	0.6463	0.0230	0.5231	0.1462
100	0.8040	0.7170	0.0870	0.5552	0.2488
10	0.0607	0.0490	0.0116	0.0337	0.0269
20	0.1059	0.0907	0.0152	0.0870	0.0189
30	0.1506	0.1490	0.0016	0.1628	0.0122
40	0.2307	0.2222	0.0085	0.2453	0.0146
50	0.2931	0.3060	0.0129	0.3218	0.0288
60	0.3887	0.3949	0.0062	0.3873	0.0014
70	0.4313	0.4837	0.0524	0.4411	0.0097
80	0.5260	0.5684	0.0424	0.4850	0.0410
90	0.6427	0.6463	0.0037	0.5231	0.1196
100	0.8020	0.7170	0.0850	0.5552	0.2468
		Average	0.0254	**Average**	0.0561

APPENDIX B: ADDITIONAL FIGURES

Figures B.1 to B.9 show fractional yield of different asphaltenes from solutions of *n*-heptane and toluene at 23°C

Figures B.10 to B.19 represent fitting results of the terminator-propagator model to the molecular weights of whole asphaltenes and their solubility cuts.

Figures B.20 to B.28 depict density measurements of whole asphaltenes for the samples used in this thesis.

Figures B.29 to B.37 depict FRI calculations of whole asphaltenes for different samples used in this thesis

Figures B.38 to B.47 represent density of heavy and light cuts of asphaltenes and their correspondent density distributions.

Figures B.48 to B.55 show regular solution modeling results in predicting of fractional yield of asphaltenes from solutions of n-heptane and toluene at 23 °C.

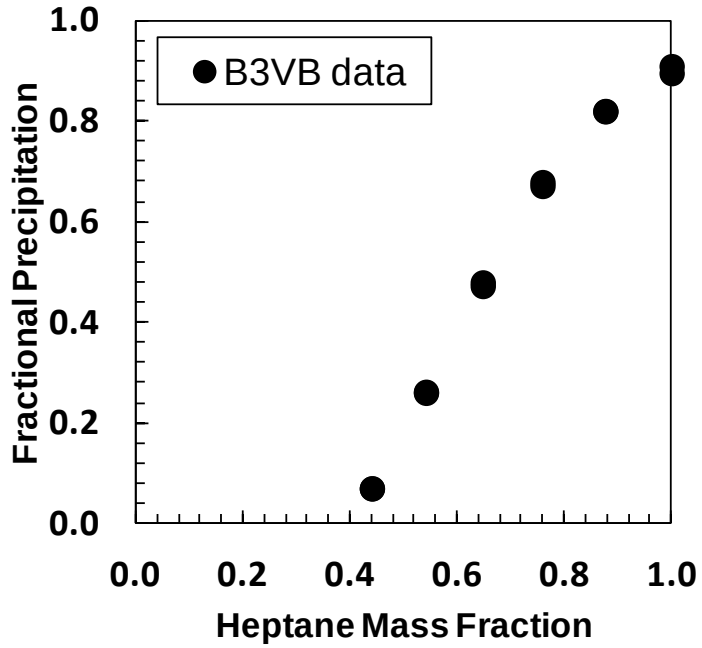

Figure B.1. Fractional precipitation of B3VB asphaltenes from solutions of *n*-heptane and toluene at 23°C

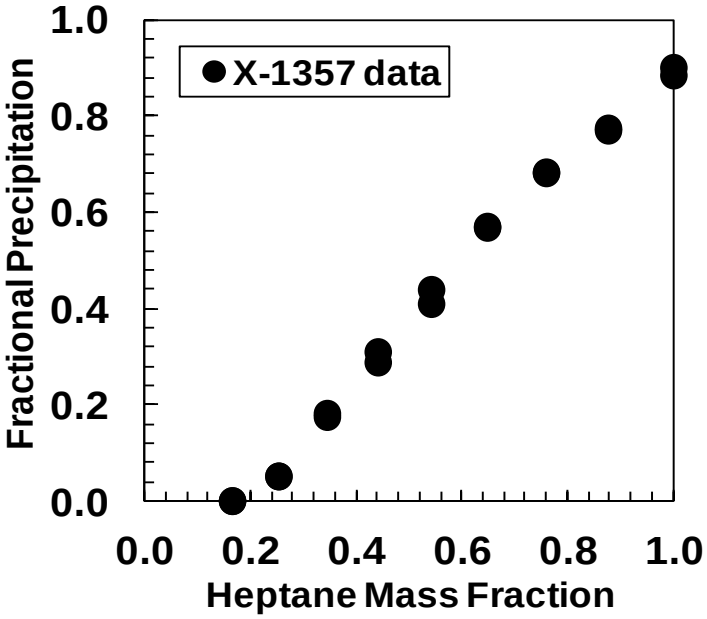

Figure B.2. Fractional precipitation of X-1357 asphaltenes from solutions of *n*-heptane and toluene at 23°C

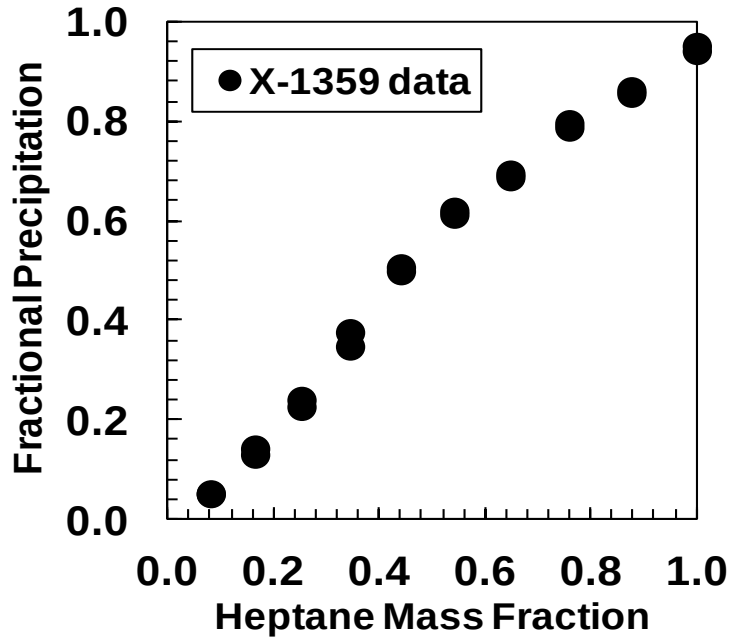

Figure B.3. Fractional precipitation of X-1359 asphaltenes from solutions of *n*-heptane and toluene at 23°C

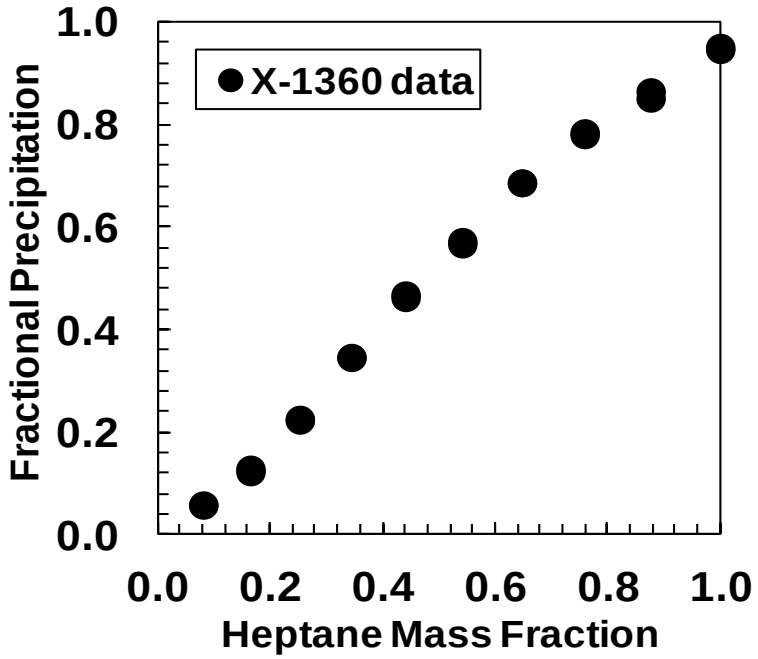

Figure B.4. Fractional precipitation of X-1360 asphaltenes from solutions of *n*-heptane and toluene at 23°C

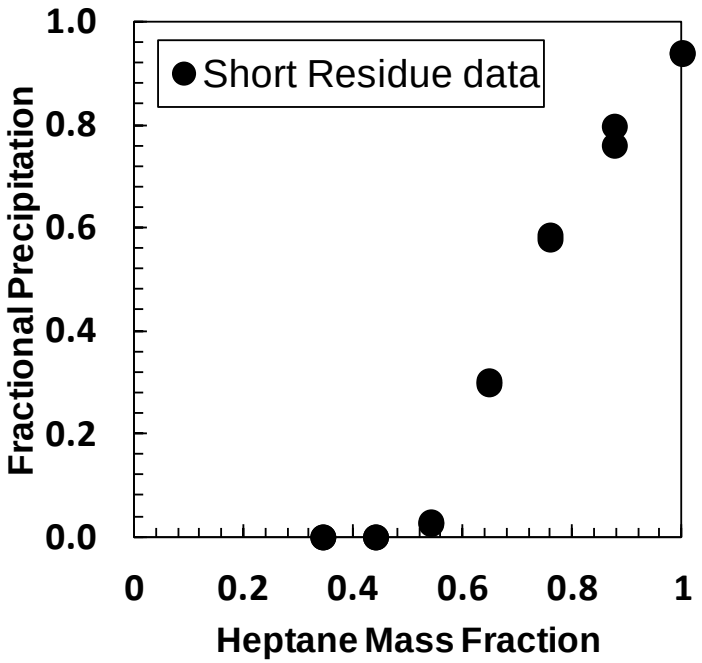

Figure B.5. Fractional precipitation of Short Residue asphaltenes from solutions of *n*-heptane and toluene at 23°C

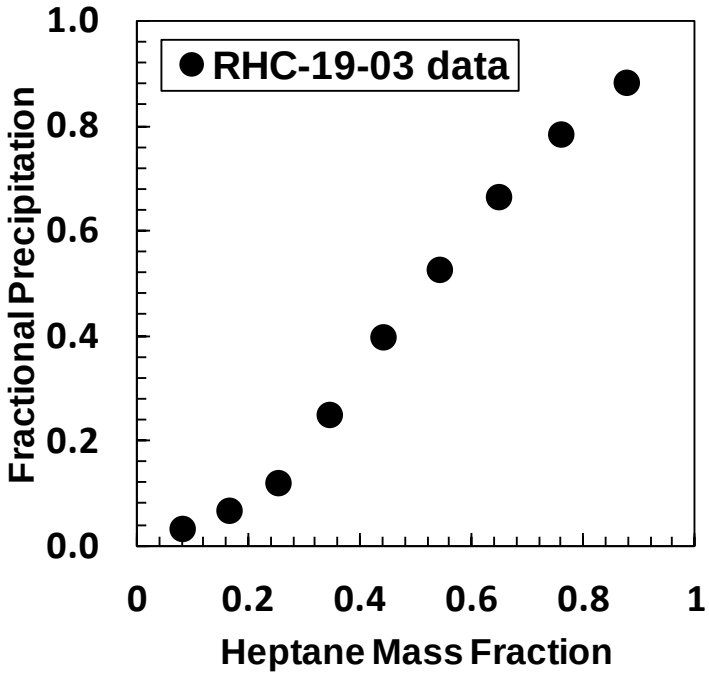

Figure B.6. Fractional precipitation of RHC-19-03 asphaltenes from solutions of *n*-heptane and toluene at 23°C

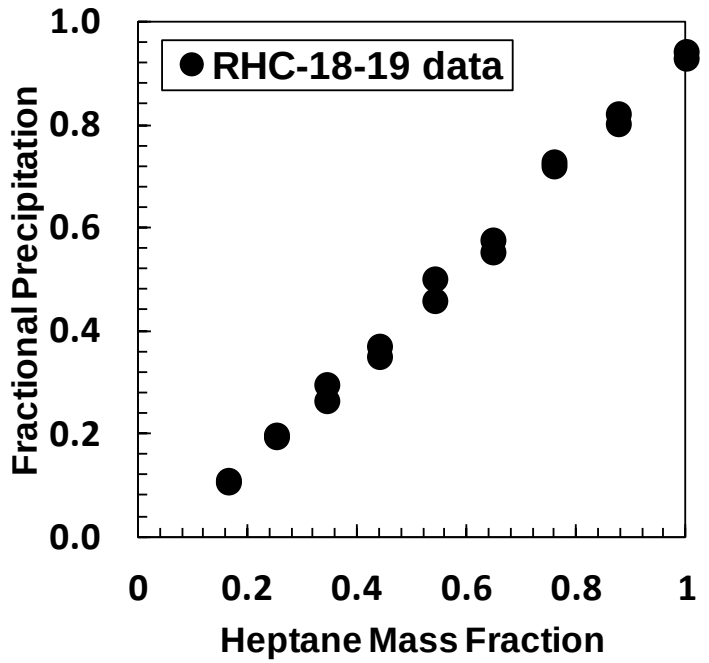

Figure B.7. Fractional precipitation of RHC-18-19 asphaltenes from solutions of *n*-heptane and toluene at 23°C

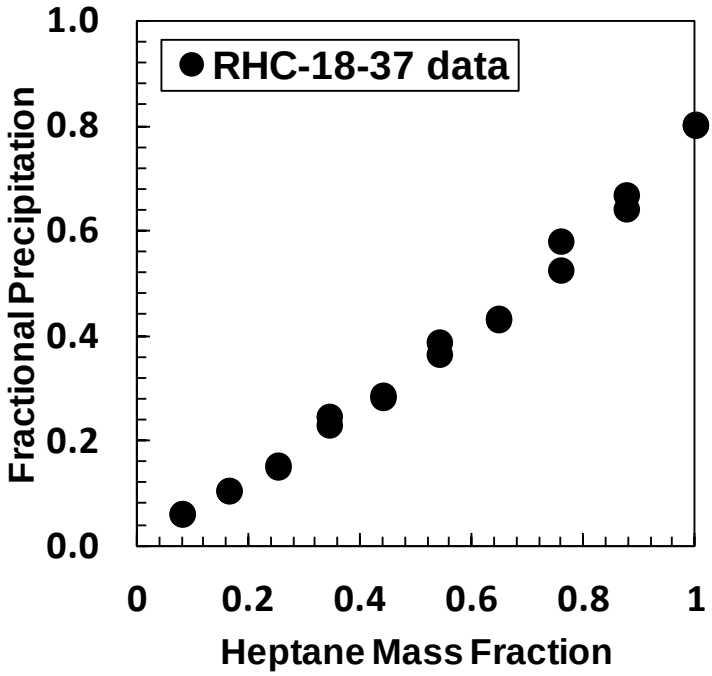

Figure B.8. Fractional precipitation of RHC-18-37 asphaltenes from solutions of *n*-heptane and toluene at 23°C

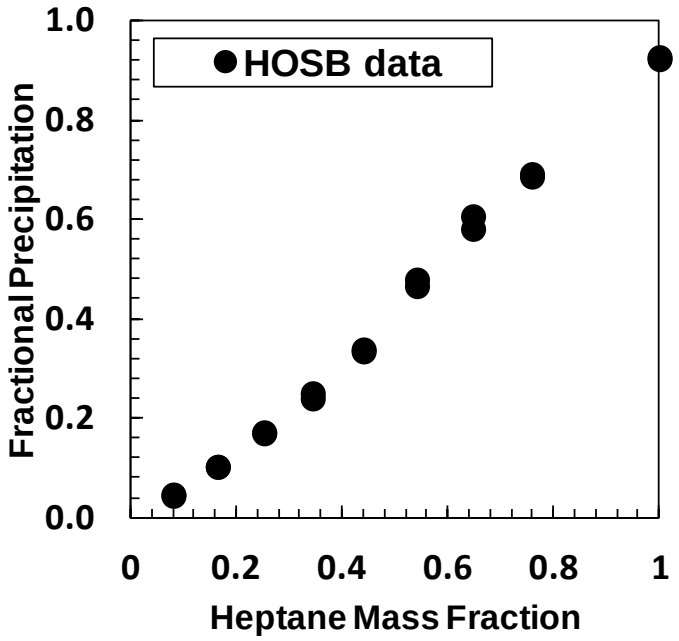

Figure B.9. Fractional precipitation of HOSB asphaltenes from solutions of *n*-heptane and toluene at 23°C

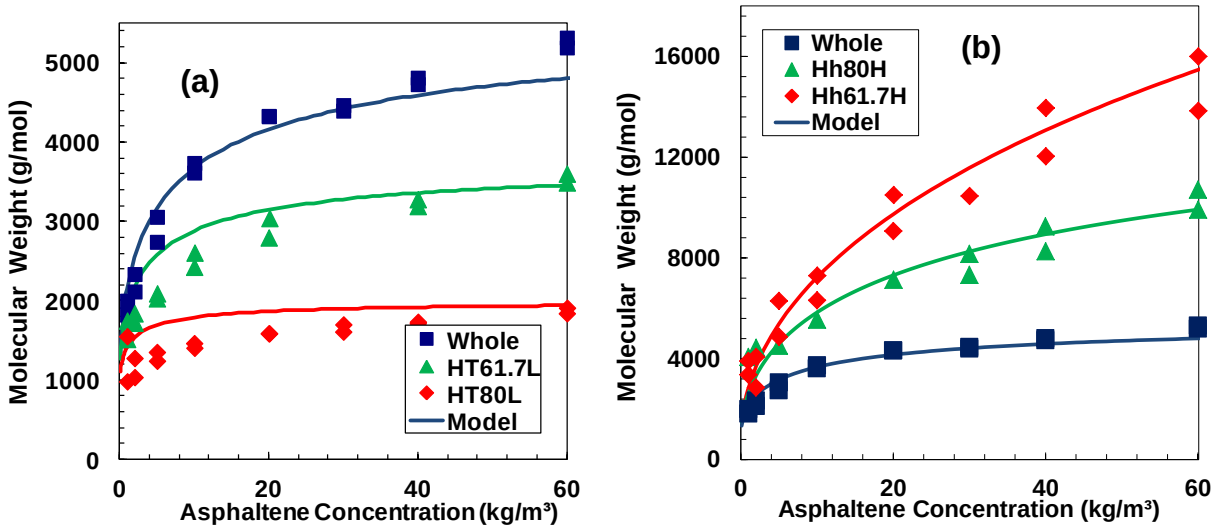

Figure B.10. Fitting of terminator-propagator model to B3VB whole asphaltenes, a) light cuts and, b) heavy cuts measured in toluene.

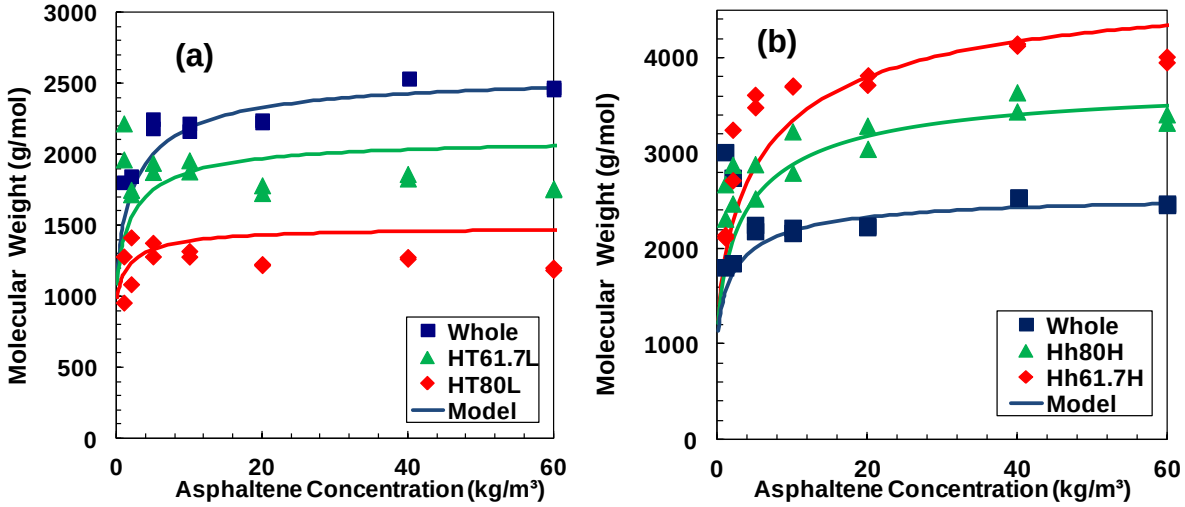

Figure B.11. Fitting of terminator-propagator model to B3VB whole asphaltenes, a) light cuts and, b) heavy cuts measured in o-dichlorobenzene.

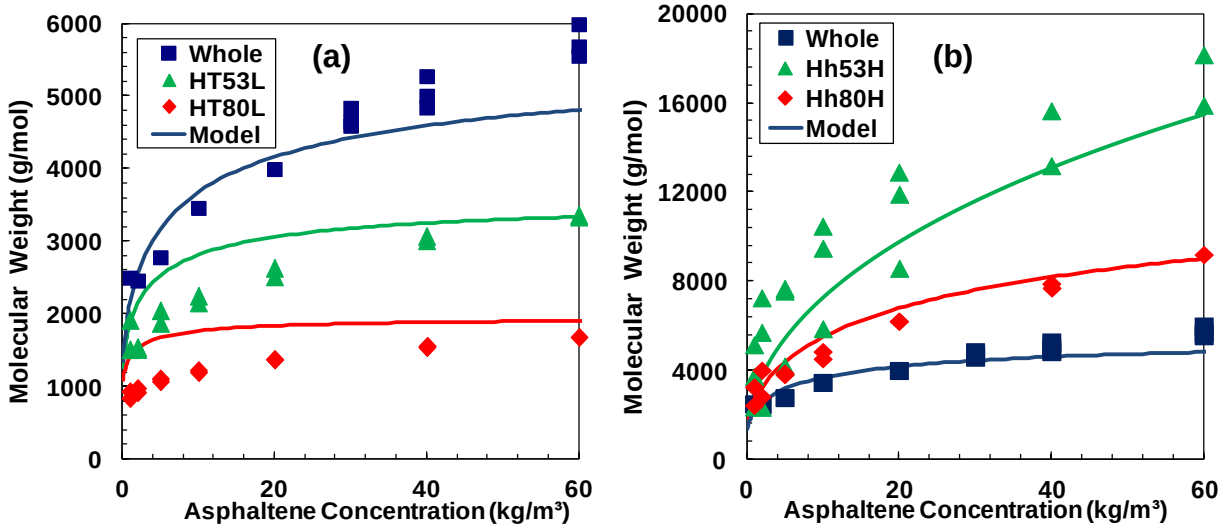

Figure B.12. Fitting of terminator-propagator model to X-1357 whole asphaltenes, a) light cuts and, b) heavy cuts measured in toluene.

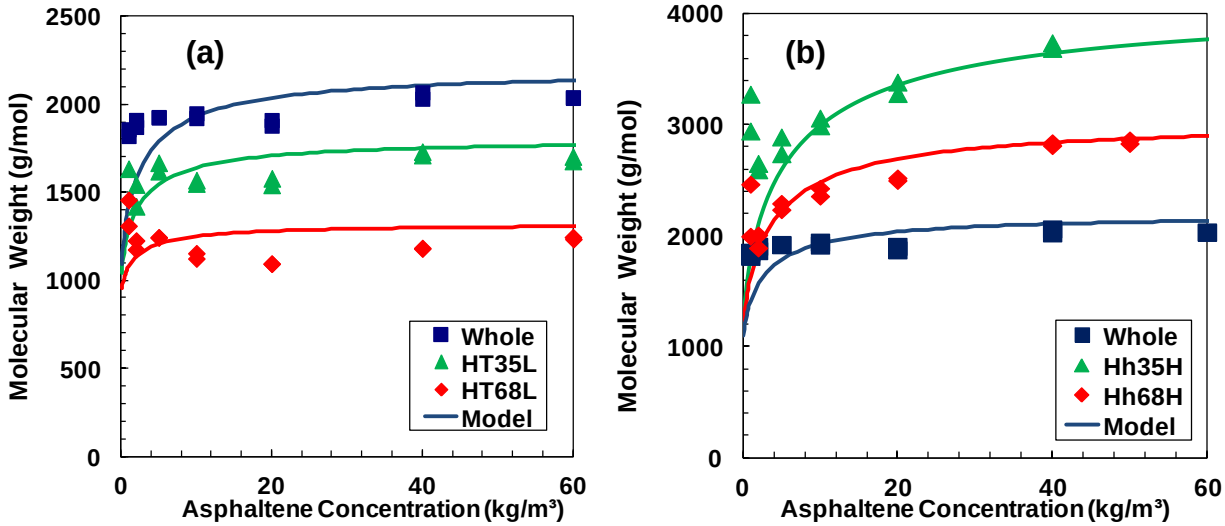

Figure B.13. Fitting of terminator-propagator model to X-1359 whole asphaltenes, a) light cuts and, b) heavy cuts measured in o-dichlorobenzene.

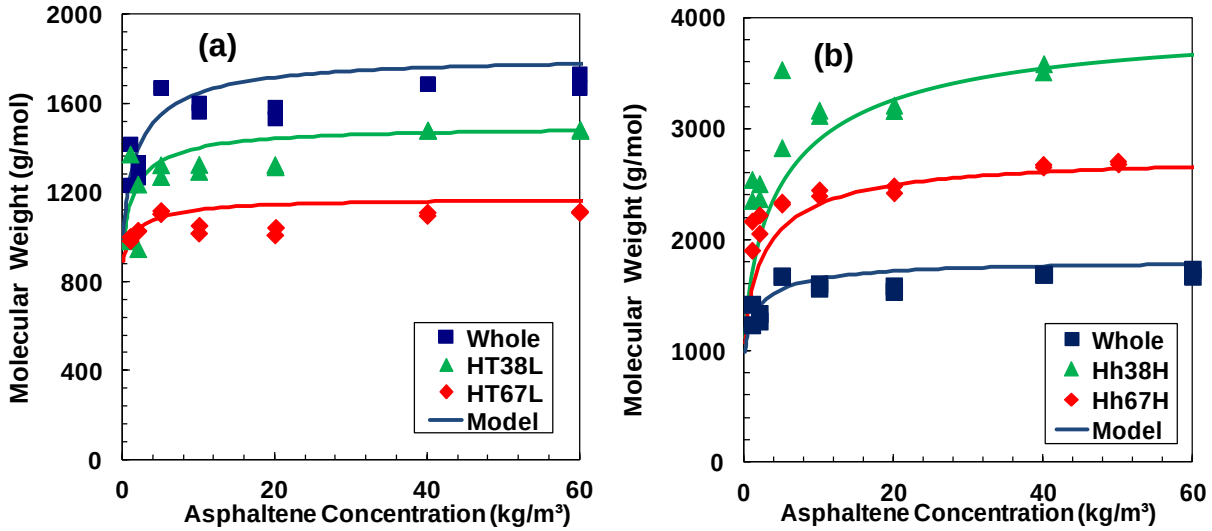

Figure B.14. Fitting of terminator-propagator model to X-1360 whole asphaltenes, a) light cuts and, b) heavy cuts measured in o-dichlorobenzene.

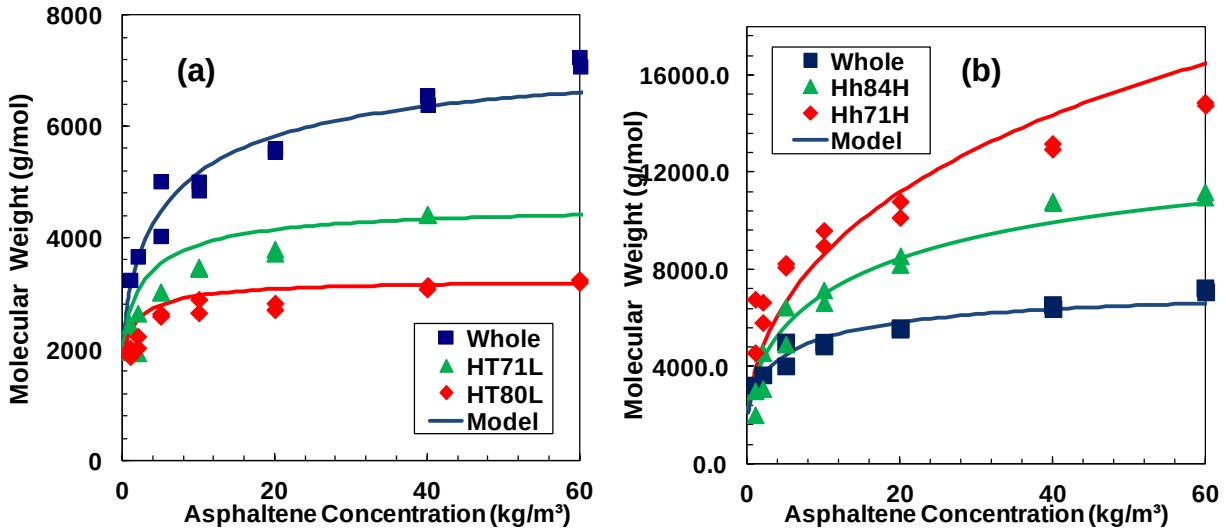

Figure B.15. Fitting of terminator-propagator model to Short Residue whole asphaltenes, a) light cuts and, b) heavy cuts measured in toluene.

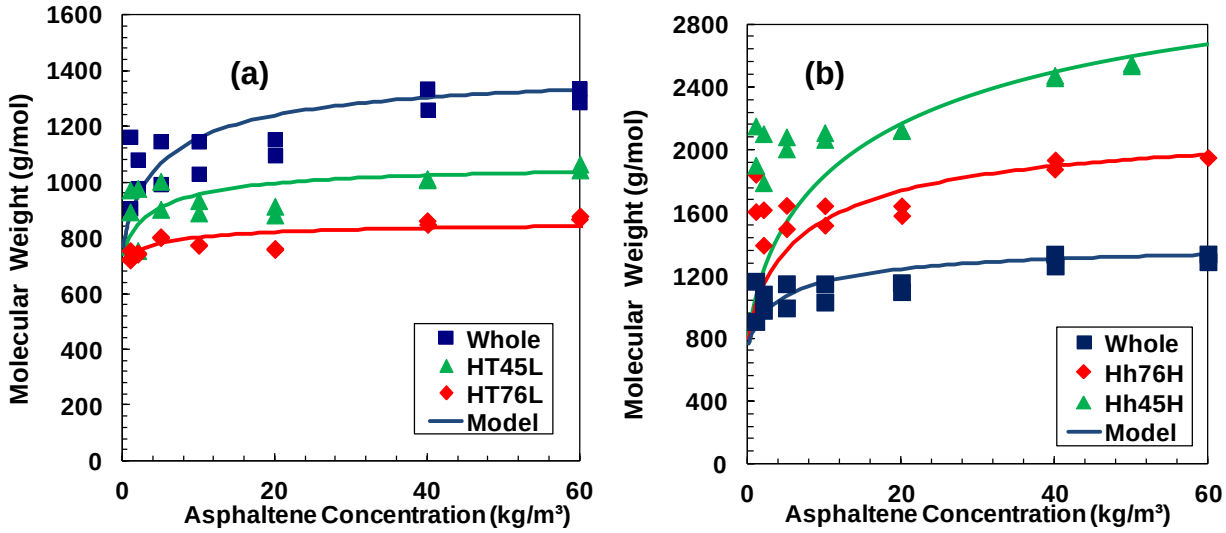

Figure B.16. Fitting of terminator-propagator model to RHC-18-19 whole asphaltenes, a) light cuts and, b) heavy cuts measured in o-dichlorobenzene.

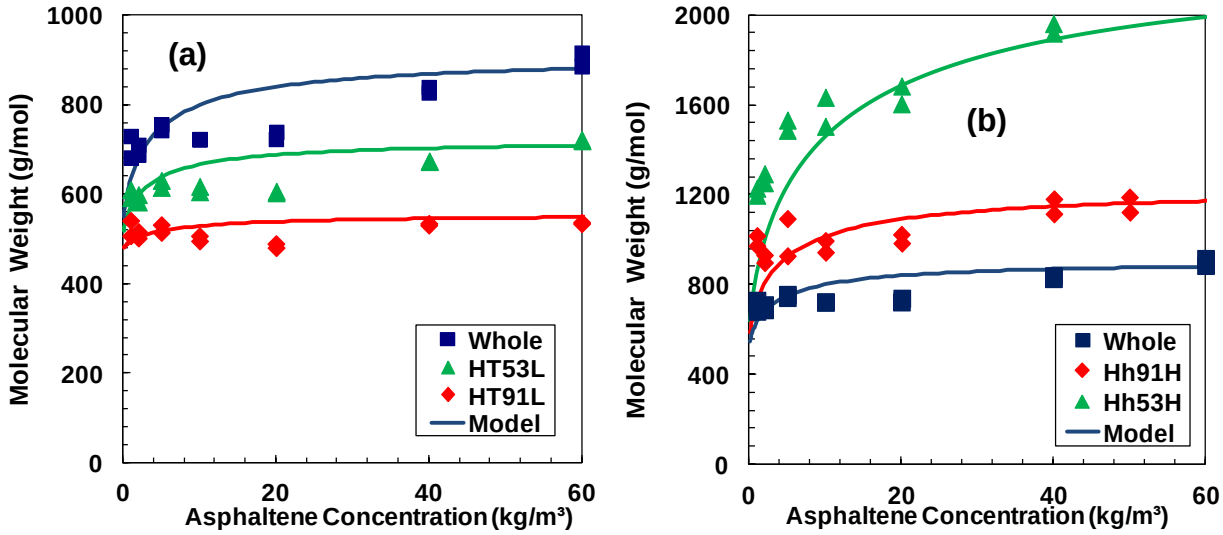

Figure B.17. Fitting of terminator-propagator model to RHC-18-37 whole asphaltenes, a) light cuts and, b) heavy cuts measured in o-dichlorobenzene.

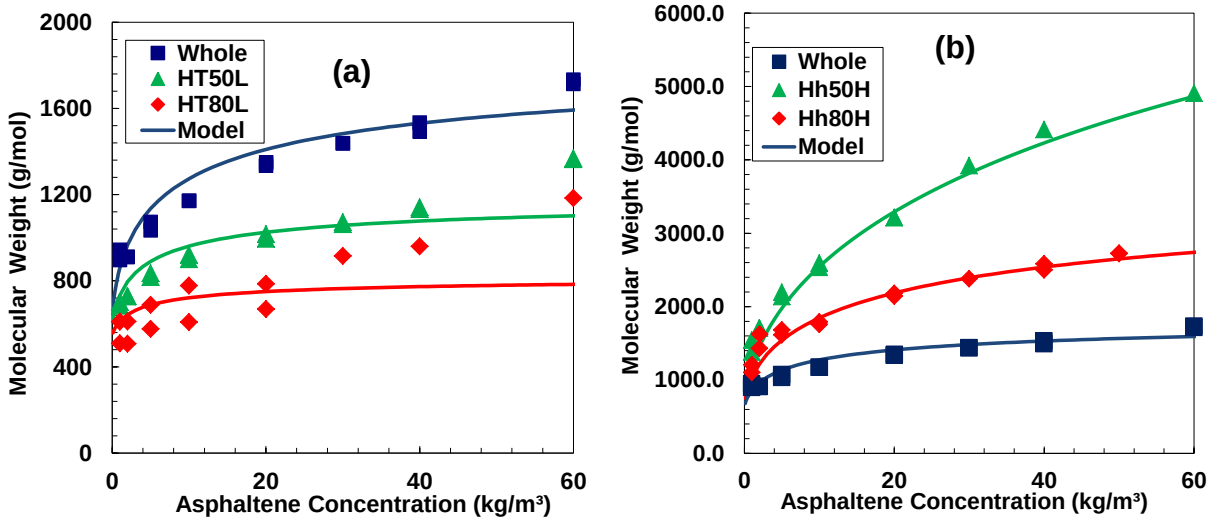

Figure B.18. Fitting of terminator-propagator model to RHC-18-37 whole asphaltenes, a) light cuts and, b) heavy cuts measured in toluene.

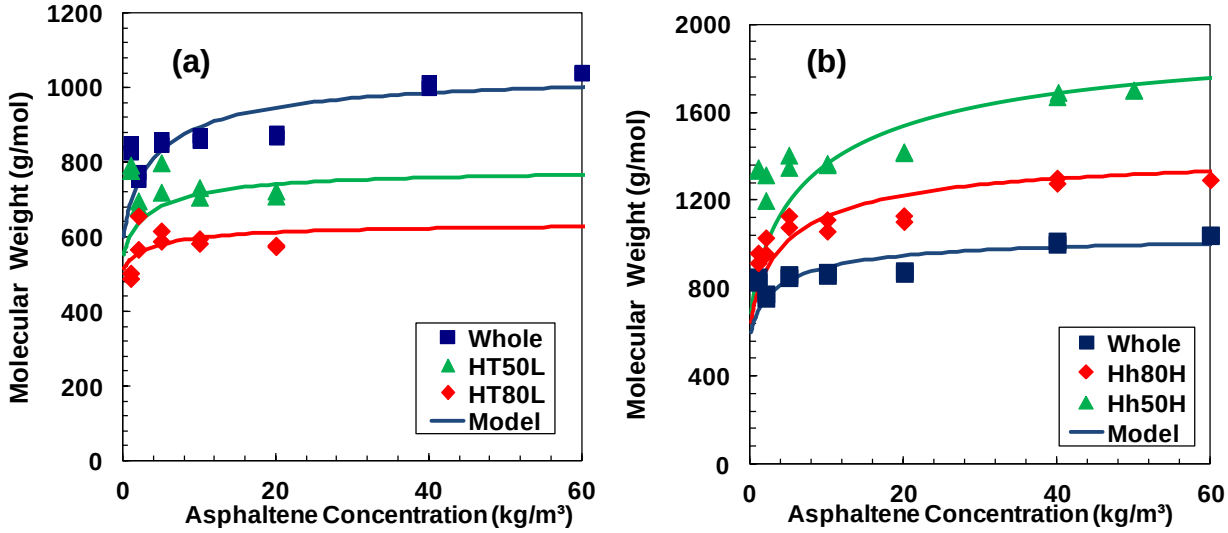

Figure B.19. Fitting of terminator-propagator model to HOSB whole asphaltenes, a) light cuts and, b) heavy cuts measured in o-dichlorobenzene.

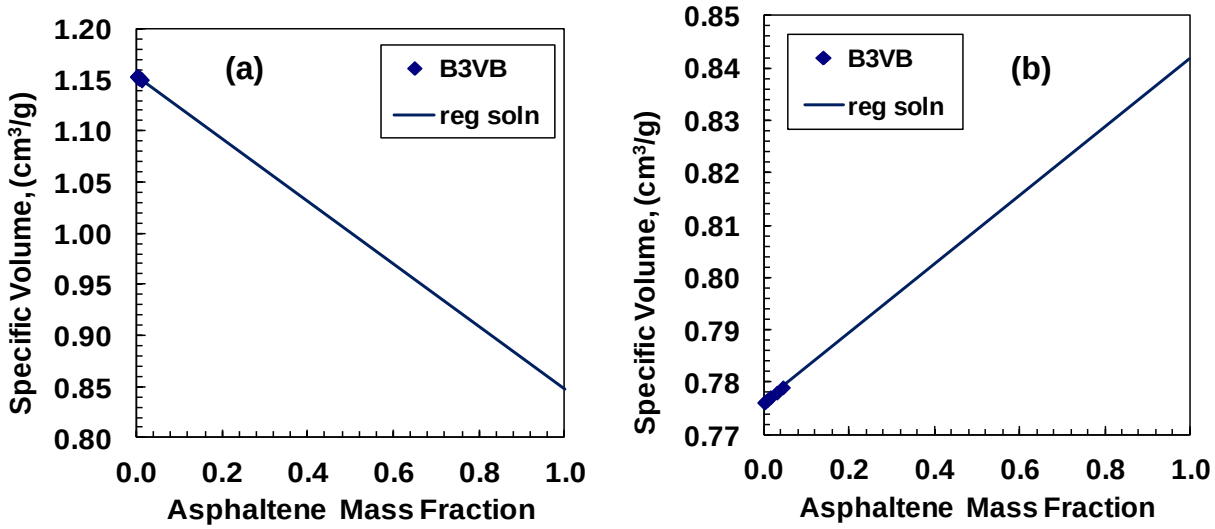

Figure B.20. Density measurements of B3VB whole asphaltenes in a) toluene and, b) o-dichlorobenzene.

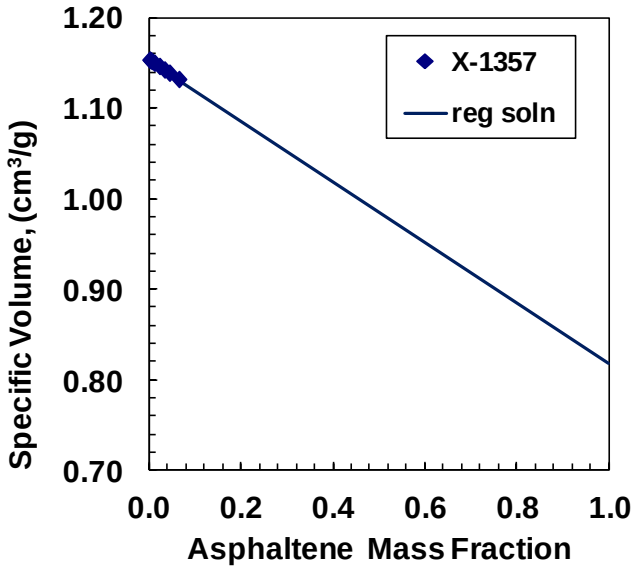

Figure B.21. Density measurements of X-1357 whole asphaltenes in toluene.

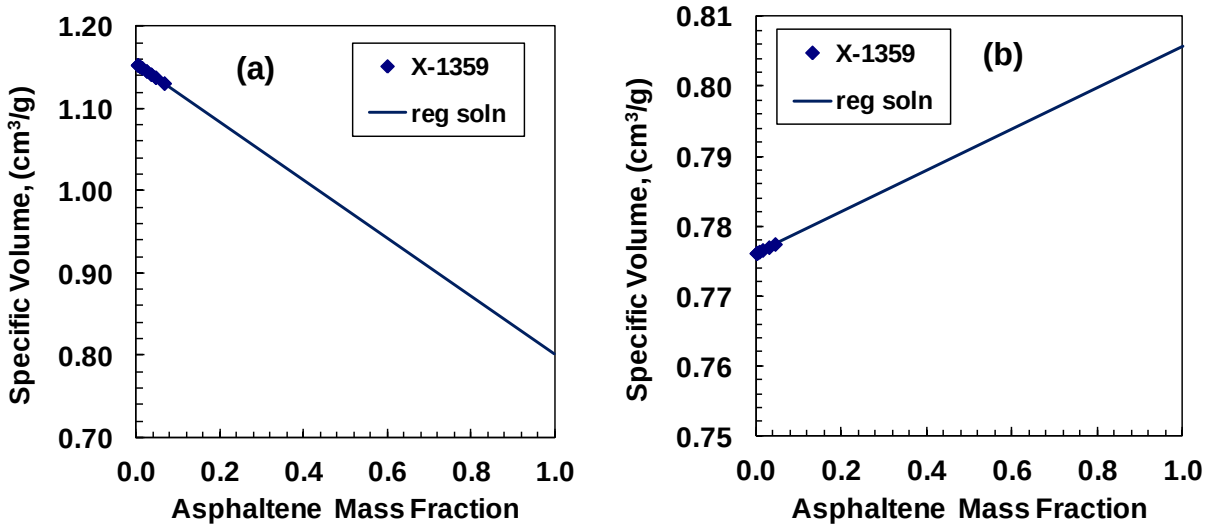

Figure B.22. Density measurements of X-1359 whole asphaltenes in a) toluene and, b) o-dichlorobenzene.

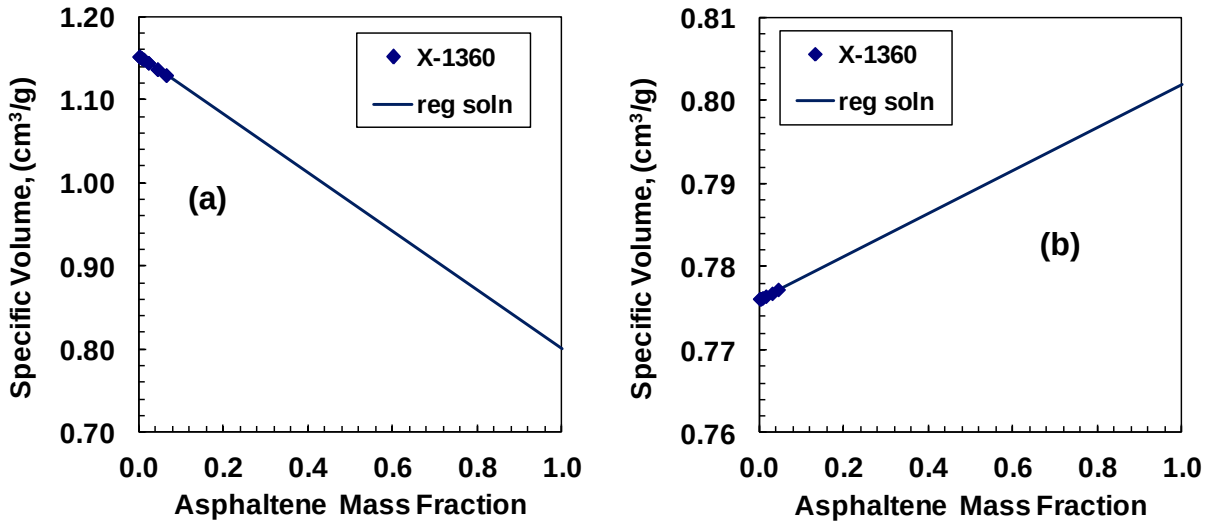

Figure B.23. Density measurements of X-1360 whole asphaltenes in a) toluene and, b) o-dichlorobenzene.

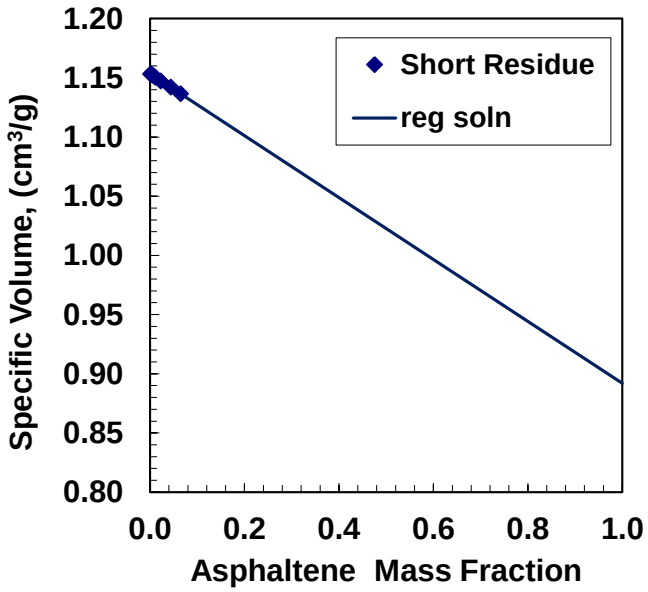

Figure B.24. Density measurements of Short Residue whole asphaltenes in toluene.

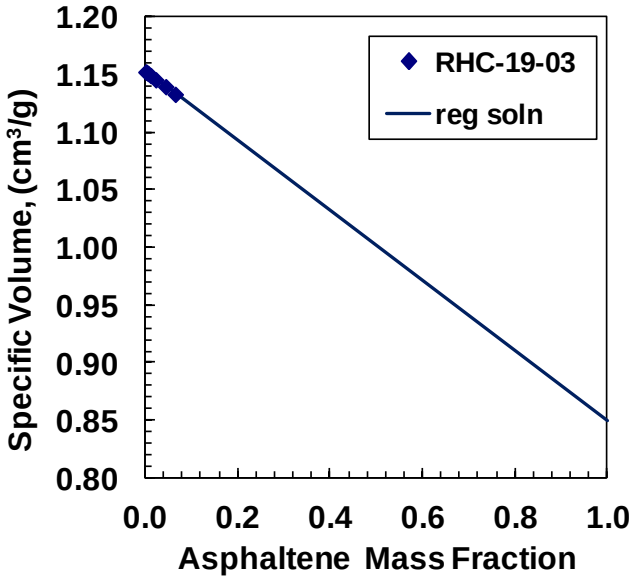

Figure B.25. Density measurements of RHC-19-03 whole asphaltenes in toluene.

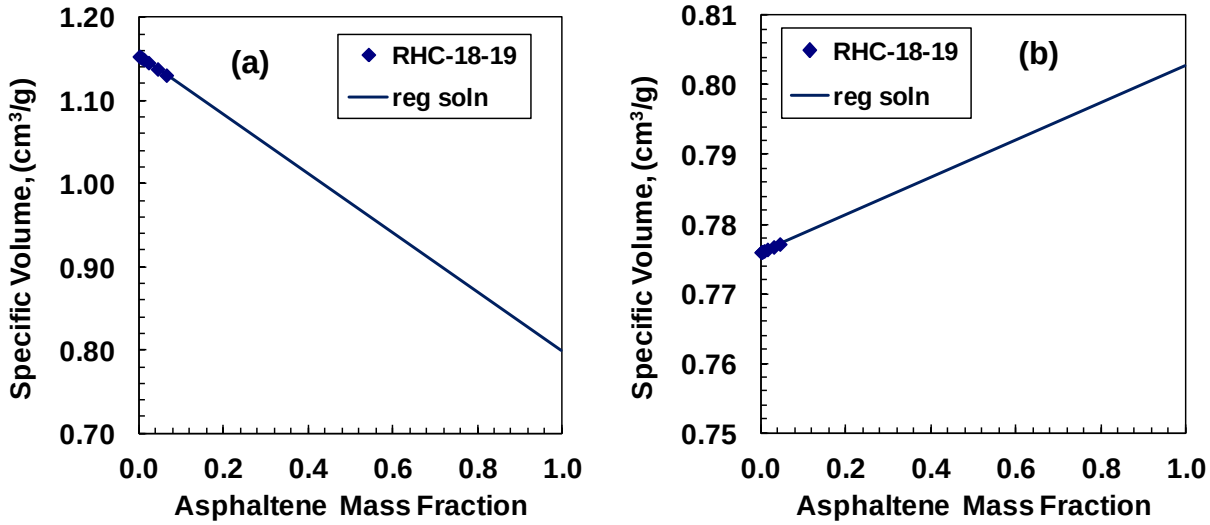

Figure B.26. Density measurements of RHC-18-19 whole asphaltenes in a) toluene and, b) o-dichlorobenzene.

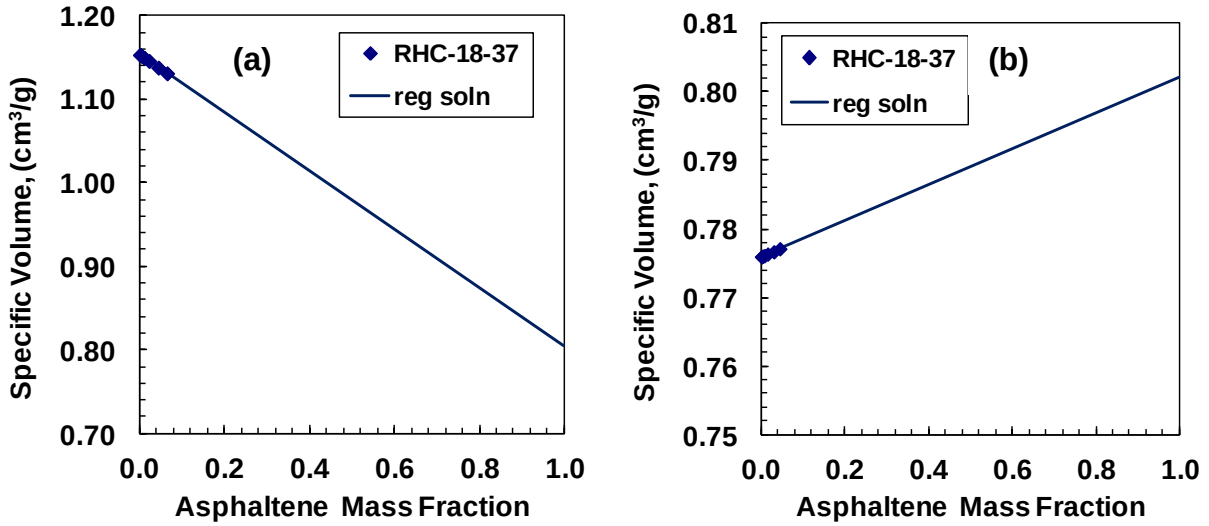

Figure B.27. Density measurements of RHC-18-37 whole asphaltenes in a) toluene and, b) o-dichlorobenzene.

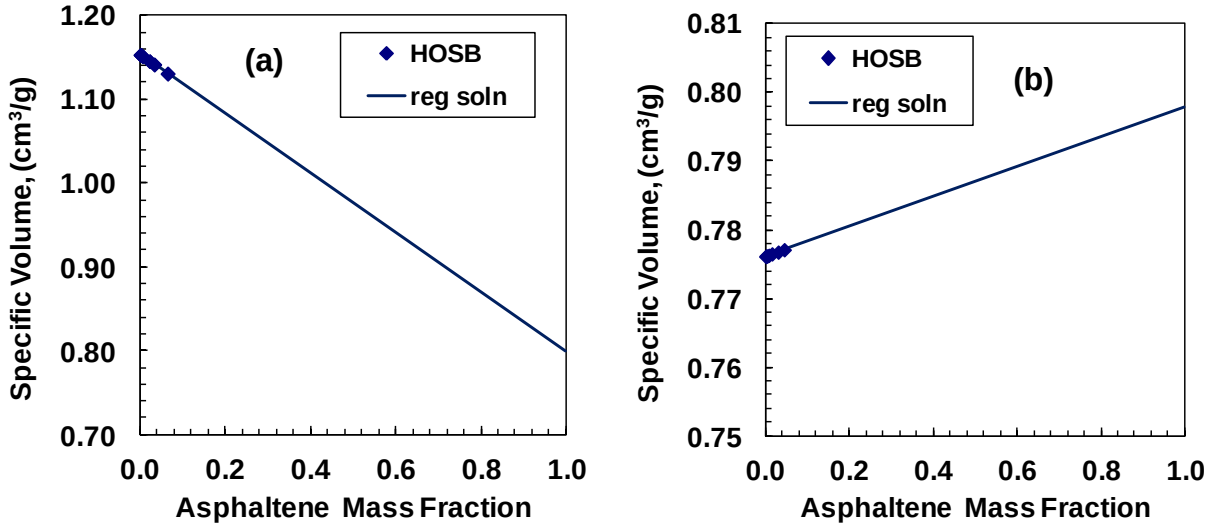

Figure B.28. Density measurements of HOSB whole asphaltenes in a) toluene and, b) o-dichlorobenzene.

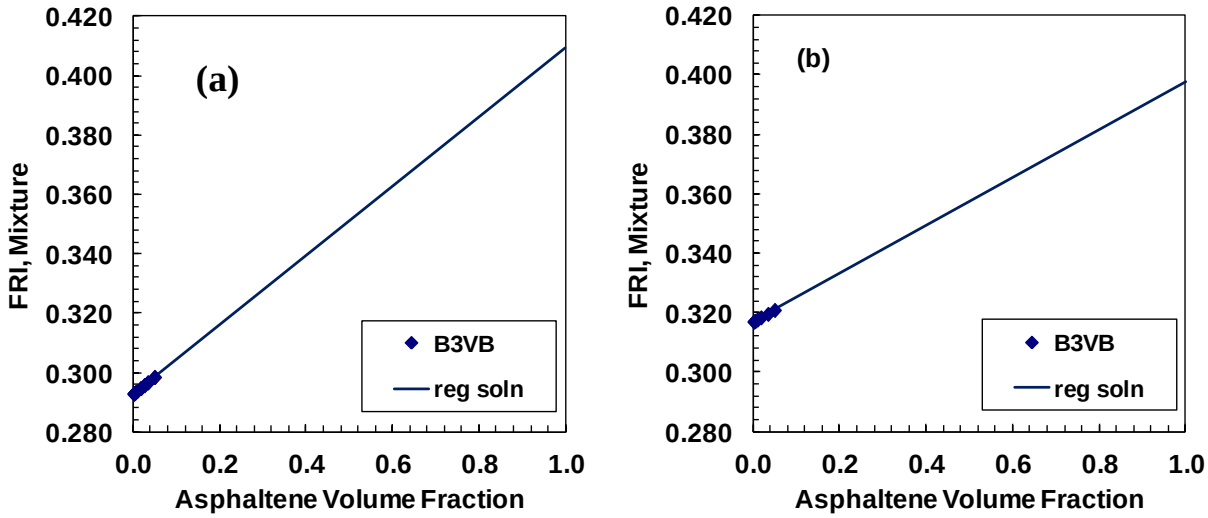

Figure B.29. FRI measurements of B3VB whole asphaltenes in a) toluene and, b) o-dichlorobenzene.

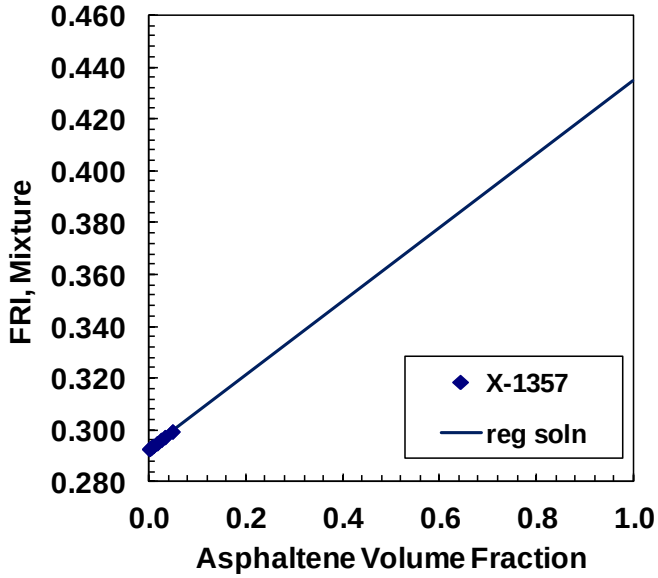

Figure B.30. FRI measurements of X-1357 whole asphaltenes in toluene.

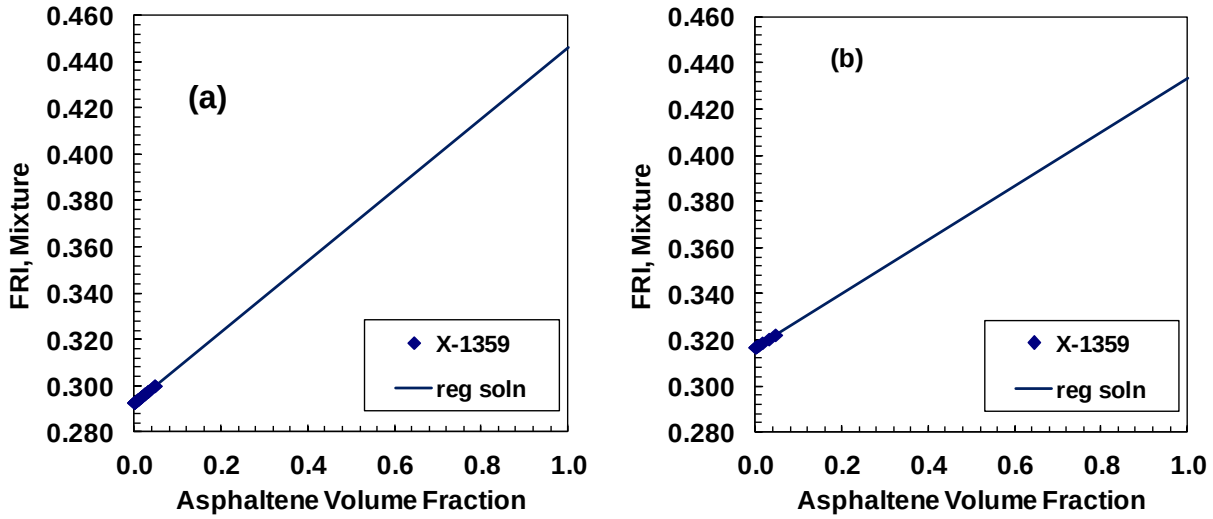

Figure B.31. FRI measurements of X-1359 whole asphaltenes in a) toluene and, b) o-dichlorobenzene.

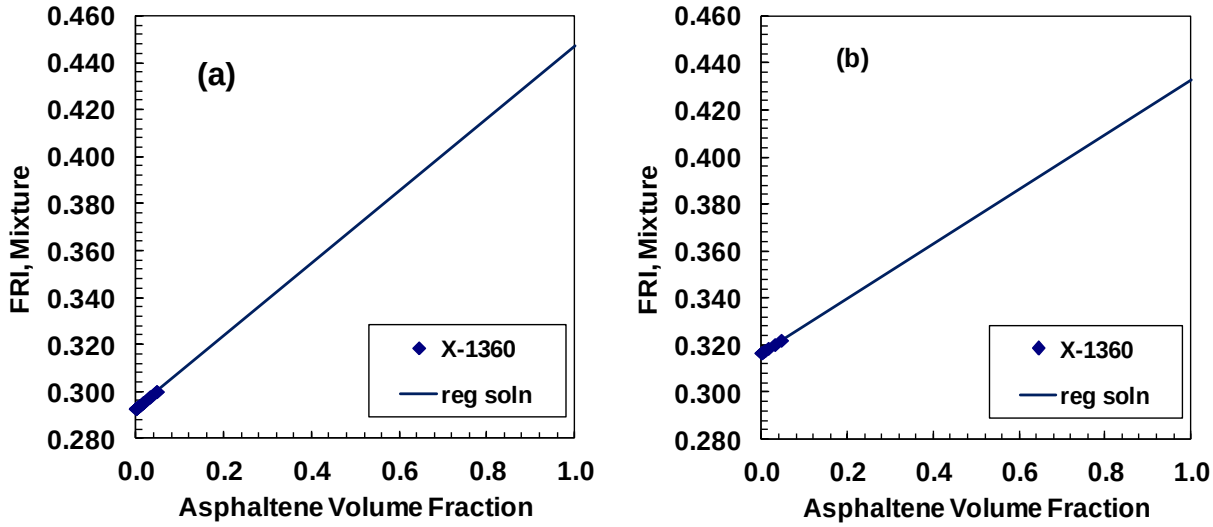

Figure B.32. FRI measurements of X-1360 whole asphaltenes in a) toluene and, b) o-dichlorobenzene.

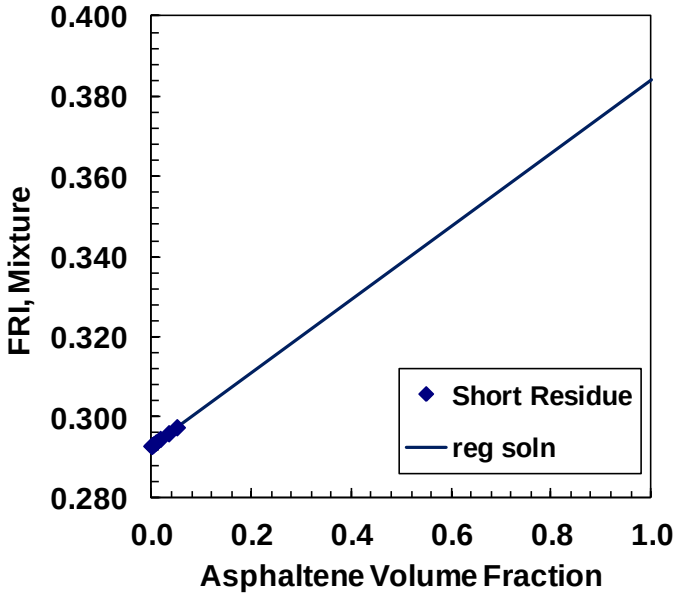

Figure B.33. FRI measurements of Short Residue whole asphaltenes in toluene.

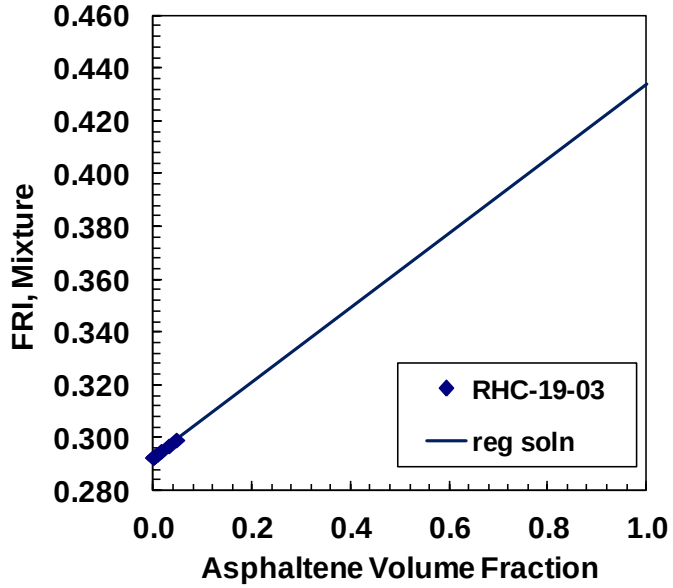

Figure B.34. FRI measurements of RHC-19-03 whole asphaltenes in toluene.

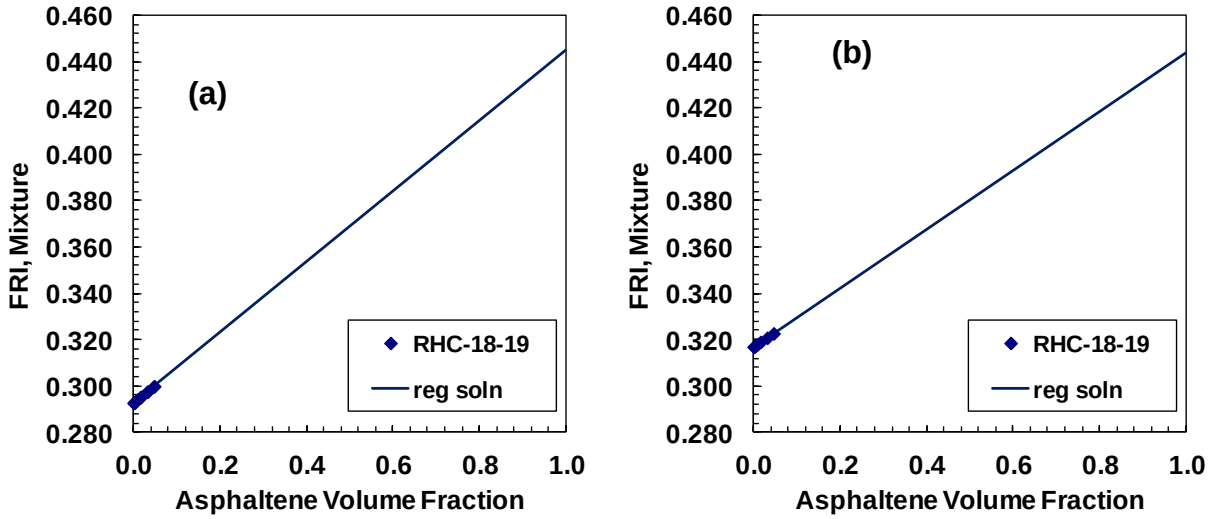

Figure B.35. FRI measurements of RHC-18-19 whole asphaltenes in a) toluene and, b) o-dichlorobenzene.

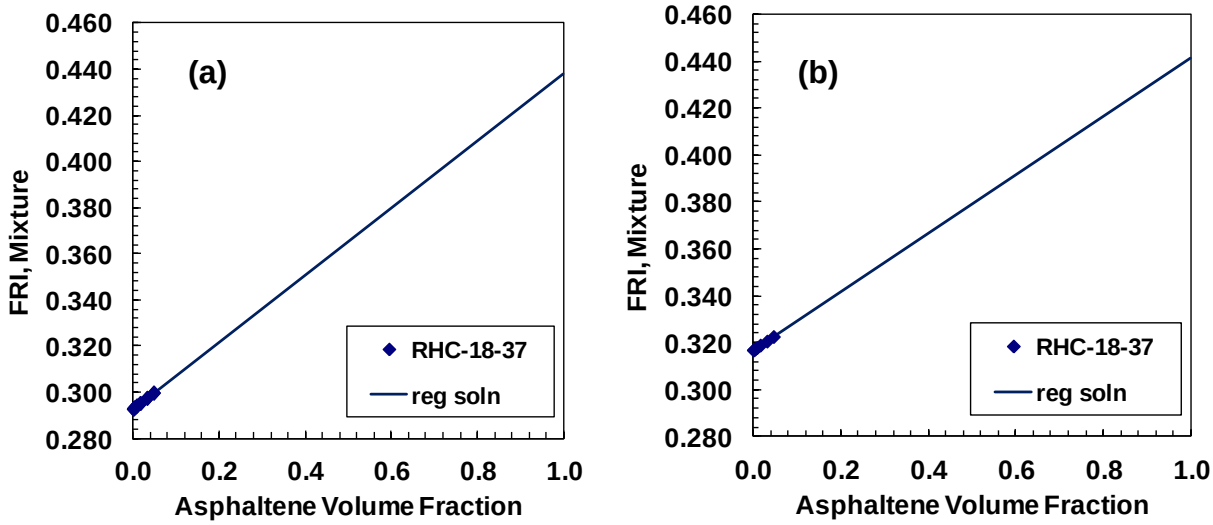

Figure B.36. FRI measurements of RHC-18-37 whole asphaltenes in a) toluene and, b) o-dichlorobenzene.

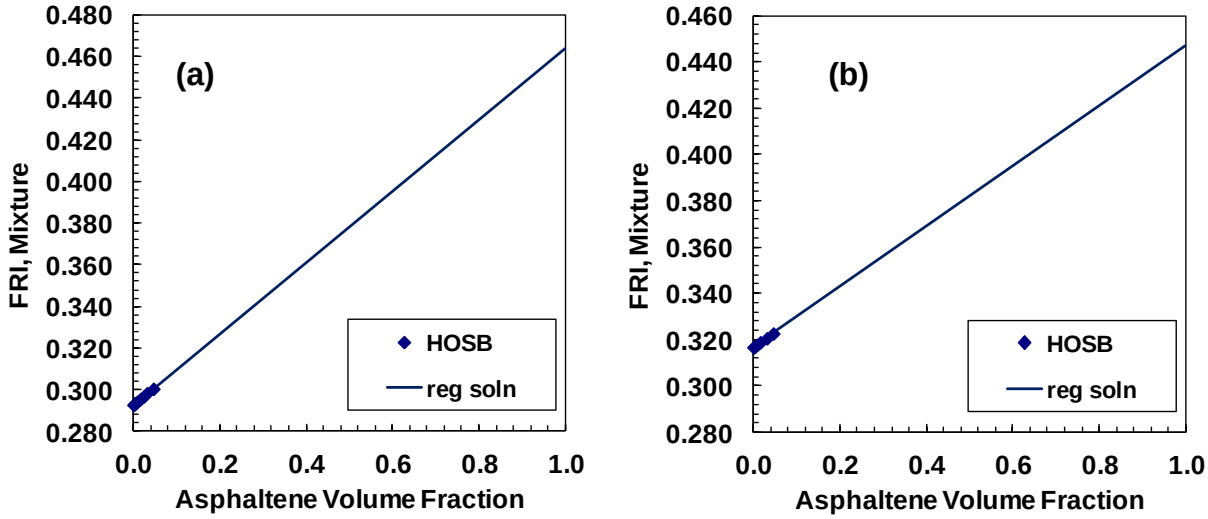

Figure B.37. FRI measurements of HOSB whole asphaltenes in a) toluene and, b) o-dichlorobenzene.

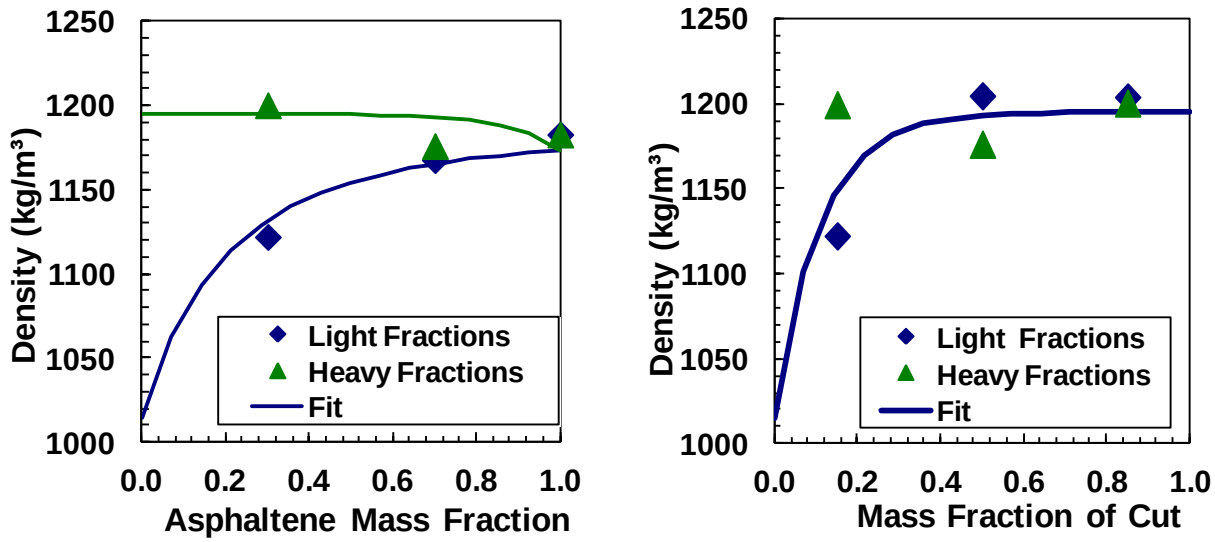

Figure B.38. Density of fractions (left plot) and density distribution (right plot) of B3VB asphaltenes measured in toluene.

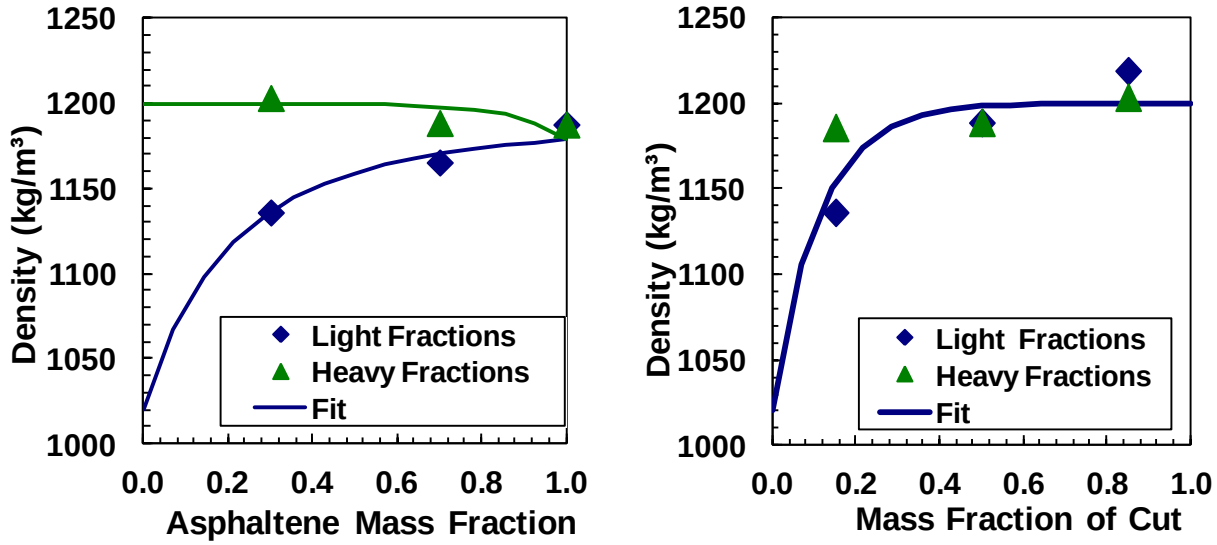

Figure B.39. Density of fractions (left plot) and density distribution (right plot) of B3VB asphaltenes measured in o-dichlorobenzene.

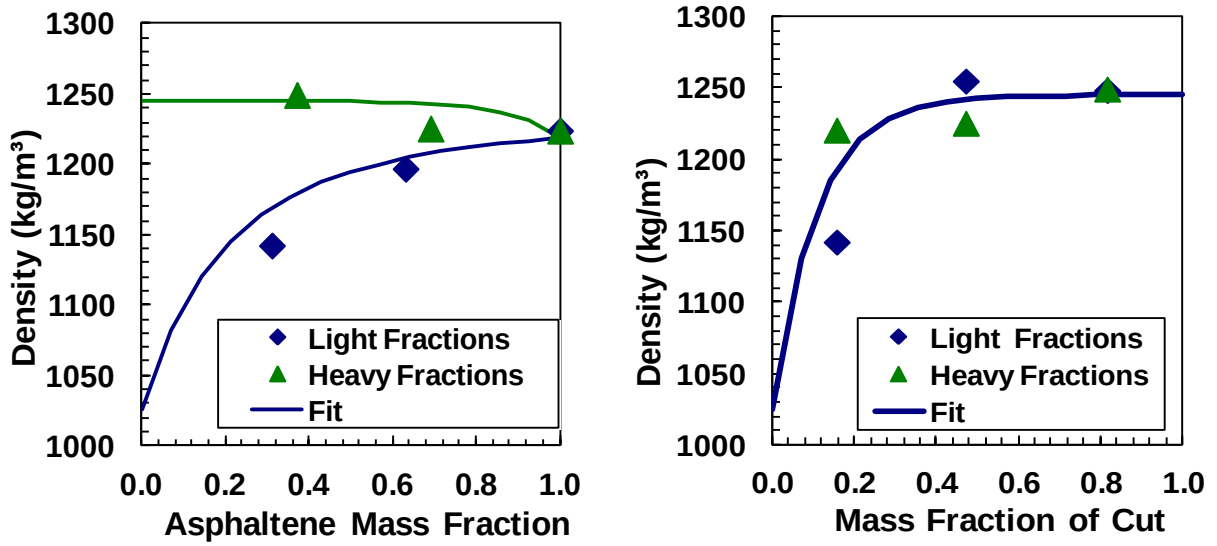

Figure B.40. Density of fractions (left plot) and density distribution (right plot) of X-1357 asphaltenes measured in toluene.

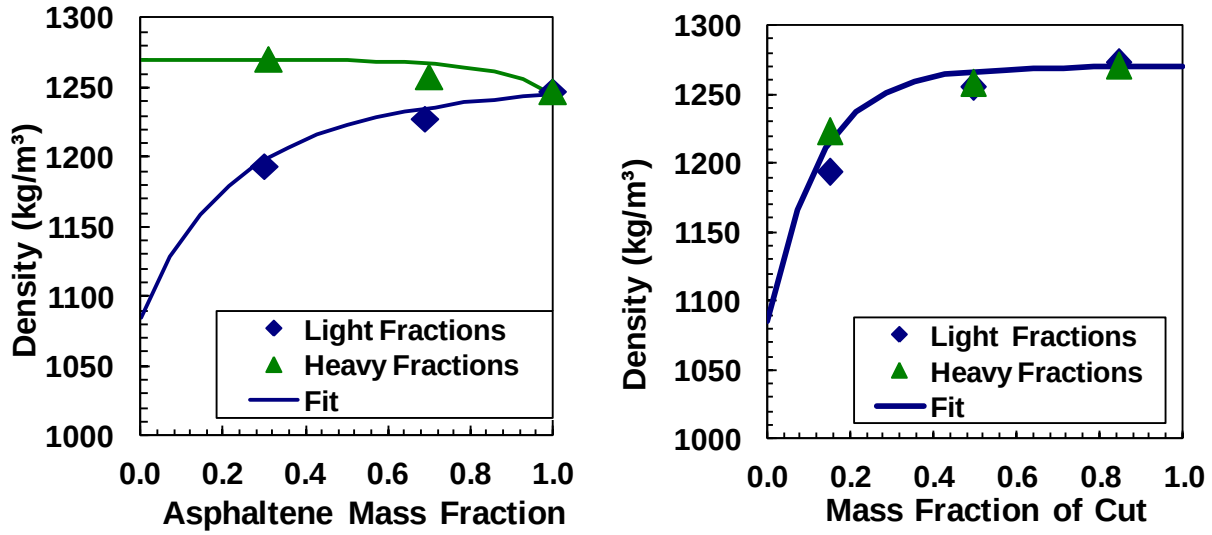

Figure B.41. Density of fractions (left plot) and density distribution (right plot) of X-1359 asphaltenes measured in o-dichlorobenzene.

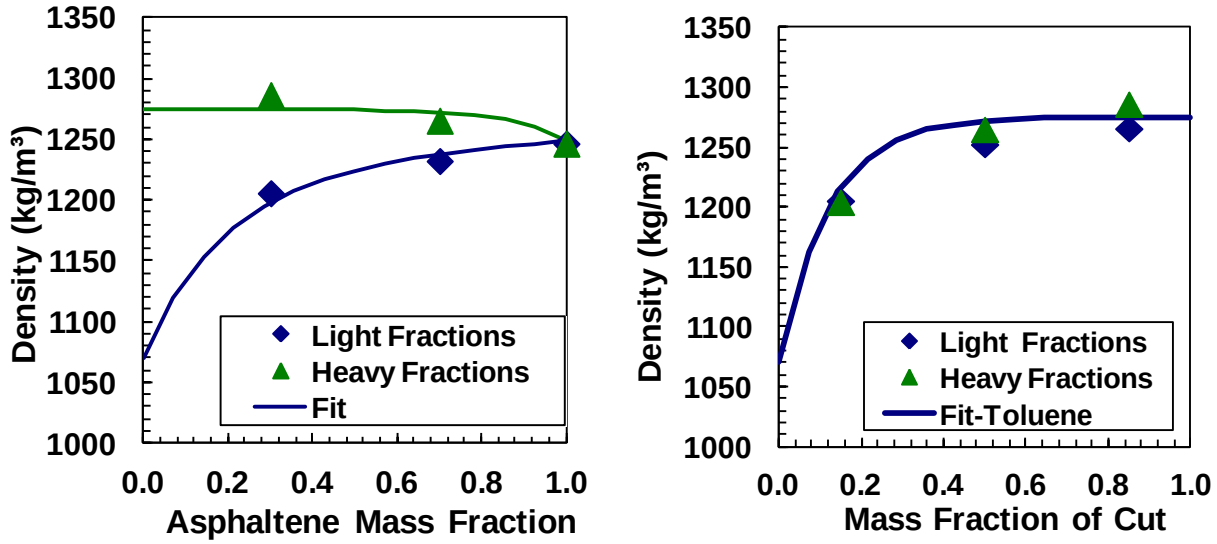

Figure B.42. Density of fractions (left plot) and density distribution (right plot) of X-1360 asphaltenes measured in o-dichlorobenzene.

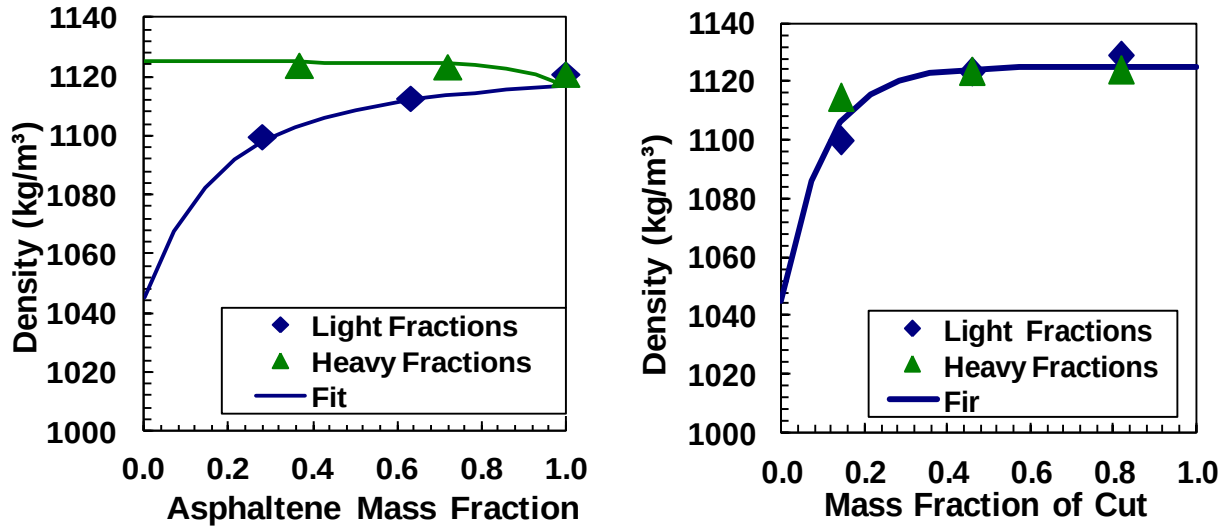

Figure B.43. Density of fractions (left plot) and density distribution (right plot) of Short Residue asphaltenes measured in toluene.

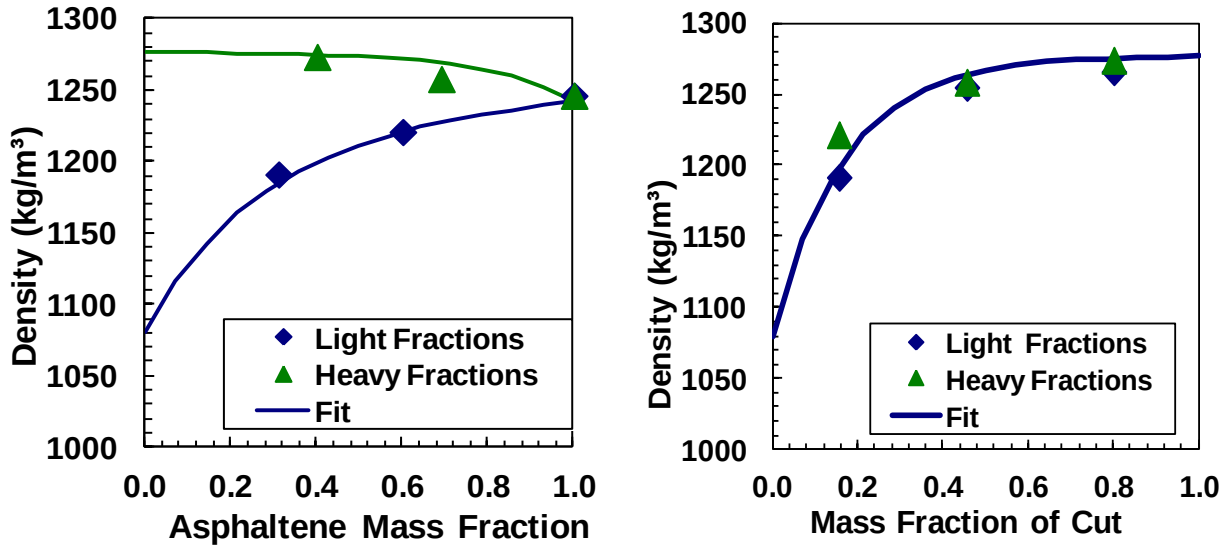

Figure B.44. Density of fractions (left plot) and density distribution (right plot) of RHC-18-19 asphaltenes measured in o-dichlorobenzene.

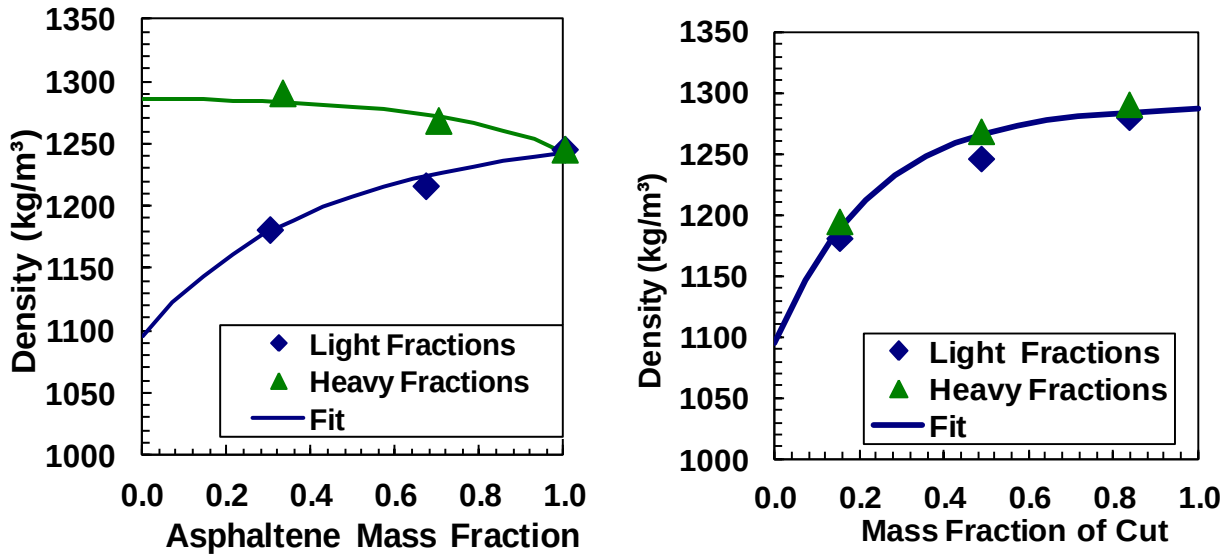

Figure B.45. Density of fractions (left plot) and density distribution (right plot) of RHC-18-37 asphaltenes measured in o-dichlorobenzene.

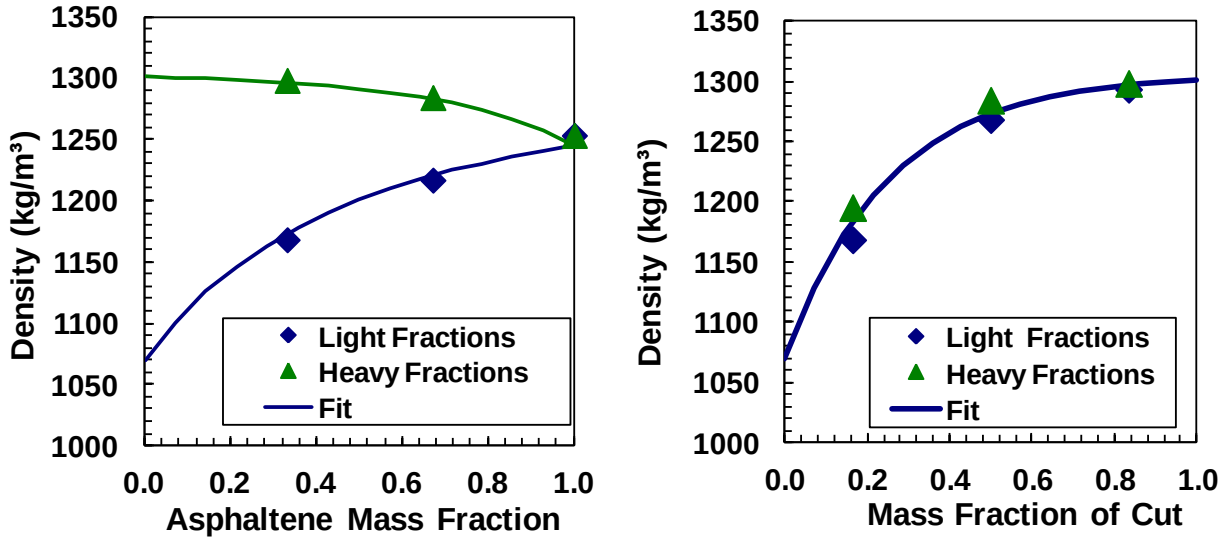

Figure B.46. Density of fractions (left plot) and density distribution (right plot) of HOSB asphaltenes measured in toluene.

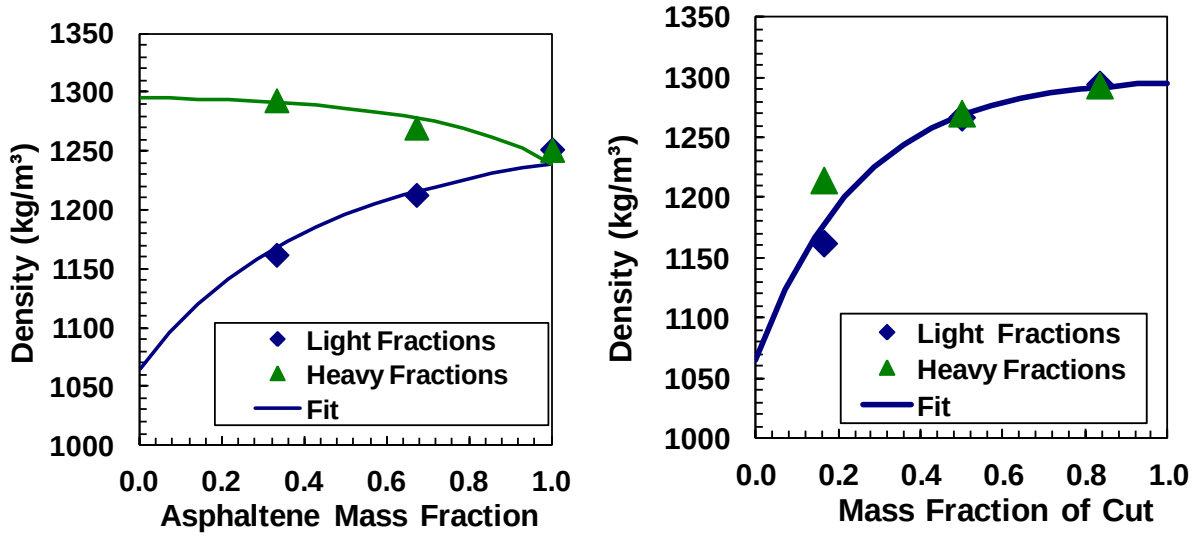

Figure B.47. Density of fractions (left plot) and density distribution (right plot) of HOSB asphaltenes measured in o-dichlorobenzene.

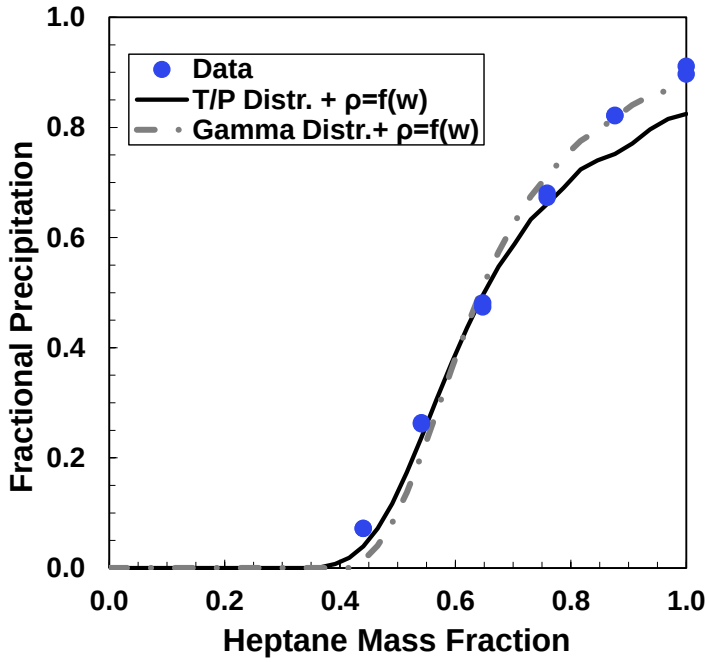

Figure B.48. RSM Model predictions for fractional yield of B3VB asphaltenes from solutions of n-heptane /toluene at 23 °C.

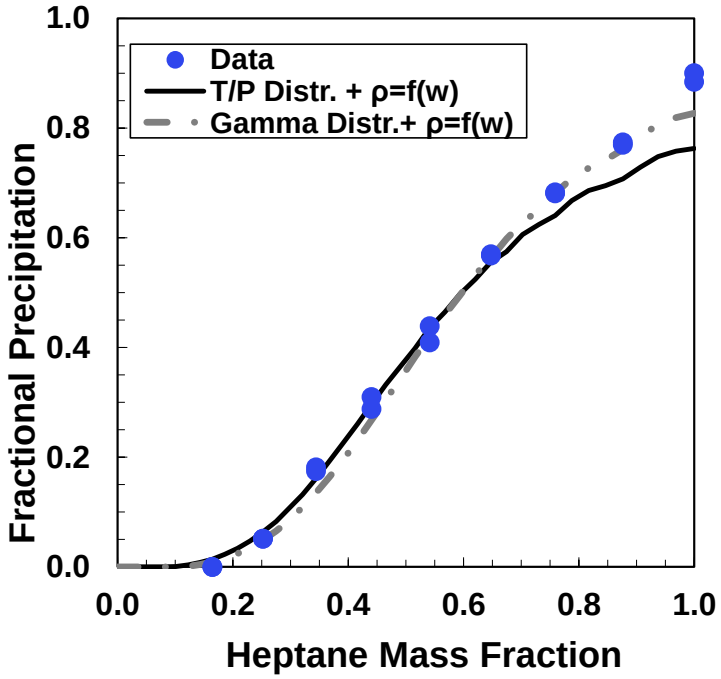

Figure B.49. RSM Model predictions for fractional yield of X-1357 asphaltenes from solutions of n-heptane /toluene at 23 °C.

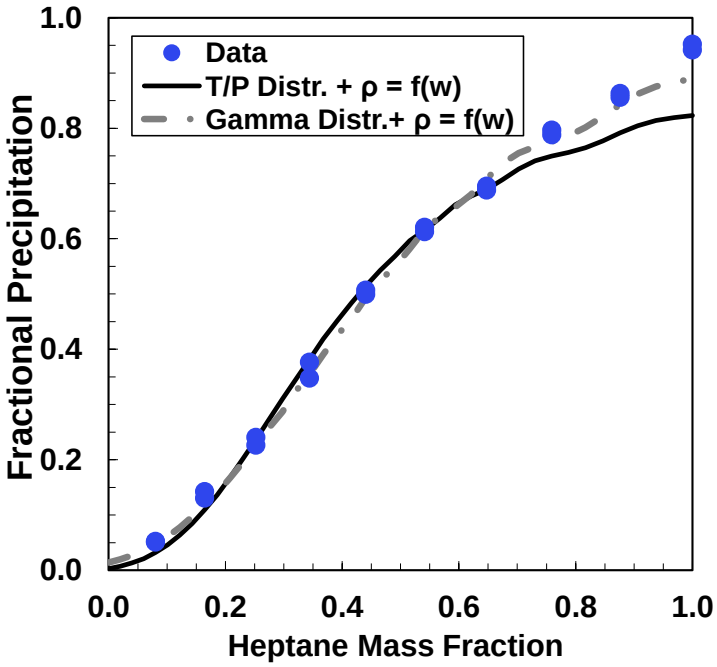

Figure B.50. RSM Model predictions for fractional yield of X-1359 asphaltenes from solutions of n-heptane /toluene at 23 °C.

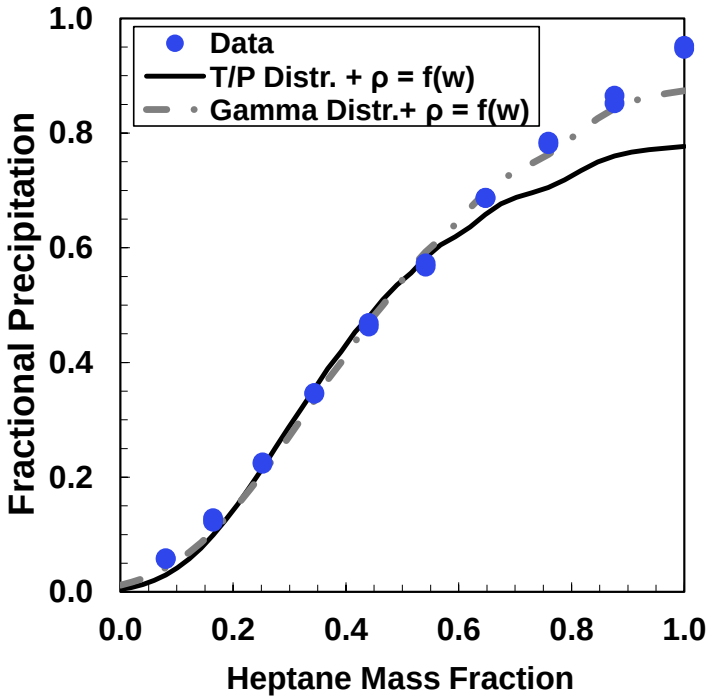

Figure B.51. RSM Model predictions for fractional yield of X-1360 asphaltenes from solutions of *n*-heptane /toluene at 23 °C.

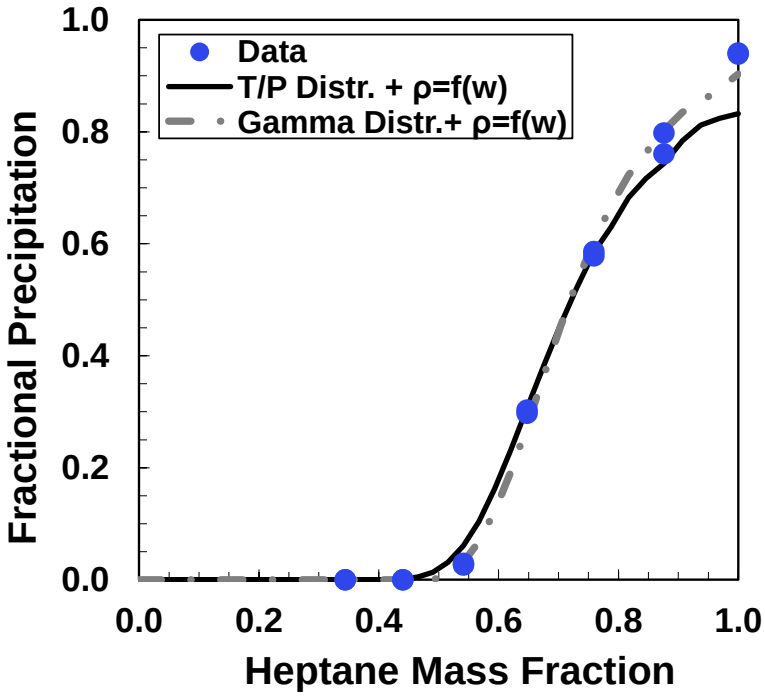

Figure B.52. RSM Model predictions for fractional yield of Short Residue asphaltenes from solutions of *n*-heptane /toluene at 23 °C.

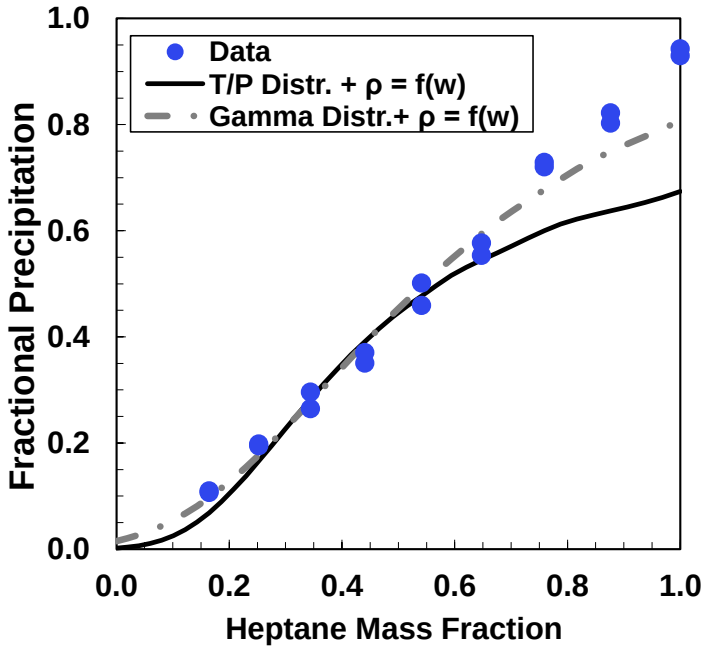

Figure B.53. RSM Model predictions for fractional yield of RHC-18-19 asphaltenes from solutions of n-heptane /toluene at 23 °C.

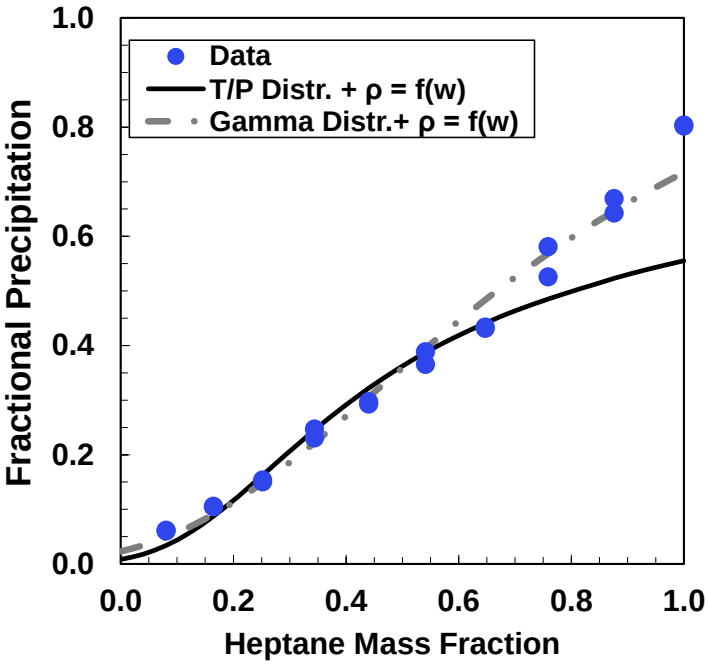

Figure B.54. RSM Model predictions for fractional yield of RHC-18-37 asphaltenes from solutions of *n*-heptane /toluene at 23 °C.

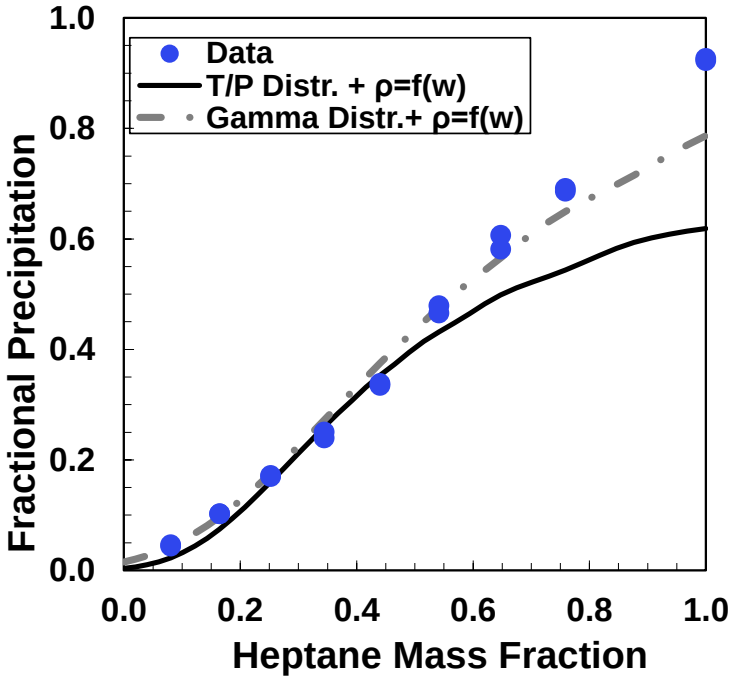

Figure B.55. RSM Model predictions for fractional yield of HOSB asphaltenes from solutions of *n*-heptane /toluene at 23 °C.